SYNTHESIS AND X-RAY POWDER DIFFRACTION STUDIES OF NOVEL NITRIDE-FLUORIDE COMPOUNDS

by

Joseph A. Potkonicky, Jr.

Submitted in Partial Fulfillment of the Requirements

for the Degree of

Master of Science

in the

Chemistry

Program

YOUNGSTOWN STATE UNIVERSITY

December, 1997

SYNTHESIS AND X-RAY POWDER DIFFRACTION STUDIES OF NOVEL NITRIDE-FLUORIDE COMPOUNDS

Joseph A. Potkonicky, Jr.

I hereby release this thesis to the public. I understand this thesis will be housed at the Circulation Desk of the University library and will be available for public access. I also authorize the University or other individuals to make copies of this thesis as needed for scholarly research.

Signature:

Joseph A. Potkonicky, Jr. — Student — 12/1/97 — Date

Approvals:

Timothy R. Wagner — Thesis Advisor — 12/8/97 — Date

Committee Member — 12/8/97 — Date

Frederick W. Wolf — Committee Member — 12/8/97 — Date

Dean of Graduate Studies — 12/11/97 — Date

ABSTRACT

Attempts to synthesize novel nitride-fluoride analogs to certain metal oxide compounds, and novel fluoride analogs to oxides with the magnetoplumbite structure were carried out under varied conditions. The novel nitride-fluoride compounds attempted for this exploratory research project were: $BaMgAl_{11}F_{10}N_9$ which is an analog of $BaMgAl_{11}O_{18.5}$ (barium β-alumina), $MgAl_2(FN)_2$ which is an analog of Al_2O_3 (corundum), and Sr_2NF which is an analog of SrO (rocksalt type). The two novel fluorides attempted for this research project were $NaLi_6Mg_6F_{19}$ and $CaLi_5Mg_6F_{19}$. Powder X-ray diffraction data for each trial synthesis of each proposed compound are presented and discussed in terms of reaction outcomes.

ACKNOWLEDGMENT

I would like to extend my deepest gratitude to my research advisor, Dr. Timothy Wagner, whose knowledge, insight, and patience guided me toward the completion of my thesis project. I wish to thank Drs. Daryl Mincey and Friedrich Koknat for reviewing my work as members of my thesis committee. I would also like to thank Dr. James Mike for mentoring me as both a graduate and undergraduate student.

I wish to dedicate this work to my wife, Janet, whose enduring support and love helped me to complete this seemingly impossible task.

I would also like to sincerely thank my parents, Joseph and Paula, for their steadfast encouragement through-out my entire academic career.

Lastly, I would like to thank all of my family, friends, and colleagues for their continual kindness and support.

TABLE OF CONTENTS

PAGE

LIST OF TABLES

LIST OF FIGURES

FIGURE PAGE

CHAPTER I

EXPLORATION OF SOLID-STATE CHEMISTRY

Introduction

Through-out modern history, solid state chemistry can be credited with some of the most beneficial innovations known to humanity. Solid state chemistry is either partially or completely responsible for such familiar devices as: telephones, radios, televisions, computers, video cassette recorders, cellular phones, pagers, and most if not all other electronic devices that utilize the technology of the integrated circuit.

Without the rudimentary experiments performed by early solid state chemists, we would not have the technology of lasers to perform remarkable tasks such as refractive eye surgery or microengraving. Lasers are also used by physicians to perform surgeries because they will instantly cauterize blood vessels that are bleeding inside of organ tissue. This small list of examples does not completely summarize the tremendous impact that the science of solid state chemistry has had on civilization. For this reason, it can be stated that solid state chemistry has been a very important tool for science as well as society, and it will

continue to play an important role in technology into the twenty-first century and beyond.

Background

The immense discipline known as inorganic chemistry encompasses all of the chemistry not directly associated with the science of hydrocarbons and the substances that are derived from them. The science of solid state chemistry is a subsection of inorganic chemistry, and it is defined as the preparation, identification, characterization, and categorization of solid materials.

An unlimited number of inorganic crystalline compounds could theoretically be synthesized, and solid state chemists work to discover these compounds through a difficult process of trial and error. The process of discovering a new species begins with nothing more than a laboratory of starting reagents and the intuition of the solid state chemist. The synthesis of previously undiscovered compounds often requires a large number of trials to get the desired result but sometimes even that is not enough to achieve the ultimate goal of the synthesis. The absolute judge of whether a proposed synthesis will work is determined by the thermodynamic properties of the system in question as well as the kinetics. The thermodynamics of the system may dictate that upon the reaction of a mixture, the desired

compound may not form because another phase may be thermodynamically more stable. In addition, the amount of energy that may be necessary to stress the system so that the reaction is forced toward the products may not be available to the system. Even if the aforementioned conditions are satisfied, the reaction may be kinetically hindered so that the desired product will still not be obtained. Inability to predict from first principles the structure a specific starting composition will form under certain reaction conditions is the foremost difficulty that most solid state chemists encounter when attempting to synthesize novel species.

After a synthesis has been performed, the solid state chemist has a large repertoire of analytical instruments and techniques available for identifying and characterizing the reaction product. Many of these methods incorporate the use of X-rays to some degree. The following list contains characterization techniques for solids that utilize X-rays: Powder X-ray Diffraction, Single Crystal X-ray Diffraction, Electron Spectroscopy for Chemical Analysis, X-ray Fluorescence, and Electron Probes. The instrumentation for these methods are equipped with X-ray detectors. Two additional techniques of value to solid state chemists are Scanning and Transmission Electron Microscopy.

Solid-State Materials

The convention in solid state chemistry is to characterize solids according to the bonding that occurs within them. Presently there are four types of solids classified in solid state chemistry. Each of the four types of solids possess specific bonding systems.

The first group of solids are referred to as molecular solids. There are two characteristics unique to molecular solids. The first characteristic is strong interatomic forces, such as covalent bonds, that hold the atoms of the molecule together. The second characteristic is weak intermolecular bonds that are known as van der Waals forces. Because the intermolecular forces are weak, the mechanical properties of the bulk solid are extremely weak. Most binary compounds of nonmetals are good examples of molecular solids.

The next group of solids are referred to as extended solids. Extended solids are non-molecular species that are characterized by a mixture of strong bonds, which can range from mostly ionic to mostly covalent in character, depending upon composition. The strong bonds join one atom to the next forming a continuous network of material known as a lattice. All crystalline solids form lattices that consist of unit cells. Identical unit cells stack in all directions

to form a crystal lattice. This is the general type of solid that is studied in this thesis.

The third type of solids are polymeric solids that are molecular solids that contain very long chains of atoms that are bonded with covalent bonds. Long polymeric chains undergo a process known as cross-linking which increases the molecular weight and dimensional stability. Cross-linking occurs when polymeric chains are linked together with covalent or ionic bonds to form a network.[1] As a polymeric solid undergoes extensive cross-linking, the increased stability causes it to behave less analogously to a molecular solid.

The fourth and final category of solids are those which are specified as low-dimensional materials. The low-dimensional materials possess very strong bonds in one or two dimensions but contain weak van der Waals forces in the other remaining dimensions. A good example of a low dimensional material is graphite which exhibits very weak mechanical properties due to van der Waals forces.

Future Outlook

"The chemistry of extended solids is perhaps the oldest chemical science, beginning perhaps with the firing of clay pots in prehistoric eras or certainly with the smelting of ores in the bronze age."[2] This statement succeeds in

reflecting on the history of solid state chemistry, but there is no such statement to predict the future direction of the science.

One of the main drawbacks of solid state chemistry is the lack of a logical predictive method to determine reactions or products. The intuitive tools that are available for other disciplines of chemistry are not readily available in solid state chemistry presently. The main problems that solid state chemistry must overcome in order to advance the science are: the inability to predict the composition of non-stoichiometric compounds, the inadequacy of calculating basic structures of compounds, and the failure to determine a feasible reaction pathway for a proposed synthesis. For these three reasons, the science of solid state chemistry moves at a markedly slower pace than other disciplines of chemistry such as organic synthesis. Organic chemists have long enjoyed a tremendous advantage with regard to the advancement of their field of chemistry because reaction mechanisms in organic chemistry are very predictable with relatively easily calculated outcomes. Organic chemists have less of a problem predicting stoichiometries because there are relatively few types of bonds that organic compounds use.

Currently, stoichiometries of inorganic compounds are predicted by employing the law of definite proportions. The

law of definite proportions is quite effective for working with normal valence compounds. A normal valence compound contains electropositive elements bonded to electronegative elements using ionic or covalent bonds. Electropositive elements are metallic in nature and are located on the left side of the periodic chart whereas electronegative elements are non-metallic and reside on the right side of the periodic chart. Metallic elements, which are positive, have an affinity to bond with negatively charged non-metallic elements to form ionic compounds. Unfortunately, the law of definite proportions is not useful for predicting the compositions of non-stoichiometric compounds like β-alumina which has the composition $Na_{2+X}Al_{22}O_{34+X/2}$ where X is in the range of 0.3 to 0.6. In contrast to the experimentally determined composition, the theoretically predicted structural composition of β-alumina is $NaA_{11}O_{17}$. Examples like that of β-alumina are usually the rule, and not the exception, in solid state chemistry.

Quantitatively predicting the structures of new compounds is impossible to do at present due to the large number of bonding possibilities for a given composition. For example, DiSalvo[3] has prepared a variety of curiously layered structures with possible superconductor properties by heating mixtures of calcium nitride and nickel powders under an atmosphere of nitrogen. This is a typical example

of the researcher being unable to predict product structures by relating them to initial reactants, thus illustrating the problem of relating structure to stoichiometry. Unlike the compounds synthesized in solid state chemistry, the structures of organic products can be predicted because the bonding that takes place between: carbon, hydrogen, nitrogen, oxygen and sulfur remains relatively consistent. This problem of predicting the structures is directly related to that of predicting the stoichiometries. Once one of these two problems has been solved, the solution to the other should follow close behind.

The final stumbling block in the science of solid state chemistry is the absence of a method to predict the reaction mechanism for a proposed synthesis. A solid state reaction contains two steps that must take place in order for the reaction to proceed. The first step occurs when the atoms diffuse through the solid material to the interface, where the particles can react with each other. The second step occurs when the atoms rearrange into a new structure. Presently the mechanism of diffusion that takes place during a reaction is understood, but the mechanism that accounts for the atoms rearranging into novel compounds is unknown. The primary reason that the rearranging of atoms cannot be understood is that the area where the reactants interface with each other is obstructed by the unreacted material.

The most logical solution to this problem would be to develop a technique that would penetrate the unreacted material enabling the observation of the atoms as they rearrange. Unfortunately such a technique has not yet been added to the solid state chemist's repertoire of analytical devices. It is the job of present and future solid state chemists to work tirelessly to attain the solutions to these stated problems in order to advance the science of solid materials.

Although the structures of inorganic compounds cannot necessarily be predicted from first principles, much has been learned about existing compounds using X-ray crystallographic methods. X-ray crystallography is perhaps the most important technique available to the solid state chemist and will be briefly discussed next.

Introduction to X-ray Crystallography

In order to fully understand the concept of X-ray crystallography, the nature and history of X-rays needs to be explored. X-rays may be defined as electromagnetic radiations whose wavelengths lie in the range of 0.1 to 10 Å. X-rays are produced when a stream of high-energy electrons bombard a material that is usually metallic. Inner electrons from atoms of the material are removed, which causes the atoms to be in an excited state. When

outer shell electrons replace the vacated inner shell electrons, the atoms return to their ground state of energy. The energy given off during this electron transition from outer shells to inner shells appears as the emission of X-rays. An intensity distribution curve of emitted X-rays for a metal exhibits the spectral line $K\alpha$ which represents an $L \rightarrow K$ electron transition and the spectral line $K\beta$ which designates the rare $M \rightarrow K$ electron transition (Figure 1.1).

X-rays were accidentally discovered in 1895 by Roentgen when he detected a new type of radiation that penetrated material such as wood, cardboard, and thin metal.[4] The next advancement occurred when von Laue pioneered a method to determine that X-rays consisted of electromagnetic waves of very short wavelengths. Von Laue's method consisted of positioning a crystal in front of an X-ray beam that was collimated or parallel, and placing a photographic plate behind the crystal to detect any diffraction patterns (Figure 1.2). This diffraction experiment, conceived by von Laue, was carried on by his assistants Friedrich and Knipping. Ultimately von Laue's hypothesis that the regular array of atoms in a crystal could act as a diffraction grating for X-rays was proved experimentally.[5] The initial work performed by those early scientists laid the foundation for the beginning of X-ray crystallography.

The next scientists to impact X-ray crystallography

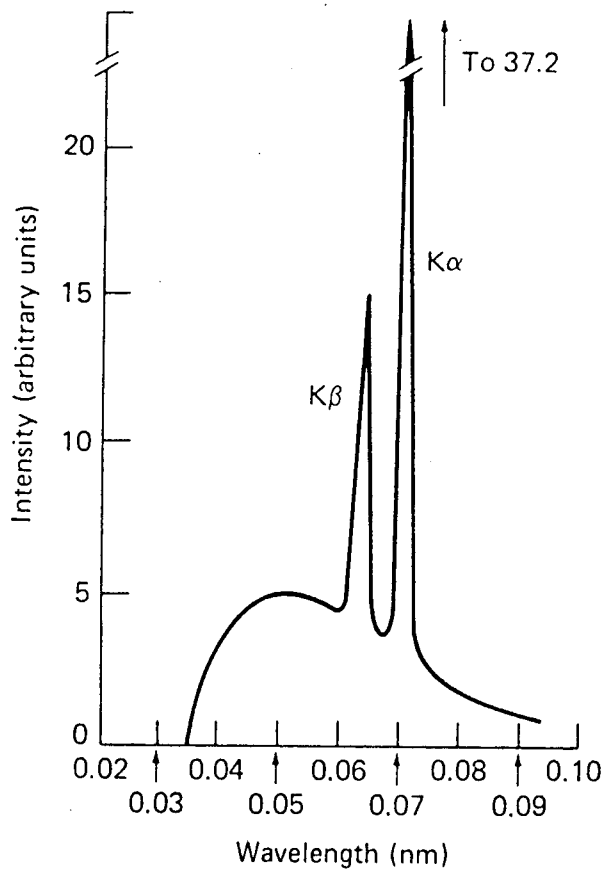

Figure 1.1. Intensity distribution curve of emitted X-rays for a metal, after Bromberg[4].

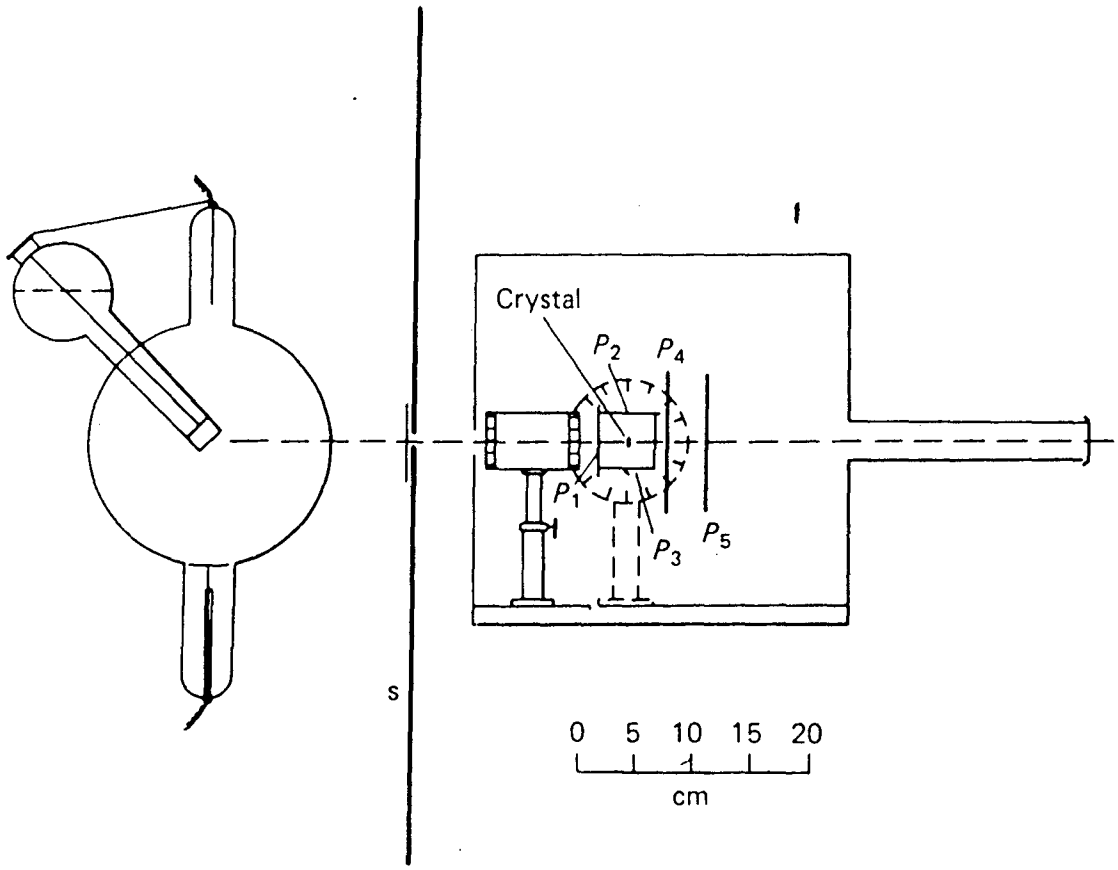

Figure 1.2. Schematic representation of Max von Laue's diffraction experiment, after Bromberg[4].

were the father and son team of William Henry Bragg and William Lawrence Bragg, who derived the fundamental equation for crystal structure determination known as Bragg's law: $n\lambda=2d_{hkl}sin\theta$, where n, an integer, is the order of diffraction, λ is the X-ray wavelength, d is the distance between the atomic planes of the crystal lattice, and θ is the angle of diffraction.[6] Bragg's law applies to a situation where an incident beam of X-rays, originating from an X-ray tube (Figure 1.3), bombards a powder sample that contains fragments of crystals ideally in every possible orientation. The X-rays are diffracted only from those crystals which are oriented in a specific set of planes (h,k,l), such that the angle of diffraction θ and the interplanar spacing d satisfies the Bragg equation, illustrated in Figure 1.4. The terms for (h,k,l) are the Miller indices, and their respective reciprocals denote the values on the three crystallographic axes that a crystal plane intercepts. The Miller indices are used to define all possible crystal planes that a specific solid can possess. This relationship outlined in the Bragg equation is permitted because the law of reflections demonstrates that the reflected X-ray beam is equal to the incident X-ray beam.

The maximum order of reflection, n, of the Bragg equation is dependent on the source of the X-rays. For many

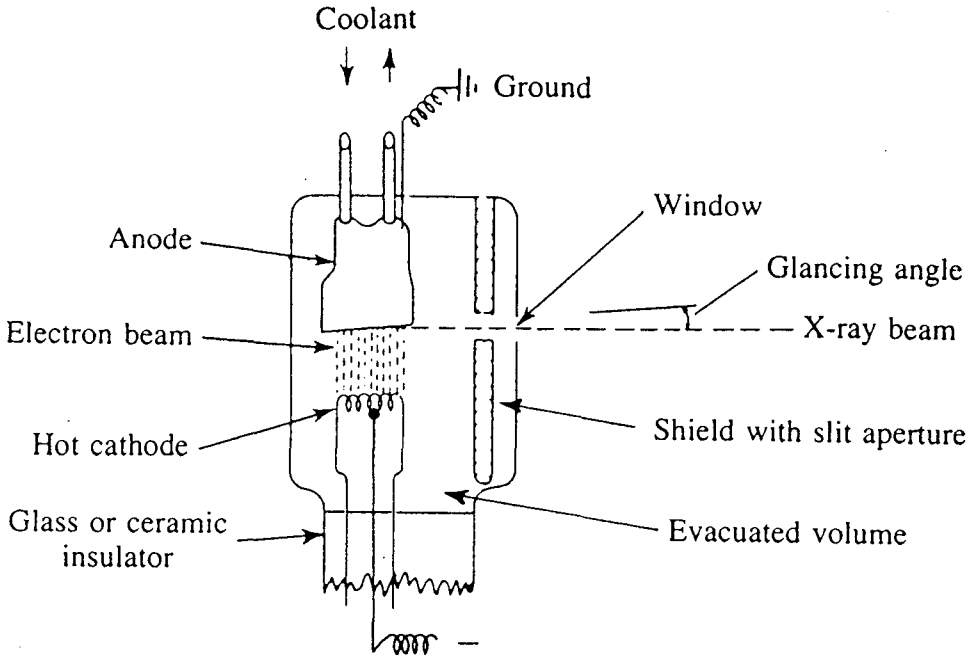

Figure 1.3. Schematic of an X-ray tube, after Willard[7].

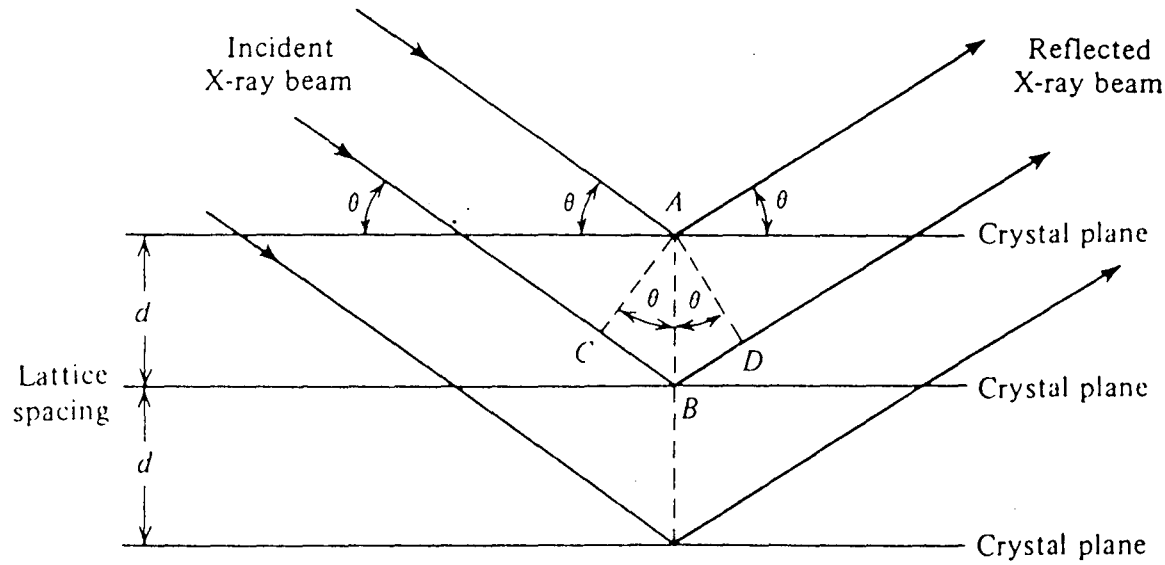

Figure 1.4. Diffraction of X-rays from a set of crystal planes, after Willard[7].

state of the art instruments, the source of the X-rays is a Cu$K\alpha$ source. A Cu$K\alpha$ X-ray source emits energy at a wavelength of 1.5418 Å, but there are other X-ray sources used such as Mo$K\alpha$ which emits energy at a wavelength of 0.7107 Å. Thus, the most important factor that determines the boundaries of the Bragg equation is the wavelength of the X-rays. In general, it is possible to obtain more data within a given range of θ using a smaller wavelength source.

Although Bragg's Law is extremely useful for indexing diffraction patterns and describing the geometry conditions necessary for diffraction to occur, its limitations should be recognized. First, Bragg's Law gives no prediction of systematic absences, which is necessary for discerning the lattice type of the sample. Second, it gives no indication of peak intensities, which is essential for the refinement of the structure. Finally, of lesser consequence to inorganic chemists, but still important to realize, is that Bragg's Law says nothing about the physics of diffraction at the atomic level.

Comparison of Powder Camera to Area Detector

One of the earliest methods used to identify powder samples via X-ray diffraction is referred to as the Debye-Scherrer method. A finely ground powder sample is placed in a glass capillary tube and mounted in a brass pin with clay.

The sample apparatus is inserted in the powder camera such that it is between the light collimator and the photographic film.[8] The Cu$K\alpha$ X-ray source is located behind the collimator such that only a very small beam of X-rays is permitted to bombard the sample as it rotates about its axis. The diffracted X-rays impinge upon the film exposing it to display a series of arcs which becomes the fingerprint of the sample compound.

The new generation of X-ray diffraction instruments all possess electronic detector devices that collect the diffraction data. The area detector used in this work for powder samples utilizes a two-dimensional multiwire grid, an integral pre-amplifier, and high resolution electronics that enable it to count single X-ray photons which significantly increases the sensitivity of the instrument. The area detector is interfaced with a computer enabling further analysis of the data with the use of distinctive software programs. The computer also is used to store the data for future reference.

The advantage of the area detector is its ability to collect a tremendously large amount of signals and separate the noise from the true sample signal. This allows the area detector to be highly sensitive as compared to the powder camera method.

CHAPTER II

SURVEY OF NITRIDE-FLUORIDE COMPOUNDS

Introduction to Nitride-Fluorides

Throughout the history of solid state chemistry, the most intensely investigated area of research has been the synthesis and characterization of oxide compounds. The primary reason that oxide research has been the forerunner is that oxide syntheses proceed uninhibited in normal atmosphere. In contrast, other solid state reactions must be contained in a closed system environment. The closed systems used for these syntheses are either under vacuum or filled with inert gases like argon or nitrogen. Consequently, literally thousands of oxides are known to exist as compared to only hundreds of nitrides and fluorides.

Another additional category of compounds, which are the focus of this thesis, are referred to as nitride-fluoride compounds. Nitride-fluoride compounds are often structural analogs of metal oxide compounds, and they consist of the replacement of two O^{2-} ions in the oxide with one N^{3-} and one F^{-} ion. Currently there are less than thirty nitride-fluorides known to exist. Research concentrating on the

synthesis of nitride-fluoride compounds has recently begun to receive more attention.

The majority of nitride-fluoride compounds that have been previously prepared contain the main group metals Mg, Ca, Sr, and Ba. The transition metals that have been used to prepare these metal-oxide analog compounds are Zn and Zr. The remaining nitride-fluorides that have been reported in the literature contain elements from the Actinide series along with the synthetically prepared element technetium. The latter compounds are not of interest to this thesis and will not be discussed further. The compounds of interest to this thesis are listed in Table 2.1 along with some pertinent background data for each compound.

Table 2.1

Known Nitride-Fluoride Compounds

Compound	Mixture	Temperature	Envir.	System	Ref.
Ba_2NF	$3Ba^0/1BaF_2$	700°C	Ar / N_2	Cubic	9
Ca_2NF	$4Ca^0/1CaF_2$	1000°C	Ar / N_2	Cubic	9
L-Mg_2FN	$1Mg^0/1MgF_2$	900-1000°C	N_2	Tetra.	10
H-Mg_2FN	L-Mg_2FN	1100-1350°C	N_2	Cubic	10
Mg_3F_3N	$1Mg^0/3MgF_2$	900-1000°C	N_2	Cubic	10
Sr_2NF	$3Sr^0/1SrF_2$	950°C	Ar / N_2	Cubic	9
α-Zn_2NF	Zn_3N_2/ZnF_2	325-400°C	N_2	Ortho.	11
β-Zn_2NF	Zn_3N_2/ZnF_2	325-400°C	N_2	Tetra.	11
α-$Zn_9N_4F_6$	Zn_3N_2/ZnF_2	325-400°C	N_2	Unknown	11
β-$Zn_9N_4F_6$	Zn_3N_2/ZnF_2	325-400°C	N_2	Unknown	11
$Zn_7N_4F_2$	Zn_3N_2/ZnF_2	325-400°C	N_2	Unknown	11
$ZrF_{1.27}N_{0.987}$	ZrF_4/NH_3	580°C	NH_3	Ortho.	12

Main Group Metal Nitride-Fluoride Compounds

The three nitride-fluoride compounds, Ca_2NF, Sr_2NF, and Ba_2NF, were first synthesized over twenty years ago by Ehrlich[9] et al. The underlying experimental technique employed within these syntheses was mixing stoichiometric amounts of the metal powder with the metal fluoride. The mole ratios of the starting materials was either three or four moles of the metal powder to one mole of the metal fluoride.[9] The reagent mixtures were heated initially in a closed argon atmosphere at 450°C to drive off any oxidation that may have formed on the metal powder. Next, the atmosphere was switched to nitrogen and the temperature was increased to 700°C for barium, 950°C for strontium, and 1000°C for calcium to start the solid state reaction.[9] The samples were heated for 24 hours to form the nitride-fluoride species, and the excess fluorine was removed from the sample product by reheating the sample under dynamic vacuum at 1000°C.[9] Debye-Scherrer patterns showed evidence that new phases were present, which were postulated to be the previously mentioned nitride-fluorides. Based on their X-ray data, the researchers concluded that the novel nitride-fluoride compounds have structures analogous to those of the corresponding oxides (CaO, SrO, BaO), all three of which have the NaCl-type structure.[9] Detailed studies to

determine the actual structures, which have not been performed, will ultimately reveal if these compounds were actually synthesized.

The other main group metal which was utilized in the preparation of nitride-fluoride compounds is magnesium. The following magnesium nitride-fluoride compounds were reported by Andersson[10] et al, Mg_3NF_3, L-Mg_2NF, and H-Mg_2NF, where L- and H- refer to low and high temperature forms respectively. As with the calcium, strontium, and barium species; the magnesium nitride-fluoride compounds were synthesized by using a mixture of magnesium metal with magnesium fluoride in a nitrogen atmosphere at relatively high temperatures.[10] The two initial products were determined to have the compositions Mg_3NF_3 and L-Mg_2NF, by density tests performed on the materials as well as structural analysis. The H-Mg_2NF compound was formed by heating L-Mg_2NF between 1100°C and 1350°C under extreme pressure.[10]

Powder X-ray diffraction patterns of the three magnesium nitride-fluoride compounds were indexed to determine their structure-types. Unlike the case for the calcium, strontium, and barium nitride-fluorides discussed previously, more quantitative structural data was obtained in this study using a least-squares crystal structure refinement program on the powder diffraction intensities. The structure of Mg_3NF_3 was determined to be cubic (NaCl-

type), analogous to that of MgO.[10] The structure of L-Mg_2NF was determined to be tetragonal and was described as an intermediate between the zinc-blende and sodium chloride structures.[10] When subjected to 20 Kb pressure and a temperature of 1300°C, L-Mg_2NF transforms to H-Mg_2NF which reportedly has the NaCl-type structure like its oxide analog MgO.[10]

Transition Metal Nitride-Fluoride Compounds

The first transition metal that forms nitride-fluoride compounds is zinc. There are five zinc nitride-fluoride compounds that have been reported by Marchand[11] et al: α-Zn_2NF, β-Zn_2NF, α-$Zn_9N_4F_6$, β-$Zn_9N_4F_6$, and $Zn_7N_4F_2$. These five compounds were prepared by mixing Zn_3N_2 and ZnF_2 together in various stoichiometric amounts and heating at relatively low temperatures in nickel crucibles from 325°C to 400°C.[11] Upon completion of the syntheses, the five distinct products were isolated. Three of the different species were reportedly discernible based on their individual colors.[11] There are two allotropes of the compound Zn_2NF, α and β. The transition from the α species to the β species occurs at 450°C, where only the β form is stable.[11] Two of the five nitride-fluoride compounds were assigned crystal structures based on the reflections observed. Those compounds were

characterized by indexing Debye-Scherrer patterns that were collected for each separate phase of the material. The lattice of α-Zn_2NF was determined to be orthorhombic whereas the lattice of β-Zn_2NF was determined to be tetragonal.[11]

The final transition metal possessing a nitride-fluoride compound is zirconium. Unlike the previous nitride-fluorides, the zirconium species has a fractional stoichiometry. The formula reported by Jung[12] et al for zirconium nitride-fluoride is $ZrN_{0.906}F_{1.28}$. Curiously, the method used to synthesize $ZrN_{0.906}F_{1.28}$ differs significantly from the methods that were used to synthesize the previous nitride-fluoride compounds listed in this chapter. The zirconium nitride-fluoride compound was synthesized by ammonolysis of ZrF_4 by a current of NH_3 at 580°C.[12] The structure of $ZrN_{0.906}F_{1.28}$ was determined to be orthorhombic by a detailed study to index the powder pattern.[12]

It is remarkable that of the few nitride-fluoride compounds reported in the literature, fewer still have been well-characterized. Of the twelve compounds discussed in this chapter, only six could be considered well-characterized: L-Mg_2FN, H-Mg_2FN, Mg_3F_3N, α-Zn_2NF, β-Zn_2NF, and $ZrN_{0.906}F_{1.28}$. The other six compounds: Ca_2NF, Sr_2NF, Ba_2NF, α-$Zn_9N_4F_6$, β-$Zn_9N_4F_6$, and $Zn_7N_4F_2$ were characterized only by indexed powder X-ray diffraction patterns, which yielded

lattice-types for Ca_2NF, Sr_2NF, and Ba_2NF. It is noteworthy that the most recent of these papers reporting nitride-fluoride work was published over twenty years ago. This has surely been a neglected field in solid state chemistry.

CHAPTER III

STATEMENT OF THE PROBLEM

As stated in the previous chapter, literally thousands of oxides are known to exist as compared to hundreds of nitrides, fluorides, and less than thirty nitride-fluoride compounds. Therefore there is a gap in basic knowledge of the solid state chemistry of nitride-fluoride compounds.

This exploratory research project involves attempts to synthesize novel nitride-fluoride compounds that are analogous to familiar metal oxide compounds. Also, attempts will be made to synthesize novel mixed metal fluoride compounds that are analogous to oxides with the magnetoplumbite structure. The syntheses will be carried out under varied conditions of temperature and reaction atmosphere, since there is no clear path to follow in the literature for most of the compounds studied.

The novel nitride-fluoride compounds that will be attempted in this exploratory research project are: $BaMgAl_{11}F_{10}N_9$ which is an analog of $BaMgAl_{11}O_{18.5}$ (barium β-alumina), $MgAl_2(FN)_2$ which is an analog of $MgAl_2O_4$ (spinel), $Al_2(FN)_{1.5}$ which is an analog of Al_2O_3 (corundum), and Sr_2NF which is an analog of SrO (rocksalt type). The two novel

mixed metal fluorides proposed for synthesis for this research project are $NaLi_6Mg_6F_{19}$ and $CaLi_5Mg_6F_{19}$.

Following the aforementioned syntheses, powder X-ray diffraction data will be collected and analyzed for each trial. The results of the X-ray diffraction data will show if the novel compounds are present or give clues as to why they are not.

This project is not only useful for expanding knowledge in nitride-fluoride crystal chemistry, but could also help increase understanding of structure to property relationships in oxides. For example, if a structural nitride-fluoride analog to a high temperature oxide superconductor could eventually be made in work continuing from this exploratory project, some insight might be gained as to why the oxides are superconductors.

The ultimate goal of this researcher is to synthesize a novel compound or at least determine the reasons why the attempted syntheses were unsuccessful.

CHAPTER IV

EXPERIMENTAL METHODS AND PROCEDURES

Introduction

The numerous methods of sample preparation and data processing that were used to obtain the results that are presented in this thesis can be summarized by the following categories: sample preparation, X-ray data collection, X-ray diffraction pattern analysis, and overall data interpretation.

Sample Preparation

There were several methods employed for the preparation and synthesis of the proposed novel nitride-fluoride and fluoride compounds. The reagents were weighed out on a Mettler model PM460 analytical balance according to the theoretically resolved mole ratios. The mole ratio was determined by calculating the probable stoichiometry for the proposed solid state chemical reaction. After all of the reagents were weighed out, they were combined in a mortar and ground up into a fine powder with a pestle. Once all of the reagents were in powder form, reagent grade acetone was added to the solid mixture to create a slurry, which was stirred for an extended period of time to allow for complete

mixing of the reagents. After mixing, the mortar was placed in the chemical fume hood to permit the evaporation of the acetone. Once the acetone had evaporated from the mortar, a finely mixed powder of starting materials remained. Portions of the reagent powder were placed in the dies of a pellet press, and a number of sample pellets were made for the proposed syntheses. The reagents that were air sensitive were mixed together without acetone in a glove bag under an inert atmosphere of argon or nitrogen.

Several devices were used to hold the starting material pellets and powders while they were undergoing solid-state reaction. Usually, the sample holders used were constructed from relatively pure nickel metal. These nickel vessels come either as a crucible with matching cover or reaction boat with no cover. Although the nickel reaction boats do not have covers available, one can be fabricated by placing one boat on top of another. This technique gives adequate coverage during the progression of the reaction. Unfortunately, the nickel crucibles and combustion boats did occasionally interact with sample material located at the interface during the solid-state reactions. The other type of sample containers used were ceramic reaction boats. These vessels were not acceptable for reactions involving fluorine because the fluorine would attack the ceramic

material and cause various side reactions that ultimately ruined the attempted synthesis.

The reactions were designed to proceed in a thick walled quartz tube which was rated to withstand temperatures up to approximately 1600°C. The reactions were carried out at temperatures well below the limit for the quartz tubes, but the tubes were attacked by the fluorine from the reactions which shortened the number of times that the tubes could be reused. The quartz tube was always used as part of a closed system for reactions involving species other than oxygen. Closed systems are usually essential because in many cases oxides will preferentially form before fluorides, nitrides, and nitride-fluorides.

The atmospheres of the closed systems were also varied. Syntheses were performed under the following atmospheric conditions: dynamic vacuum, static vacuum, dynamic nitrogen, and static nitrogen. After careful consideration of the dynamics of the reactions being attempted; it was determined that nitrogen atmospheres, either static or dynamic, would yield the best chances of synthesizing nitride-fluoride compounds.

X-ray Data Collection

The instrument that was used to collect X-ray data for the powder samples, from the raw starting materials to the

syntheses products, was a Siemens model P4 X-ray diffractometer equipped with a X1000 multi-wire area detector. The function of the area detector is to collect data for the analysis of powder samples of solids. The X-ray diffractometer and area detector are hard-wired to a Pentium™ PC complete with *GADDS* (General Area Detector Diffraction Software) software installed.

It is of course necessary to calibrate the instrument before meaningful data can be obtained. The procedure that is used for instrument calibration employs the mineral corundum, Al_2O_3, as the calibration standard. A two frame powder diffraction pattern of corundum is periodically collected and stored on the hard drive to serve as the calibration frames for the instrument. Here, a frame of data refers to a data collection range of about 40° in 2θ. This is the maximum range of data the area detector can collect at once. Thus, a typical diffraction pattern obtained for calibration has a 2θ range of approximately 5 to 80°, corresponding to two frames of data. To calibrate the instrument, the diffraction peaks that are displayed on the raw area detector image must be precisely aligned to match the preset peak locations for corundum that have been fixed in the software. In order to achieve the best possible instrument calibration, each frame must be aligned several times because the spatial orientations of the peaks

are interdependent. Note that prior to calibration of the area detector against corundum, flood-field and spatial corrections are usually performed. These corrections compensate for imperfections inherent in the multi-wire detection hardware.

Since the instrument remains powered up continually, the first task to accomplish in order to collect data for a sample is to align the sample capillary tube such that it is centered in the beam path. This is necessary to ensure that the sample, which rotates 360° during data collection, is continually exposed to X-rays. The first step in the centering procedure is to switch the goniometer, where the sample is mounted, of the diffractometer from computer to manual control. The manual control box has buttons which move the sample to four preprogrammed positions, which are 90° apart. An optical microscope mounted on the goniometer is used to center the sample in the beam path at each of the four positions.

For most of the samples studied in this thesis, three frames of data were collected by positioning the area detector at 2θ positions of 25°, 55°, and 75°. As these instrumental 2θ positions mark the area detector center for each frame, and since the area detector window spans about 40° in 2θ, the total data range collected is about 5° to 95° in 2θ. Since only a maximum 2θ range of 30° is used per

frame to avoid possible errors in the peripheral regions of the area detector window, the actual 2θ range for most of the diffraction patterns reported in this thesis is 10° to 85° in 2θ.

The data collection time for each frame was 5 minutes, and the data at this point is in the form of a raw data image of the area detector window. The diffraction peaks seen on the image look very much like the areas present on exposed film for a Debye-Scherrer camera. Before the data can be analyzed, each raw frame must be processed using the 'unwarp' and 'spatial' routines available in the *GADDS* software menu. These routines provide the corrections needed to compensate for inherent distortions of the area detector, as mentioned earlier. Following this step, each frame must be integrated to give an intensity versus 2θ plot, or a standard X-ray diffractogram. Finally, the 3 integrated plots are merged into one plot.

X-ray Diffraction Pattern Analysis

Refinement of the merged powder X-ray diffraction pattern is accomplished in the *DOS* based program *Diffrac-At*. The raw data file is selected from a list of powder X-ray diffraction files. The refinement begins by adjusting the two axes such that the entire powder X-ray diffraction pattern is within the ranges for 2θ and the d-spacings.

Next, the background noise is subtracted out, so that the powder X-ray diffraction pattern appears cleaned. Finally, the true peak signals are identified from those that are just noise, and the refined powder X-ray diffraction pattern is saved. A plot of the refined powder X-ray diffraction pattern along with a print out of the "*DIF*" file can be obtained after completion of the refinement routines.

Overall Data Interpretation

The approach taken for interpretation of the results collected is a two step process. The first step is to establish the progress of the solid-state reaction by comparing the powder X-ray diffraction patterns of intermediate and final products to those of the starting materials. The second step consists of identifying the most intense peaks contained in the powder X-ray diffraction pattern. The identification of phases present in the products from powder X-ray diffraction data can be accomplished by accessing the 1995 CD-ROM version of *JCPDS*, which is a database of solid state compounds. A universal search of the database may yield meaningful matches, or various elements can be selected or deselected from the search parameters to further narrow the possibility of achieving a match. Unidentified peaks must be compared to all possible diffraction peaks of known phases present

either by calculating them by hand or by using the *DOS* based program, *D-CALC* written by T. R. Wagner.[13] If after determining that none of the possible *d*-spacings for known phases match, then it is possible that a novel compound has been synthesized.

CHAPTER V

EXPERIMENTAL RESULTS AND DISCUSSION

Introduction

The objective of this chapter is to present the results of the syntheses or attempted syntheses of the target compounds listed in Table 5.1. In addition, synthesis techniques and conditions will be presented for each trial completed for the six target compounds. The results will be interpreted based on the powder X-ray diffraction patterns obtained for the intermediate and final products.

Table 5.1

Target Compounds For Proposed Syntheses

Proposed Reaction	Product	Trials
$BaF_2 + MgF_2 + 9AlN + 2AlF_3 \rightarrow BaMgAl_{11}F_{10}N_9$	$BaMgAl_{11}F_{10}N_9$	4
$2AlN + MgF_2 \rightarrow MgAl_2(FN)_2$	$MgAl_2(FN)_2$	3
$6Al^0 + 2AlF_3 + 3N_2 \rightarrow Al_8(FN)_6$	$Al_2(FN)_{1.5}$	4
$NaF + 6LiF + 6MgF_2 \rightarrow NaLi_6Mg_6F_{19}$	$NaLi_6Mg_6F_{19}$	2
$CaF_2 + 5LiF + 6MgF_2 \rightarrow CaLi_5Mg_6F_{19}$	$CaLi_5Mg_6F_{19}$	2
$3Sr^0 + SrF_2 + N_2 \rightarrow (Sr_2NF)_2$	Sr_2NF	1

The compositions for the four novel nitride-fluoride compounds were designed as analogs to certain metal-oxide

compounds, simply by replacing two O^{-2} ions of the oxides with one NF^{-4} group. Thus, this exploratory research project involved attempts to synthesize novel non-oxide structural analogs of well known oxide systems: $BaMgAl_{11}O_{18.5}$ (barium β-alumina), $MgAl_2O_4$ (spinel), Al_2O_3 (corundum), and SrO (rocksalt type).

The two fluoride compounds were selected to be synthesized after several trials of nitride-fluoride syntheses were unsuccessful. The fluoride compounds were designed as analogs of oxides with the magnetoplumbite structure[14], which have been extensively studied in Dr. T. R. Wagner's laboratory. Of the syntheses attempted, only Sr_2NF was successfully made, and it was the only attempted product which has been previously reported.[9]

The previous study of Sr_2NF did not provide a detailed structural analysis, and this was the main purpose for synthesizing it for this work. The study of Sr_2NF will be discussed at the end of this chapter.

The bulk of the chapter will discuss the reaction conditions used in each of the trial syntheses, and the actual results will be presented and discussed.

Order of Syntheses

The first novel nitride-fluoride synthesis attempted was for $BaMgAl_{11}F_{10}N_9$. The compound $BaMgAl_{11}F_{10}N_9$ was chosen

as an exploratory synthesis to determine whether or not a non-oxide ternary compound could be made. It appeared that perhaps the ternary nitride-fluoride compound was too complicated so the binary non-oxide analog, $MgAl_2(FN)_2$, was attempted. Next, efforts were focused on synthesizing the oxide analog $Al_2(FN)_{1.5}$. In the interim period, the two mixed metal fluoride compounds were attempted. Finally, the Sr_2NF compound was synthesized in order to quantify the structural parameters.

Attempted Synthesis of $BaMgAl_{11}F_{10}N_9$

All of the attempts to synthesize the novel ternary nitride-fluoride compound, $BaMgAl_{11}F_{10}N_9$, were carried out according to the following stoichiometrically balanced equation:

$$BaF_2 + MgF_2 + 9AlN + 2AlF_3 \rightarrow BaMgAl_{11}F_{10}N_9.$$

The details for each of the trial syntheses attempted will be discussed next.

Trial 1

A mixture containing 1.256 grams of BaF_2, 1.212 grams of AlF_3, 0.448 grams of MgF_2, and 2.657 grams of AlN was ground up with a mortar and pestle. The mole ratio was one mole of BaF_2, two moles of AlF_3, one mole of MgF_2, and nine moles of AlN. A sample was prepared and analyzed on the X-

ray diffractometer. The X-ray diffraction pattern for that sample is illustrated in Figure 5.1, and the corresponding statistical data is in Table 5.2.

Note that Table 5.2 contains a column showing the absolute value of the difference between the *d*-values obtained in this study and those from the literature. In general, errors of +/- 0.05° for angles is considered typical for diffractometer work.[15] Thus, in terms of *d*-spacings, an error of +/- 0.005Å can be considered good agreement on average. Examination of Bragg's Law, $n\lambda=2d_{hkl}sin\theta$, indicates at low angles, high *d*-values, one would expect to see larger uncertainty ranges in *d*-spacings.

Calibration studies performed on the equipment used for this work show that differences up to 0.01Å are typical at lower angles, 25° or less, and will be considered good agreement for the purpose of this research. Note that this criterion applies to the data presented in this chapter.

The mixture of starting materials was placed in a stainless steel die and pressed into a sample pellet. The sample pellet was placed in a new nickel reaction boat. The nickel boat was placed in a new quartz tube. The quartz tube was then placed inside of the Thermolyne model 21100 tube furnace, and the tube was connected to a dynamic vacuum atmosphere. The sample mixture was fired for three days at 800°C. The sample was removed from the quartz tube and

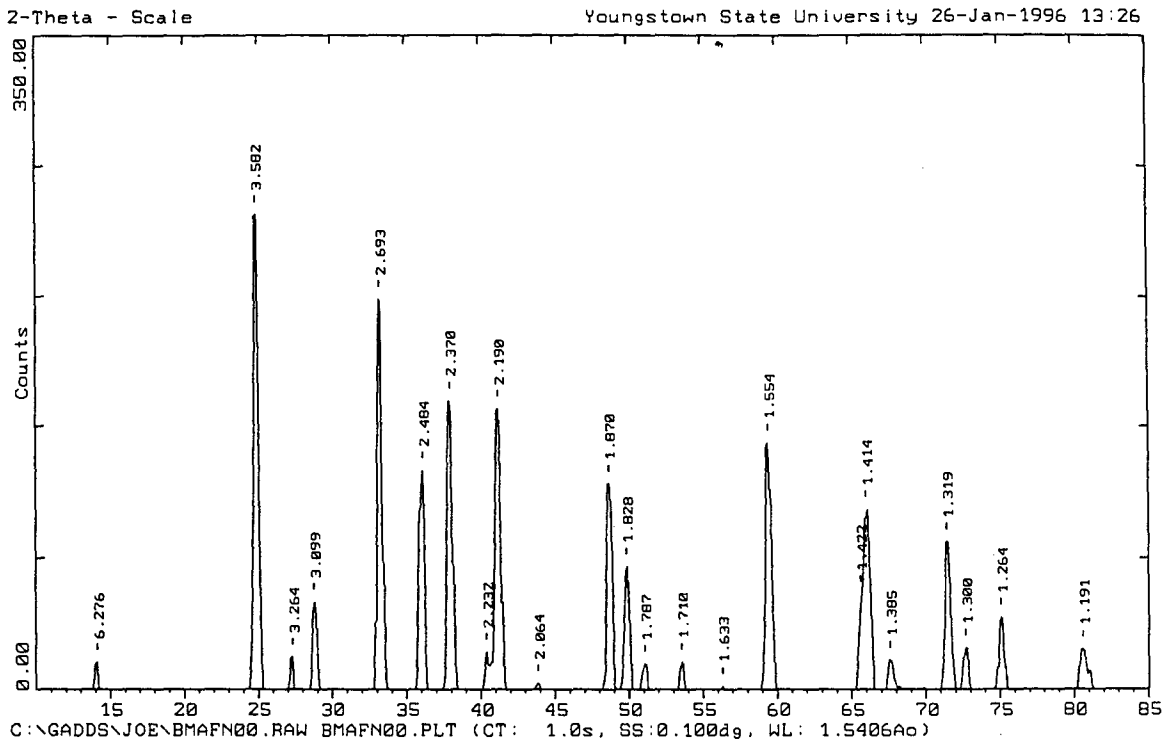

Figure 5.1. X-ray diffraction pattern for $BaMgAl_{11}F_{10}N_9$ synthesis trial 1 starting materials.

Table 5.2

Statistical Data For Figure 5.1

Peak	Counts (%)	2θ (°)	$d_{Exp.}$ (Å)	$d_{Lit.}$ (Å)	$\lvert d_{Exp.}-d_{Lit.} \rvert$ (Å)	Phase	PDF Card
1	5.57	14.100	6.2761	-	-	-	-
2	100.00	24.834	3.5824	3.579	0.0034	BaF_2	4-452
3	6.71	27.300	3.2641	3.267	0.0029	MgF_2	41-1443
4	18.28	28.787	3.0988	3.100	0.0012	BaF_2	4-452
5	82.12	33.239	2.6933	2.695	0.0017	AlN	25-1133
6	45.85	36.132	2.4840	2.490	0.0060	AlN	25-1133
7	60.65	37.941	2.3696	2.371	0.0014	AlN	25-1133
8	7.83	40.372	2.2323	2.2309	0.0014	MgF_2	41-1443
9	58.78	41.186	2.1900	2.193	0.0030	BaF_2	4-452
10	1.13	43.834	2.0637	2.0672	0.0035	MgF_2	41-1443
11	43.15	48.663	1.8696	1.870	0.0004	BaF_2	4-452
12	25.67	49.833	1.8284	1.829	0.0006	AlN	25-1133
13	5.28	51.071	1.7869	1.790	0.0031	BaF_2	4-452
14	5.67	53.560	1.7096	1.7112	0.0016	MgF_2	41-1443
15	0.62	56.300	1.6327	1.6335	0.0008	MgF_2	41-1443
16	51.67	59.438	1.5538	1.550	0.0038	BaF_2	4-452
17	19.85	65.600	1.4220	1.423	0.0010	BaF_2	4-452
18	37.60	66.016	1.4140	1.4133	0.0007	AlN	25-1133
19	6.10	67.574	1.3852	1.386	0.0008	BaF_2	4-452
20	30.81	71.444	1.3193	1.3194	0.0001	AlN	25-1133
21	8.62	72.679	1.2999	1.3007	0.0008	AlN	25-1133
22	15.06	75.082	1.2642	1.266	0.0018	BaF_2	4-452
23	8.28	80.591	1.1911	1.1933	0.0022	BaF_2	4-452

analyzed by X-ray diffraction. The X-ray diffraction pattern is illustrated in Figure 5.2, and the corresponding statistical data is in Table 5.3.

The X-ray diffraction pattern indicated that the majority of the synthesis product was unreacted aluminum nitride and magnesium fluoride. The reaction did form a small amount of barium magnesium aluminum fluoride.

Trial 2

Since the initial product consisted of mainly starting material, the trial 1 product was repressed into a pellet and placed back in the nickel boat. The nickel boat was placed in the quartz tube, which was placed in the tube furnace. The sample was fired for three more days at 1,100°C in a dynamic vacuum atmosphere. The sample was removed from the quartz tube, then analyzed by X-ray diffraction. The X-ray diffraction pattern is shown in Figure 5.3, and the corresponding statistical data is provided in Table 5.4.

The data indicated that the product still consisted of aluminum nitride. The data also showed that there was a small amount of barium magnesium aluminum fluoride present.

Trial 3

Once again, the sample was repressed into a pellet and

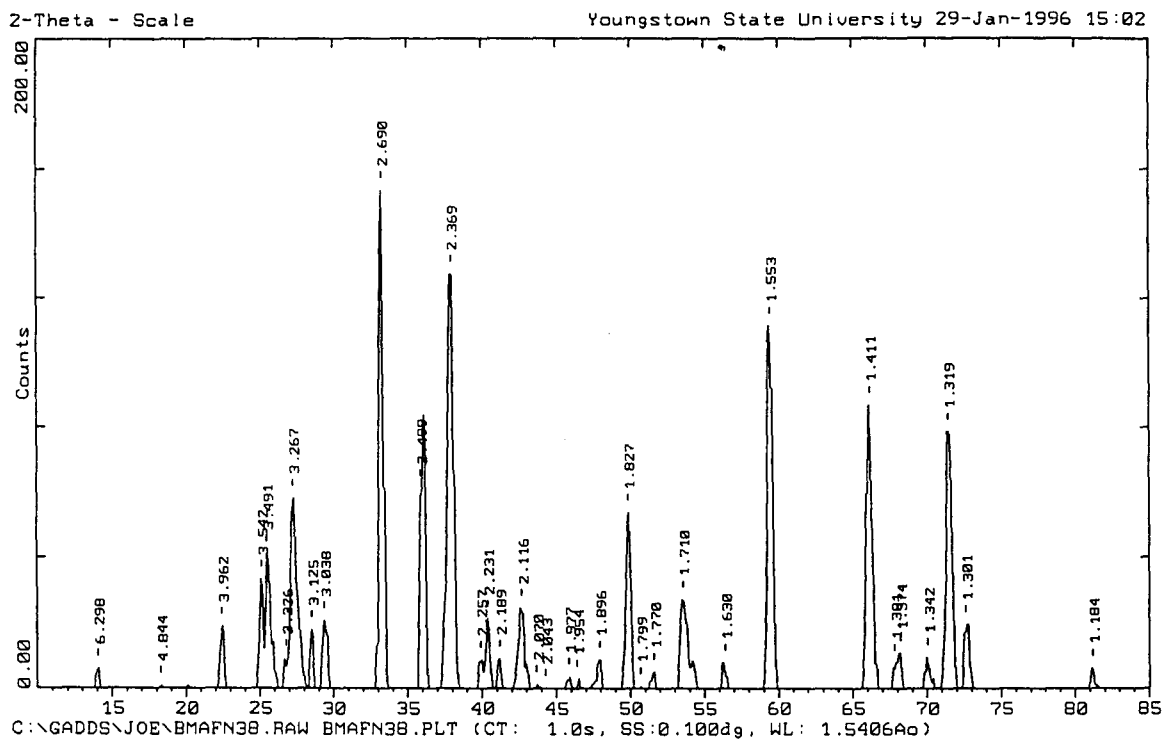

Figure 5.2. X-ray diffraction pattern for $BaMgAl_{11}F_{10}N_9$ synthesis trial 1 product.

Table 5.3

Statistical Data For Figure 5.2

Peak	Counts (%)	2θ (°)	$d_{Exp.}$ (Å)	$d_{Lit.}$ (Å)	$\lvert d_{Exp.}-d_{Lit.} \rvert$ (Å)	Phase	PDF Card
1	3.85	14.050	6.2981	-	-	-	-
2	0.38	18.300	4.8441	-	-	-	-
3	12.19	22.422	3.9619	-	-	-	-
4	21.59	25.124	3.5417	3.550	0.0083	Ba_2MgAlF_9	44-1047
5	26.72	25.491	3.4915	-	-	-	-
6	5.85	26.779	3.3264	3.346	0.0196	Ba_2MgAlF_9	44-1047
7	37.98	27.274	3.2671	3.267	0.0001	MgF_2	41-1443
8	11.49	28.540	3.1250	3.1890	0.0640	Ba_2MgAlF_9	44-1047
9	13.32	29.380	3.0376	3.037	0.0006	Ba_2MgAlF_9	44-1047
10	100.00	33.275	2.6904	2.695	0.0046	AlN	25-1133
11	39.88	35.900	2.4995	2.490	0.0095	AlN	25-1133
12	83.07	37.956	2.3686	2.371	0.0024	AlN	25-1133
13	5.62	39.903	2.2575	-	-	-	-
14	13.79	40.388	2.2314	2.2309	0.0005	MgF_2	41-1443
15	5.73	41.200	2.1893	2.1918	0.0025	Ba_2MgAlF_9	44-1047
16	16.00	42.693	2.1162	2.120	0.0041	Ba_2MgAlF_9	44-1047
17	0.75	43.696	2.0699	2.0672	0.0027	MgF_2	41-1443
18	0.01	44.300	2.0431	2.0448	0.0017	Ba_2MgAlF_9	44-1047
19	2.28	45.854	1.9774	-	-	-	-
20	1.85	46.431	1.9541	-	-	-	-
21	5.57	47.929	1.8965	1.8853	0.0112	Ba_2MgAlF_9	44-1047
22	34.88	49.862	1.8274	1.829	0.0016	AlN	25-1133
23	0.36	50.700	1.7991	1.8035	0.0044	Ba_2MgAlF_9	44-1047
24	3.21	51.605	1.7697	1.7756	0.0059	Ba_2MgAlF_9	44-1047
25	17.57	53.558	1.7097	1.7112	0.0015	MgF_2	41-1443
26	4.92	56.400	1.6301	1.6335	0.0034	MgF_2	41-1443
27	72.58	59.462	1.5532	1.5559	0.0027	AlN	25-1133
28	56.54	66.175	1.4110	1.4133	0.0023	AlN	25-1133
29	4.96	67.824	1.3807	1.3821	0.0014	MgF_2	41-1443
30	6.90	68.193	1.3741	1.3745	0.0004	MgF_2	41-1443
31	6.13	70.06	1.3420	1.3475	0.0055	AlN	25-1133
32	51.21	71.47	1.3190	1.3194	0.0004	AlN	25-1133
33	12.62	72.61	1.3011	1.3007	0.0004	AlN	25-1133
34	3.95	81.20	1.1837	1.1850	0.0013	AlN	25-1133

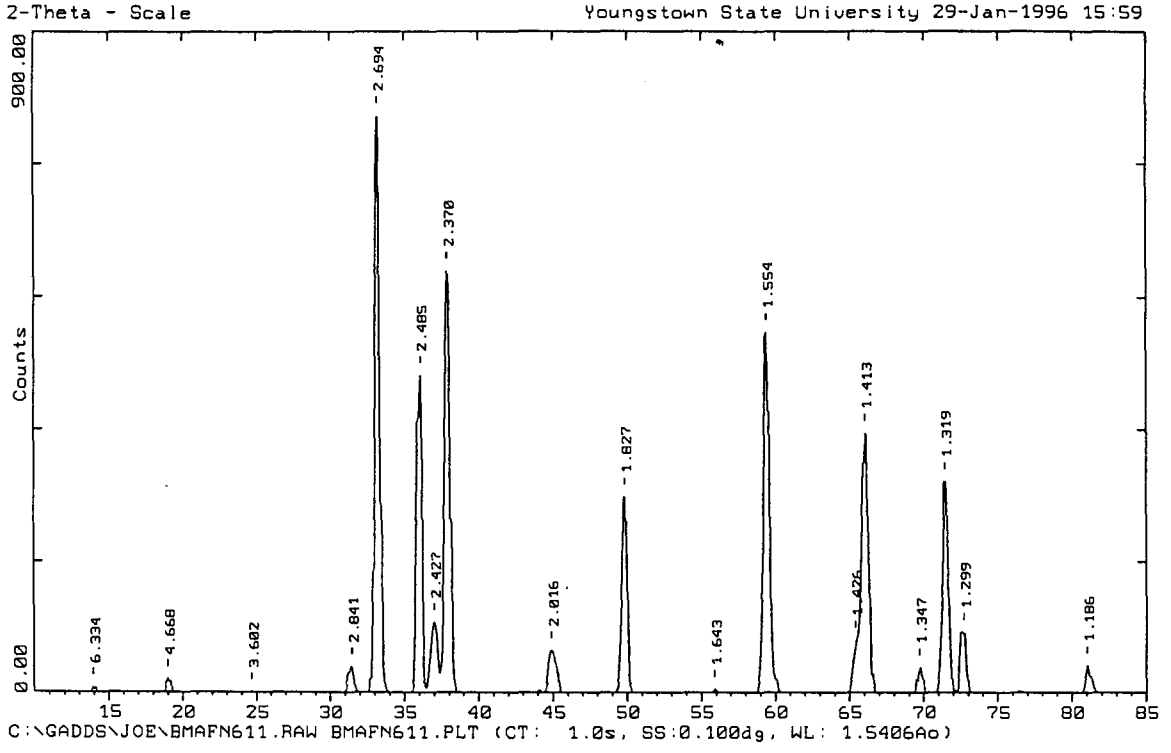

Figure 5.3. X-ray diffraction pattern for $BaMgAl_{11}F_{10}N_9$ synthesis trial 2 product.

Table 5.4

Statistical Data For Figure 5.3

Peak	Counts (%)	2θ (°)	$d_{Exp.}$ (Å)	$d_{Lit.}$ (Å)	$\lvert d_{Exp.}-d_{Lit.} \rvert$ (Å)	Phase	PDF Card
1	0.86	13.971	6.3337	-	-	-	-
2	2.33	18.995	4.6684	-	-	-	-
3	0.04	24.700	3.6015	3.626	0.0245	Ba_2MgAlF_9	44-1047
4	4.56	31.467	2.8408	2.846	0.0052	Ba_2MgAlF_9	44-1047
5	100.00	33.231	2.6939	2.695	0.0011	AlN	25-1133
6	54.68	36.114	2.4851	2.490	0.0049	AlN	25-1133
7	12.27	37.017	2.4266	2.419	0.0076	Ba_2MgAlF_9	44-1047
8	72.54	37.938	2.3697	2.371	0.0013	AlN	25-1133
9	7.36	44.924	2.0161	-	-	-	-
10	33.93	49.870	1.8271	1.829	0.0019	AlN	25-1133
11	0.55	55.933	1.6426	1.6402	0.0024	Ba_2MgAlF_9	44-1047
12	62.09	59.428	1.5541	1.5559	0.0018	AlN	25-1133
13	9.14	65.400	1.4258	-	-	-	-
14	44.82	66.066	1.4131	1.4133	0.0002	AlN	25-1133
15	4.41	69.738	1.3474	1.3475	0.0001	AlN	25-1133
16	36.58	71.435	1.3195	1.3194	0.0001	AlN	25-1133
17	10.52	72.719	1.2993	1.3007	0.0014	AlN	25-1133
18	4.74	81.031	1.1857	1.1850	0.0007	AlN	25-1133

placed back in the nickel boat. The nickel boat was placed in the quartz tube, which was placed in the tube furnace. The sample was fired for three more days at 1,100°C in a dynamic vacuum atmosphere. The sample was removed from the quartz tube, then analyzed by X-ray diffraction. The X-ray diffraction pattern is shown in Figure 5.4, and the corresponding statistical data is provided in Table 5.5.

Similar to the first two trials, the third attempt to synthesize this compound was unsuccessful as well. The data indicated that the product for this trial consisted mainly of aluminum nitride along with a trace of barium nitride fluoride. The aluminum nitride compound appears to be too stable in that environment, thus inhibiting the formation of the novel nitride-fluoride compound.

The next attempt to synthesize $BaMgAl_{11}F_{10}N_9$ will begin with unused starting materials since the previous sample was fired for a total of nine days with no positive results.

Trial 4

Another synthesis was attempted for the novel ternary nitride-fluoride compound $BaMgAl_{11}F_{10}N_9$. A new sample of the initial starting materials was placed in a die and pressed into a sample pellet. The sample pellet was placed in a new nickel reaction boat, which was then placed in a new quartz tube. The quartz tube was placed inside of the Thermolyne

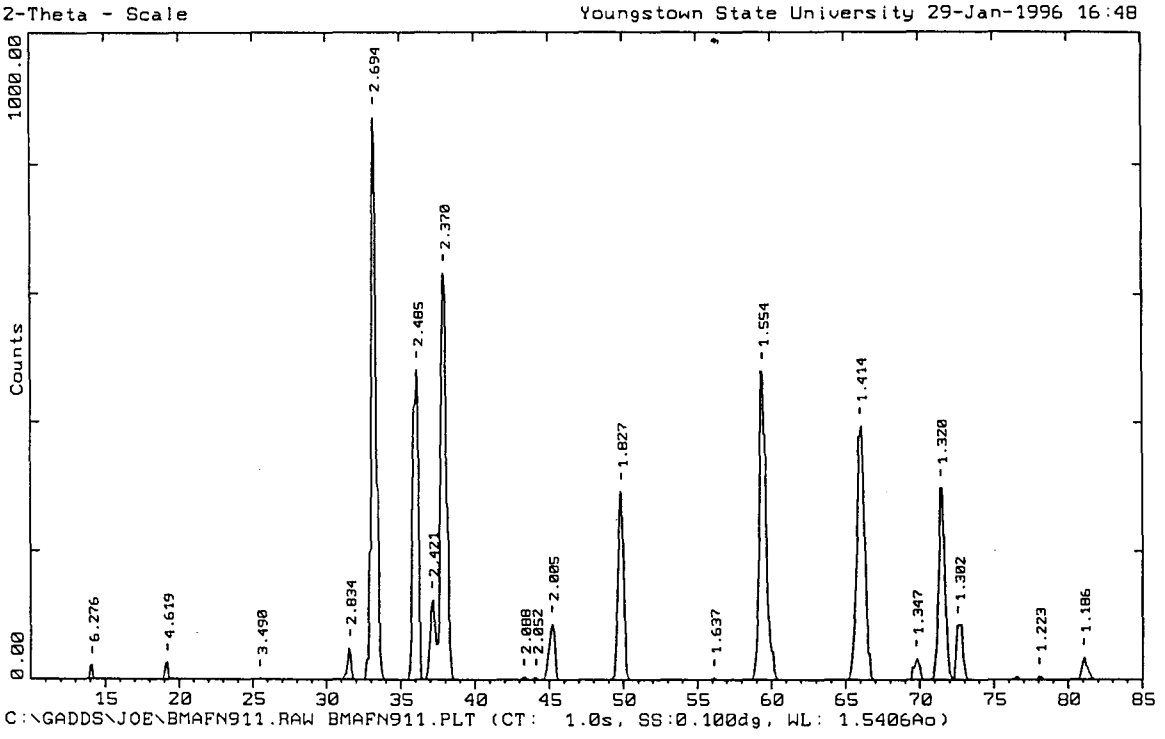

Figure 5.4. X-ray diffraction pattern for $BaMgAl_{11}F_{10}N_9$ synthesis trial 3 product.

Table 5.5

Statistical Data For Figure 5.4

Peak	Counts (%)	2θ (°)	$d_{Exp.}$ (Å)	$d_{Lit.}$ (Å)	$\lvert d_{Exp.}-d_{Lit.} \rvert$ (Å)	Phase	PDF Card
1	2.27	14.100	6.2761	-	-	-	-
2	2.94	19.200	4.6190	-	-	-	-
3	0.06	25.500	3.4903	-	-	-	-
4	5.44	31.541	2.8342	2.849	0.0148	Ba_2NF	24-114
5	100.00	33.228	2.6941	2.695	0.0009	AlN	25-1133
6	54.50	36.111	2.4854	2.490	0.0046	AlN	25-1133
7	13.94	37.105	2.4210	-	-	-	-
8	71.59	37.937	2.3698	2.371	0.0012	AlN	25-1133
9	0.36	43.295	2.0881	-	-	-	-
10	0.36	44.100	2.0519	-	-	-	-
11	9.73	45.184	2.0051	2.015	0.0099	Ba_2NF	24-114
12	33.17	49.864	1.8273	1.829	0.0017	AlN	25-1133
13	0.39	56.123	1.6375	1.635	0.0025	Ba_2NF	24-114
14	54.37	59.420	1.5542	1.5559	0.0017	AlN	25-1133
15	44.67	66.005	1.4142	1.4133	0.0009	AlN	25-1133
16	3.62	69.746	1.3472	1.3475	0.0003	AlN	25-1133
17	33.74	71.423	1.3197	1.3194	0.0003	AlN	25-1133
18	9.61	72.573	1.3016	1.3020	0.0004	Ba_2NF	24-114
19	0.60	78.044	1.2234	-	-	-	-
20	3.89	81.032	1.1857	1.1850	0.0007	AlN	25-1133

model 21100 tube furnace, and the tube was connected to a vacuum pump. The tube was evacuated with the vacuum pump and closed off. The sample was fired for one day at 1,200°C in a static vacuum atmosphere. The sample was removed from the quartz tube, and analyzed by X-ray diffraction. The X-ray diffraction pattern for the sample is illustrated in Figure 5.5, and the corresponding statistical data is listed in Table 5.6.

The X-ray diffraction data collected for this sample indicated that the fourth synthesis attempted for the novel ternary nitride-fluoride compound $BaMgAl_{11}F_{10}N_9$ had failed just as the previous three attempts. The two products that were formed during the solid-state reaction were aluminum oxide and barium aluminum silicate. It is evident that oxygen and silicon infiltrated the system and contaminated the reaction environment leading to the formation of these products.

Future research focusing on syntheses that attempt to make the novel ternary nitride-fluoride compound $BaMgAl_{11}F_{10}N_9$, must assure an oxygen free atmosphere for the reaction to proceed in. Also, it may be necessary to use intermediate compounds for this type of reaction.

Attempted Synthesis of $MgAl_2(FN)_2$

All of the attempts to synthesize the proposed novel

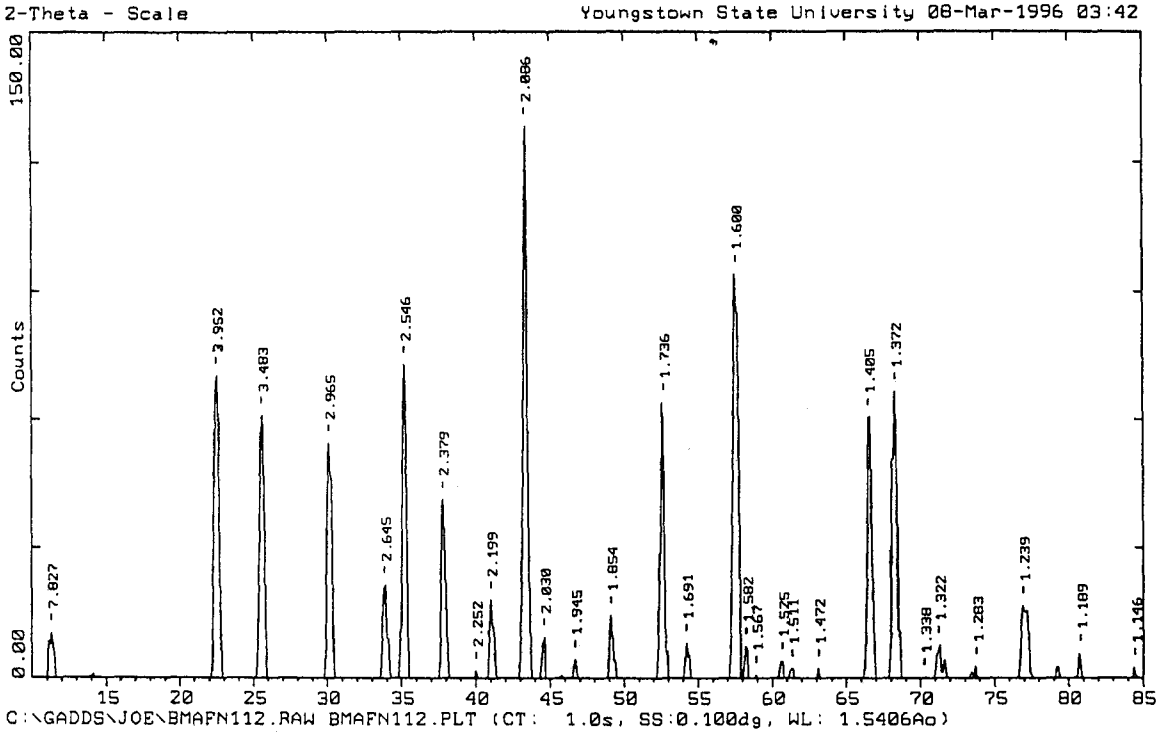

Figure 5.5. X-ray diffraction pattern for $BaMgAl_{11}F_{10}N_9$ synthesis trial 4 product.

Table 5.6

Statistical Data For Figure 5.5

Peak	Counts (%)	2θ (°)	$d_{Exp.}$ (Å)	$d_{Lit.}$ (Å)	$\lvert d_{Exp.}-d_{Lit.} \rvert$ (Å)	Phase	PDF Card
1	7.90	11.296	7.8269	7.79	0.0369	$BaAl_2Si_2O_8$	12-725
2	54.65	22.479	3.9520	3.949	0.0030	$BaAl_2Si_2O_8$	12-725
3	47.44	25.553	3.4832	3.48	0.0032	Al_2O_3	42-1468
4	42.44	30.112	2.9654	2.968	0.0026	$BaAl_2Si_2O_8$	12-725
5	16.59	33.861	2.6451	2.647	0.0019	$BaAl_2Si_2O_8$	12-725
6	56.71	35.216	2.5465	2.551	0.0045	Al_2O_3	42-1468
7	32.14	37.785	2.3790	2.379	0.0000	Al_2O_3	42-1468
8	1.29	40.000	2.2522	2.259	0.0068	$BaAl_2Si_2O_8$	12-725
9	13.86	41.005	2.1993	2.195	0.0043	$BaAl_2Si_2O_8$	12-725
10	100.00	43.335	2.0863	2.085	0.0013	Al_2O_3	42-1468
11	7.22	44.600	2.0300	-	-	-	-
12	3.28	46.668	1.9448	1.947	0.0022	$BaAl_2Si_2O_8$	12-725
13	11.11	49.107	1.8537	1.853	0.0007	$BaAl_2Si_2O_8$	12-725
14	49.90	52.676	1.7362	1.7398	0.0036	Al_2O_3	42-1468
15	6.14	54.200	1.6909	-	-	-	-
16	73.27	57.574	1.5996	1.6014	0.0018	Al_2O_3	42-1468
17	5.63	58.257	1.5825	-	-	-	-
18	0.55	58.900	1.5667	-	-	-	-
19	2.91	60.669	1.5252	1.5147	0.0105	Al_2O_3	42-1468
20	1.63	61.321	1.5105	1.5109	0.0004	Al_2O_3	42-1468
21	1.72	63.120	1.4717	-	-	-	-
22	47.21	66.517	1.4046	1.4045	0.0001	Al_2O_3	42-1468
23	51.87	68.315	1.3719	1.3738	0.0019	Al_2O_3	42-1468
24	0.11	70.277	1.3384	1.3360	0.0024	Al_2O_3	42-1468
25	5.76	71.248	1.3225	-	-	-	-
26	2.04	73.771	1.2834	1.2755	0.0079	Al_2O_3	42-1468
27	12.82	76.914	1.2386	1.2390	0.0004	Al_2O_3	42-1468
28	4.30	80.790	1.1886	1.1898	0.0012	Al_2O_3	42-1468
29	1.83	84.453	1.1462	1.1471	0.0009	Al_2O_3	42-1468

binary nitride-fluoride compound $MgAl_2(FN)_2$ were performed according to the following stoichiometrically balanced equation:

$$2AlN + MgF_2 \rightarrow MgAl_2(FN)_2.$$

The synthesis conditions of each trial will be discussed next.

Trial 1

A sample mixture was prepared by adding 2.848 grams of MgF_2 along with 3.747 grams of AlN. The mole ratio of the mixture was one mole of magnesium fluoride to two moles of aluminum nitride. The starting materials were ground into a powder with a mortar and pestle, and a sample was prepared for analysis on the X-ray diffractometer. The X-ray diffraction pattern for that sample is illustrated in Figure 5.6, and the corresponding statistical data is listed in Table 5.7.

The mixture of starting reagents was placed in a die and pressed into a sample pellet. The sample pellet was then placed in a new nickel reaction vessel. The nickel boat was loaded into a new quartz tube, and the tube was placed in the Thermolyne model 21100 tube furnace. The quartz tube was connected to a vacuum pump, to allow the reaction to proceed under dynamic vacuum. The sample was then fired for three days at 900°C. The sample product was

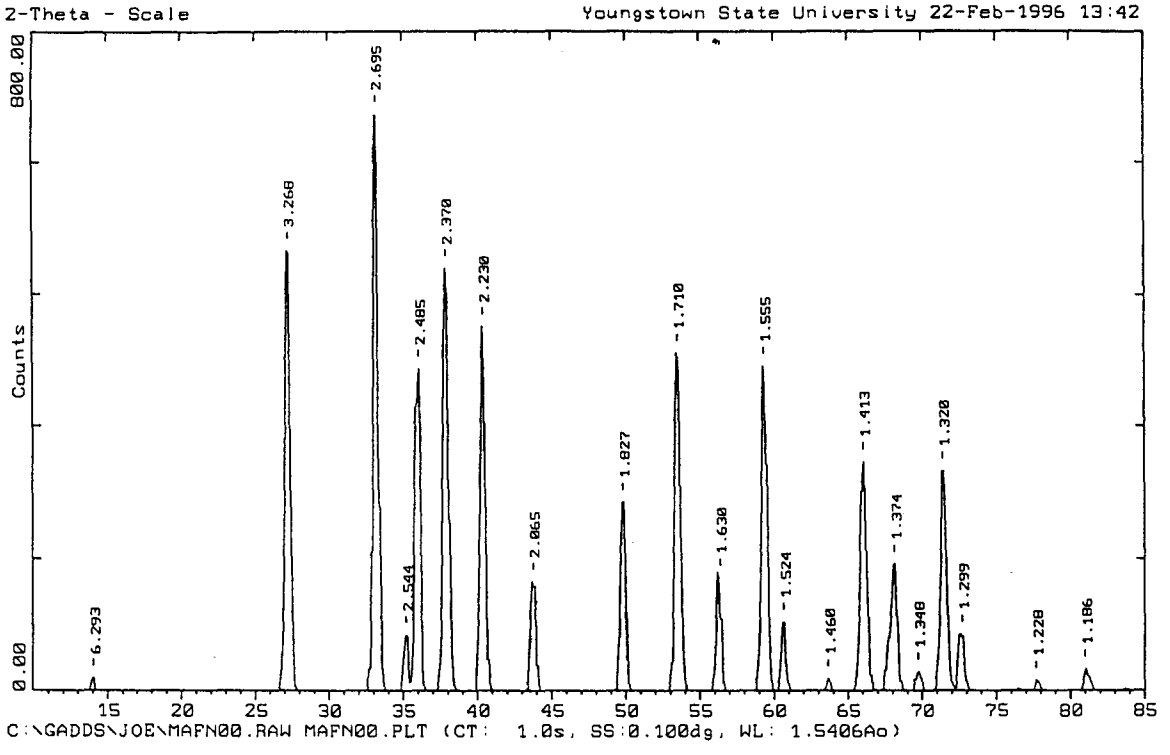

Figure 5.6. X-ray diffraction pattern for $MgAl_2(FN)_2$ synthesis trial 1 starting materials.

Table 5.7

Statistical Data For Figure 5.6

Peak	Counts (%)	2θ (°)	$d_{Exp.}$ (Å)	$d_{Lit.}$ (Å)	$\lvert d_{Exp.}-d_{Lit.} \rvert$ (Å)	Phase	PDF Card
1	2.09	14.061	6.2934	-	-	-	-
2	74.20	27.265	3.2682	3.267	0.0012	MgF_2	41-1443
3	100.00	33.219	2.6948	2.695	0.0002	AlN	25-1133
4	9.41	35.244	2.5445	2.5474	0.0029	MgF_2	41-1443
5	54.16	36.110	2.4854	2.490	0.0046	AlN	25-1133
6	71.19	37.928	2.3703	2.371	0.0007	AlN	25-1133
7	61.43	40.412	2.2302	2.2309	0.0007	MgF_2	41-1443
8	18.38	43.803	2.0651	2.0672	0.0021	MgF_2	41-1443
9	31.79	49.868	1.8272	1.829	0.0018	AlN	25-1133
10	56.85	53.542	1.7102	1.7112	0.0010	MgF_2	41-1443
11	19.03	56.400	1.6301	1.6335	0.0034	MgF_2	41-1443
12	54.64	59.398	1.5548	1.5559	0.0011	AlN	25-1133
13	11.59	60.703	1.5244	1.5259	0.0015	MgF_2	41-1443
14	2.05	63.682	1.4601	1.4607	0.0006	MgF_2	41-1443
15	38.62	66.070	1.4130	1.4133	0.0003	AlN	25-1133
16	21.24	68.182	1.3743	1.3745	0.0002	MgF_2	41-1443
17	3.24	69.730	1.3475	1.3475	0.0000	AlN	25-1133
18	36.98	71.431	1.3196	1.3176	0.0020	MgF_2	41-1443
19	9.59	72.713	1.2994	1.3007	0.0013	AlN	25-1133
20	1.76	77.719	1.2277	1.2272	0.0005	MgF_2	41-1443
21	3.69	81.016	1.1859	1.1850	0.0009	AlN	25-1133

removed from the quartz tube, ground into a powder with a mortar and pestle, and analyzed on the X-ray diffractometer. The X-ray diffraction pattern for that sample is illustrated in Figure 5.7, and the corresponding statistical data is listed in Table 5.8.

The X-ray diffraction pattern for this reaction product indicated that the attempted synthesis of $MgAl_2(FN)_2$ was unsuccessful. The only phases present in the product were aluminum nitride and magnesium fluoride. The reaction may not have proceeded because either the reaction temperature was not high enough to compel the elements to rearrange into the new compound or the sample was not permitted to react long enough.

Trial 2

A second attempt to synthesize the novel binary nitride-fluoride compound $MgAl_2(FN)_2$ was performed. Another portion of unreacted starting material was placed in the die and pressed into a sample pellet. The sample pellet was placed in a nickel reaction boat, which was placed in a new quartz tube. The quartz tube was connected to the vacuum pump, and the air was evacuated from it. The quartz tube was placed in the Thermolyne model 21100 tube furnace, and the sample was fired for one day at 1,100°C in static vacuum. The sample was removed from the tube and analyzed

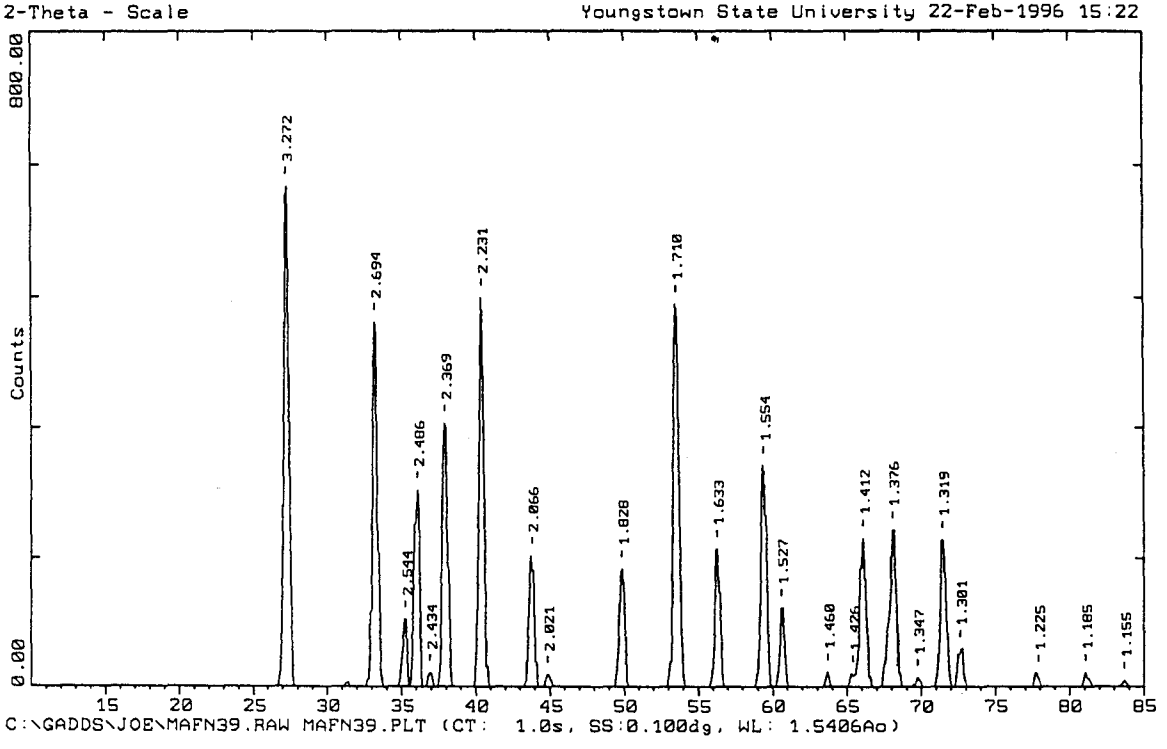

Figure 5.7. X-ray diffraction pattern for $MgAl_2(FN)_2$ synthesis trial 1 product.

Table 5.8

Statistical Data For Figure 5.7

Peak	Counts (%)	2θ (°)	$d_{Exp.}$ (Å)	$d_{Lit.}$ (Å)	$\lvert d_{Exp.}-d_{Lit.} \rvert$ (Å)	Phase	PDF Card
1	100.00	27.229	3.2724	3.267	0.0054	MgF_2	41-1443
2	73.34	33.235	2.6936	2.695	0.0014	AlN	25-1133
3	13.66	35.257	2.5436	2.5474	0.0038	MgF_2	41-1443
4	39.73	36.101	2.4860	2.490	0.0040	AlN	25-1133
5	2.90	36.905	2.4337	-	-	-	-
6	53.04	37.949	2.3691	2.371	0.0019	AlN	25-1133
7	78.14	40.406	2.2305	2.2309	0.0004	MgF_2	41-1443
8	26.59	43.786	2.0658	2.0672	0.0014	MgF_2	41-1443
9	2.52	44.819	2.0206	-	-	-	-
10	23.86	49.844	1.8280	1.829	0.0010	AlN	25-1133
11	76.86	53.546	1.7100	1.7112	0.0012	MgF_2	41-1443
12	27.85	56.275	1.6334	1.6335	0.0001	MgF_2	41-1443
13	44.85	59.434	1.5539	1.5559	0.0020	AlN	25-1133
14	16.01	60.598	1.5268	1.5259	0.0009	MgF_2	41-1443
15	2.93	63.707	1.4596	1.4607	0.0011	MgF_2	41-1443
16	2.66	65.400	1.4258	-	-	-	-
17	30.10	66.127	1.4119	1.4133	0.0014	AlN	25-1133
18	31.65	68.109	1.3756	1.3745	0.0011	MgF_2	41-1443
19	1.87	69.763	1.3470	1.3475	0.0005	AlN	25-1133
20	29.65	71.454	1.3192	1.3176	0.0016	MgF_2	41-1443
21	7.73	72.629	1.3007	1.3007	0.0000	AlN	25-1133
22	2.69	77.900	1.2253	1.2272	0.0019	MgF_2	41-1443
23	2.87	81.085	1.1851	1.1850	0.0001	AlN	25-1133
24	1.20	83.700	1.1546	1.1549	0.0003	MgF_2	41-1443

on the X-ray diffractometer. The X-ray diffraction pattern for the sample is illustrated in Figure 5.8, and the corresponding statistical data is listed in Table 5.9.

The X-ray diffraction data indicated that the second trial synthesis attempt for the proposed novel binary nitride-fluoride compound, $MgAl_2(FN)_2$, failed like the previous synthesis. The data showed that the phases present in the product matrix were again the starting materials, aluminum nitride and magnesium fluoride. As noted for the previous synthesis attempt for this compound, the failure may be due to the reaction temperature being too low or the reaction time being too short.

Trial 3

A third attempt to synthesize the novel binary nitride-fluoride compound $MgAl_2(FN)_2$ was performed. Another portion of unreacted starting material was pressed into a sample pellet. The sample pellet was loaded into a nickel boat which was placed in a quartz tube. The tube was placed in the Thermolyne model 21100 tube furnace, but it remained open to atmosphere. The sample was fired for three days at 1,200°C. Two products were discovered in the tube. The first product was in the nickel boat, and the second was scraped from the inner surface of the quartz tube.

Product 1. The product retrieved from the nickel boat

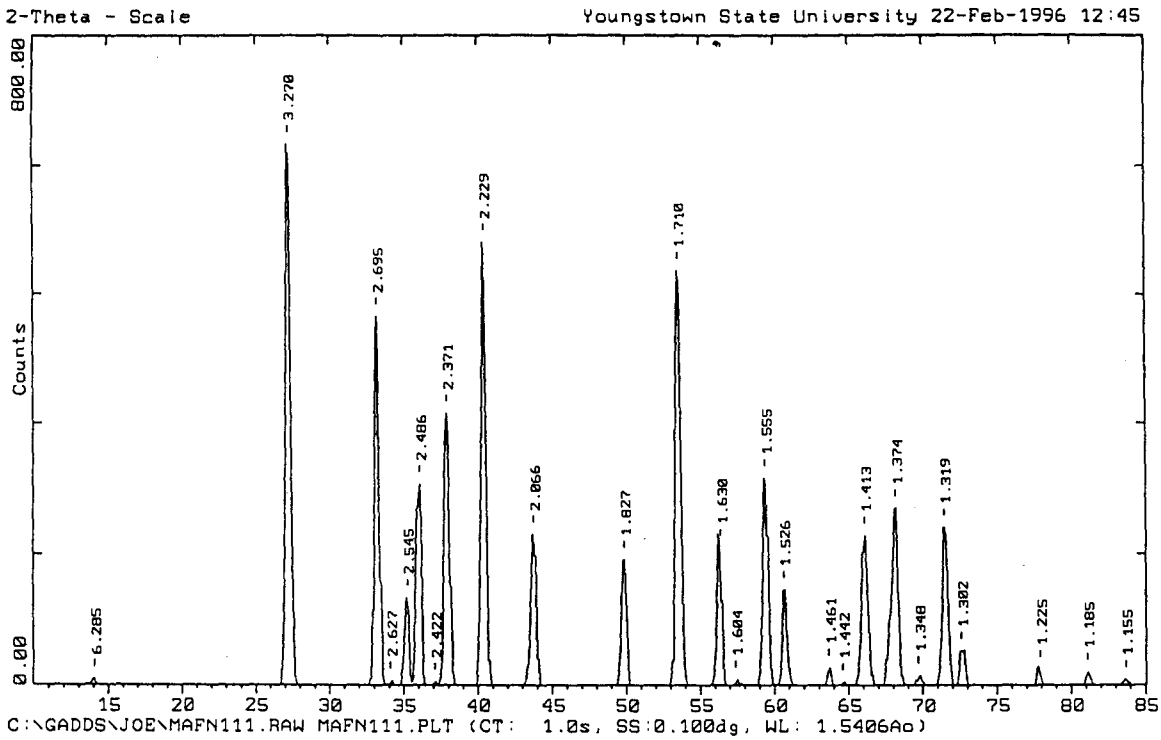

Figure 5.8. X-ray diffraction pattern for $MgAl_2(FN)_2$ synthesis trial 2 product.

Table 5.9

Statistical Data For Figure 5.8

Peak	Counts (%)	2θ (°)	$d_{Exp.}$ (Å)	$d_{Lit.}$ (Å)	$\lvert d_{Exp.}-d_{Lit.} \rvert$ (Å)	Phase	PDF Card
1	1.08	14.079	6.2855	-	-	-	-
2	100.00	27.254	3.2696	3.267	0.0026	MgF_2	41-1443
3	67.87	33.222	2.6945	2.695	0.0005	AlN	25-1133
4	0.76	34.103	2.6269	-	-	-	-
5	15.97	35.232	2.5453	2.5474	0.0021	MgF_2	41-1443
6	36.78	36.105	2.4857	2.490	0.0043	AlN	25-1133
7	0.57	37.082	2.4225	-	-	-	-
8	49.82	37.924	2.3706	2.371	0.0004	AlN	25-1133
9	81.71	40.430	2.2292	2.2309	0.0017	MgF_2	41-1443
10	27.61	43.780	2.0661	2.0672	0.0011	MgF_2	41-1443
11	22.92	49.876	1.8269	1.829	0.0021	AlN	25-1133
12	76.35	53.539	1.7102	1.7112	0.0010	MgF_2	41-1443
13	25.13	56.400	1.6301	1.6335	0.0034	MgF_2	41-1443
14	1.05	57.389	1.6043	-	-	-	-
15	37.99	59.407	1.5545	1.5559	0.0014	AlN	25-1133
16	17.34	60.622	1.5263	1.5259	0.0004	MgF_2	41-1443
17	3.19	63.658	1.4606	1.4607	0.0001	MgF_2	41-1443
18	0.47	64.579	1.4420	1.4403	0.0017	MgF_2	41-1443
19	27.39	66.070	1.4130	1.4133	0.0003	AlN	25-1133
20	32.43	68.184	1.3742	1.3745	0.0003	MgF_2	41-1443
21	1.76	69.695	1.3481	1.3475	0.0006	AlN	25-1133
22	28.78	71.444	1.3193	1.3176	0.0017	MgF_2	41-1443
23	6.25	72.572	1.3016	1.3007	0.0009	AlN	25-1133
24	2.77	77.900	1.2253	1.2272	0.0019	MgF_2	41-1443
25	2.33	81.081	1.1851	1.1850	0.0001	AlN	25-1133
26	0.97	83.666	1.1549	1.1549	0.0000	MgF_2	41-1443

was ground into a powder. The sample was then analyzed on the X-ray diffractometer. The X-ray diffraction pattern for the sample is shown in Figure 5.9, and the statistical data is listed in Table 5.10.

The X-ray diffraction pattern for product 1 of trial 3 showed that the most intense peaks matched indexed peaks for magnesium aluminum oxide.

Product 2. This off-white material, which was scraped from the inner surface of the quartz tube, was prepared and analyzed on the X-ray diffractometer. The X-ray diffraction pattern for that sample is illustrated in Figure 5.10, and the corresponding statistical data is listed in Table 5.11.

The X-ray diffraction data for product 2 of the trial 3 synthesis indicated that the product consisted of nickel aluminum oxide and nickel silicate.

Future attempts to synthesize the unknown nitride-fluoride compound $MgAl_2(FN)_2$, should be performed in oxygen free systems. The reactions may have a better probability of success at higher temperatures and longer reaction times.

Attempted Synthesis of $Al_2(FN)_{1.5}$

All four of the attempts to synthesize the compound $Al_2(FN)_{1.5}$ were carried out according to the following stoichiometrically balanced equation:

$$6Al^0 + 2AlF_3 + 3N_2 \rightarrow Al_8(FN)_6.$$

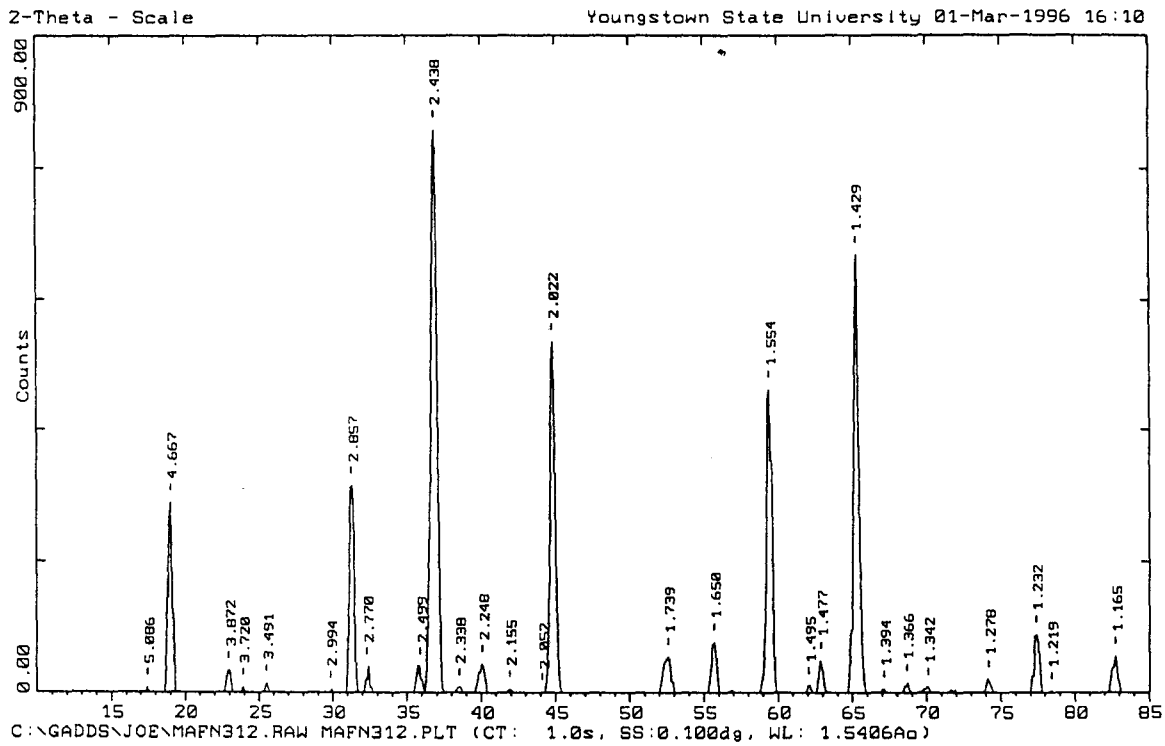

Figure 5.9. X-ray diffraction pattern for $MgAl_2(FN)_2$ synthesis trial 3 product from nickel boat.

Table 5.10

Statistical Data For Figure 5.9

Peak	Counts (%)	2θ (°)	$d_{Exp.}$ (Å)	$d_{Lit.}$ (Å)	$\lvert d_{Exp.}-d_{Lit.} \rvert$ (Å)	Phase	PDF Card
1	0.91	17.422	5.0860	-	-	-	-
2	33.55	19.000	4.6671	4.66	0.0071	$MgAl_2O_4$	21-1152
3	3.93	22.952	3.8716	-	-	-	-
4	0.99	23.900	3.7202	-	-	-	-
5	1.57	25.497	3.4908	-	-	-	-
6	0.43	29.819	2.9938	-	-	-	-
7	36.65	31.287	2.8567	2.858	0.0013	$MgAl_2O_4$	21-1152
8	4.64	32.295	2.7698	-	-	-	-
9	4.65	35.900	2.4995	-	-	-	-
10	100.00	36.840	2.4378	2.437	0.0008	$MgAl_2O_4$	21-1152
11	0.95	38.482	2.3375	2.335	0.0025	$MgAl_2O_4$	21-1152
12	5.16	40.079	2.2480	-	-	-	-
13	0.63	41.890	2.1549	-	-	-	-
14	0.09	44.091	2.0523	-	-	-	-
15	62.30	44.788	2.0219	2.020	0.0019	$MgAl_2O_4$	21-1152
16	6.42	52.580	1.7391	-	-	-	-
17	8.99	55.675	1.6496	1.650	0.0004	$MgAl_2O_4$	21-1152
18	53.80	59.436	1.5539	1.5554	0.0015	$MgAl_2O_4$	21-1152
19	1.23	62.035	1.4949	-	-	-	-
20	5.72	62.878	1.4768	-	-	-	-
21	77.93	65.234	1.4291	1.4289	0.0002	$MgAl_2O_4$	21-1152
22	0.58	67.100	1.3938	-	-	-	-
23	1.74	68.641	1.3662	1.3662	0.0000	$MgAl_2O_4$	21-1152
24	1.04	70.071	1.3418	-	-	-	-
25	2.46	74.166	1.2775	1.2780	0.0005	$MgAl_2O_4$	21-1152
26	10.33	77.368	1.2324	1.2330	0.0006	$MgAl_2O_4$	21-1152
27	0.29	78.400	1.2188	1.2187	0.0001	$MgAl_2O_4$	21-1152
28	6.50	82.745	1.1654	1.1666	0.0012	$MgAl_2O_4$	21-1152

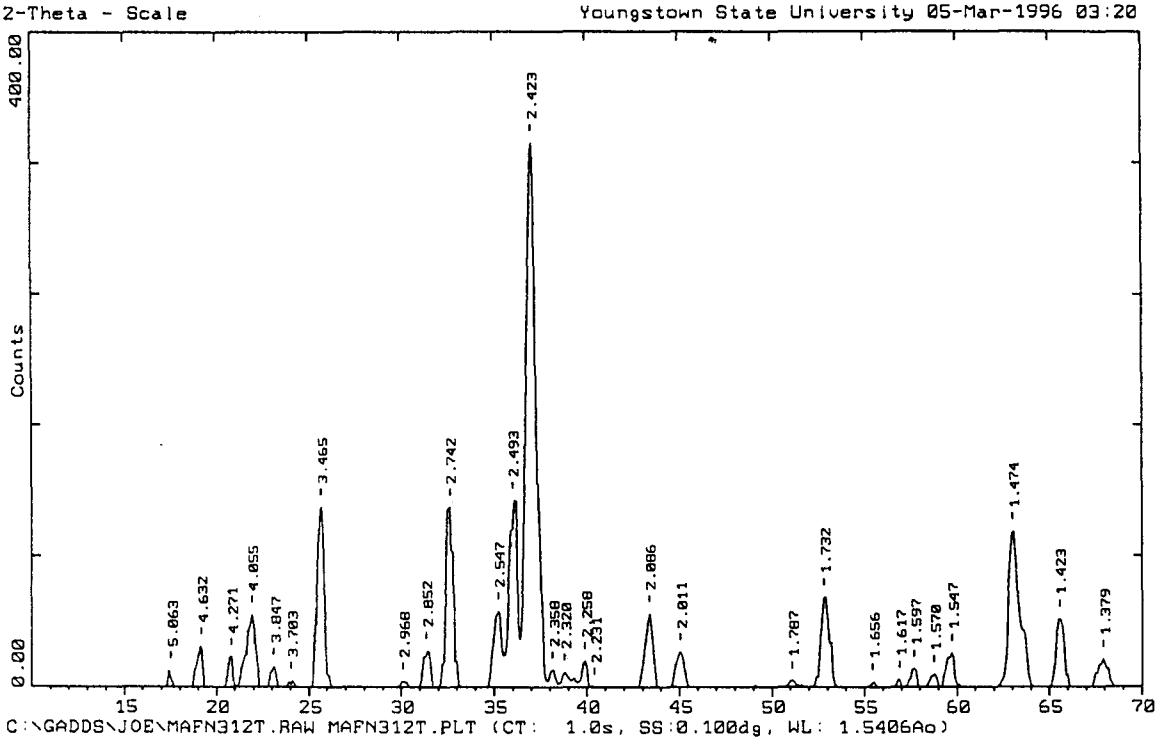

Figure 5.10. X-ray diffraction pattern for $MgAl_2(FN)_2$ synthesis trial 3 product from quartz tube.

Table 5.11

Statistical Data For Figure 5.10

Peak	Counts (%)	2θ (°)	$d_{Exp.}$ (Å)	$d_{Lit.}$ (Å)	$\lvert d_{Exp.}-d_{Lit.} \rvert$ (Å)	Phase	PDF Card
1	3.00	17.501	5.0633	5.058	0.0053	Ni_2SiO_4	15-388
2	7.43	19.145	4.6322	-	-	-	-
3	5.46	20.781	4.2711	4.281	0.0099	Ni_2SiO_4	15-388
4	13.20	21.900	4.0552	-	-	-	-
5	3.74	23.100	3.8472	3.845	0.0022	Ni_2SiO_4	15-388
6	1.12	24.012	3.7031	3.690	0.0131	Ni_2SiO_4	15-388
7	33.09	25.687	3.4653	3.469	0.0037	Ni_2SiO_4	15-388
8	1.08	30.082	2.9683	2.983	0.0147	Ni_2SiO_4	15-388
9	6.71	31.334	2.8525	-	-	-	-
10	33.11	32.629	2.7422	2.744	0.0018	Ni_2SiO_4	15-388
11	13.82	35.212	2.5467	2.551	0.0043	Ni_2SiO_4	15-388
12	34.34	36.000	2.4927	2.488	0.0047	Ni_2SiO_4	15-388
13	100.00	37.071	2.4231	2.430	0.0069	Ni_2SiO_4	15-388
14	3.10	38.141	2.3576	2.362	0.0044	Ni_2SiO_4	15-388
15	2.63	38.777	2.3204	2.324	0.0036	Ni_2SiO_4	15-388
16	4.76	39.885	2.2585	-	-	-	-
17	0.06	40.400	2.2308	2.228	0.0028	Ni_2SiO_4	15-388
18	13.40	43.352	2.0855	-	-	-	-
19	6.36	45.045	2.0110	2.011	0.0000	$NiAl_2O_4$	15-388
20	1.12	51.080	1.7866	1.789	0.0024	Ni_2SiO_4	15-388
21	16.37	52.817	1.7319	1.733	0.0011	Ni_2SiO_4	15-388
22	0.91	55.430	1.6563	1.657	0.0007	Ni_2SiO_4	15-388
23	1.26	56.900	1.6169	1.618	0.0011	Ni_2SiO_4	15-388
24	3.30	57.689	1.5967	1.600	0.0033	Ni_2SiO_4	15-388
25	2.27	58.756	1.5702	1.574	0.0038	Ni_2SiO_4	15-388
26	6.23	59.728	1.5470	1.554	0.0070	$NiAl_2O_4$	15-388
27	28.45	63.036	1.4735	-	-	-	-
28	12.43	65.555	1.4228	1.427	0.0042	$NiAl_2O_4$	15-388
29	5.07	67.926	1.3788	1.378	0.0008	Ni_2SiO_4	15-388

The details for each of the trial syntheses attempted will be discussed next.

Trial 1

A sample mixture was prepared by adding 5.040 grams of aluminum metal to 3.910 grams of AlF_3. The mole ratio of the mixture was four moles of aluminum metal to one mole of AlF_3. The starting materials were ground into a powder with a mortar and pestle. A sample of the starting materials was analyzed on the X-ray diffractometer. The X-ray diffraction pattern for that sample is illustrated in Figure 5.11, and the corresponding statistical data is listed in Table 5.12.

The X-ray diffraction pattern for the starting materials verifies the presence of aluminum metal and aluminum fluoride. There were also three unidentifiable peaks with high *d*-spacings that were outside of the literature data ranges. These low intensity peaks were probably due to trace impurities.

The mixture of starting materials was placed in an uncovered nickel boat and fired one day at 1000°C, inside a sealed quartz tube, using the Thermolyne model 21100 tube furnace. For this trial, a pure dynamic atmosphere of high purity N_2 (99.999%) was used, where dynamic atmosphere refers to a steady flow of gas over the sample. Upon removal of the sample boat, it was noted that white fibers

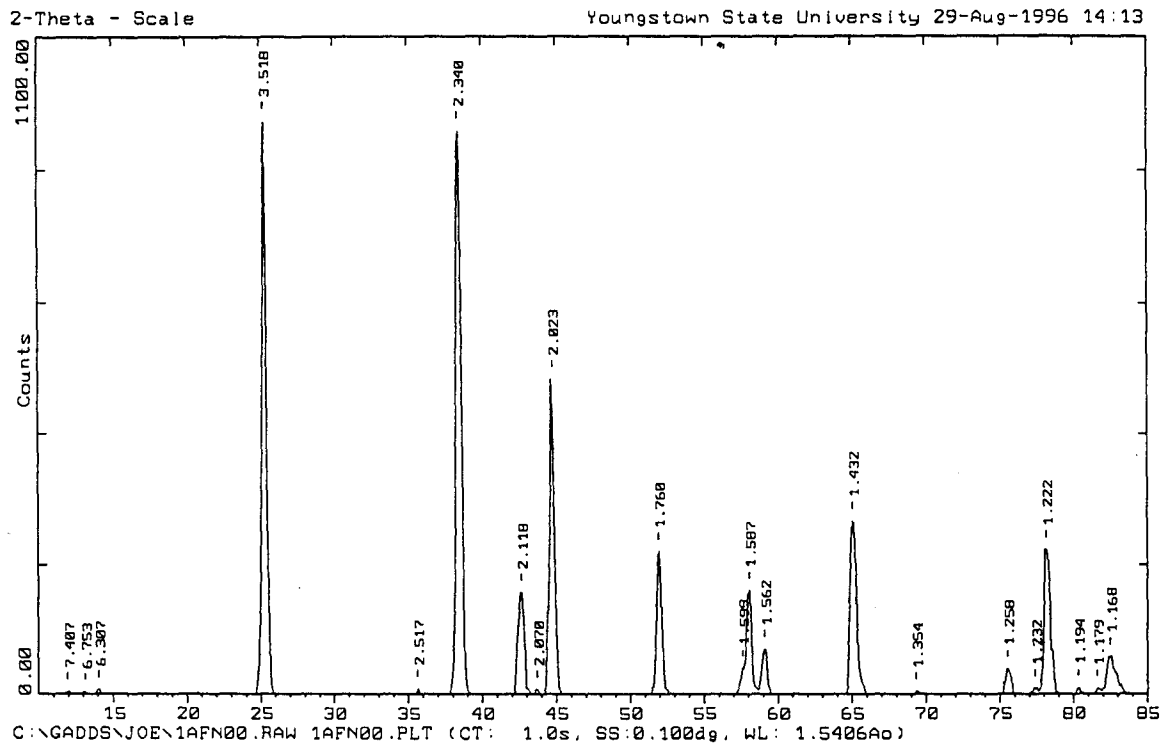

Figure 5.11. X-ray diffraction pattern for $Al_2(FN)_{1.5}$ synthesis trial 1 starting materials.

Table 5.12

Statistical Data For Figure 5.11

Peak	Counts (%)	2θ (°)	$d_{Exp.}$ (Å)	$d_{Lit.}$ (Å)	$\lvert d_{Exp.}-d_{Lit.} \rvert$ (Å)	Phase	PDF Card
1	0.43	11.938	7.4074	-	-	-	-
2	0.36	13.100	6.7529	-	-	-	-
3	0.67	14.031	6.3069	-	-	-	-
4	100.00	25.298	3.5177	3.517	0.0007	AlF_3	44-231
5	0.95	35.635	2.5174	2.5137	0.0037	AlF_3	44-231
6	94.43	38.444	2.3397	2.338	0.0017	Al	4-787
7	17.27	42.658	2.1178	2.1187	0.0009	AlF_3	44-231
8	0.82	43.700	2.0697	2.0742	0.0045	AlF_3	44-231
9	53.17	44.774	2.0225	2.024	0.0015	Al	4-787
10	24.21	51.924	1.7596	1.7599	0.0003	AlF_3	44-231
11	4.40	57.600	1.5989	1.5995	0.0006	AlF_3	44-231
12	17.57	58.069	1.5871	1.5869	0.0002	AlF_3	44-231
13	7.68	59.111	1.5616	1.5614	0.0002	AlF_3	44-231
14	29.37	65.074	1.4322	1.431	0.0012	Al	4-787
15	0.41	69.348	1.3540	1.3536	0.0004	AlF_3	44-231
16	4.26	75.533	1.2577	1.2572	0.0005	AlF_3	44-231
17	1.00	77.408	1.2319	1.2319	0.0000	AlF_3	44-231
18	24.51	78.173	1.2217	1.221	0.0007	Al	4-787
19	1.05	80.331	1.1943	1.1947	0.0004	AlF_3	44-231
20	0.88	81.622	1.1786	1.1783	0.0003	AlF_3	44-231
21	6.37	82.500	1.1683	1.169	0.0007	Al	4-787

appeared to grow out of the sample area of the nickel boat. After further examination of the sample boat, two additional areas of different colored products were discovered. A white powder was observed in the middle of the mixture, whereas a bluish powder was noted at the bottom. In addition, there were two areas of condensed material on the inner surface of the quartz tube. A gray region of material was above the sample vessel, and an off-white region of material was at the end of the tube, which was outside of the furnace during the synthesis. All five of the product areas were isolated, sampled, and analyzed on the X-ray diffractometer, in order to better quantify the relationship between the reaction conditions and the results.

Product 1. The X-ray diffraction pattern for the white fibrous sample product from the nickel boat is illustrated in Figure 5.12, and the corresponding numerical data is listed in Table 5.13.

The data indicated that the product consisted mostly of aluminum nitride. This conclusion was based on the fact that the most intense peaks matched known indexed peaks, from the literature, for AlN. The data also shows that a small amount of Al_2O_3 was present in the sample product.

Product 2. The X-ray diffraction pattern for the white powder from the middle of the sample vessel is shown in Figure 5.13, and Table 5.14 contains the numerical data.

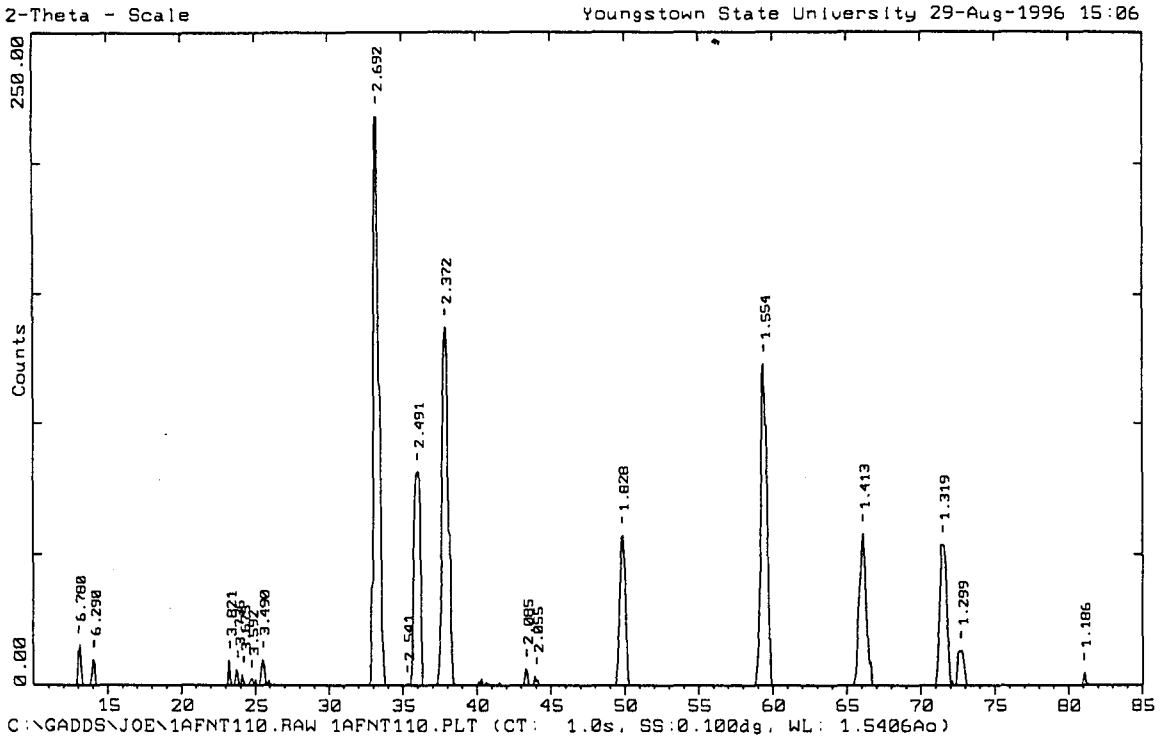

Figure 5.12. X-ray diffraction pattern for $Al_2(FN)_{1.5}$ synthesis trial 1 product 1.

Table 5.13

Statistical Data For Figure 5.12

Peak	Counts (%)	2θ (°)	$d_{Exp.}$ (Å)	$d_{Lit.}$ (Å)	$\lvert d_{Exp.}-d_{Lit.} \rvert$ (Å)	Phase	PDF Card
1	6.55	13.047	6.7803	-	-	-	-
2	4.24	14.069	6.2900	-	-	-	-
3	4.08	23.259	3.8213	-	-	-	-
4	2.54	23.800	3.7356	-	-	-	-
5	1.72	24.200	3.6748	-	-	-	-
6	0.99	24.766	3.5921	-	-	-	-
7	4.17	25.504	3.4898	3.48	0.0098	Al_2O_3	42-1468
8	100.00	33.261	2.6915	2.695	0.0035	AlN	25-1133
9	0.14	35.300	2.5406	2.551	0.0104	Al_2O_3	42-1468
10	35.26	36.030	2.4907	2.490	0.0007	AlN	25-1133
11	59.25	37.896	2.3723	2.371	0.0013	AlN	25-1133
12	2.71	43.353	2.0855	2.085	0.0005	Al_2O_3	42-1468
13	1.41	44.022	2.0553	-	-	-	-
14	24.68	49.830	1.8285	1.829	0.0005	AlN	25-1133
15	53.14	59.437	1.5538	1.5559	0.0021	AlN	25-1133
16	24.99	66.089	1.4127	1.4133	0.0006	AlN	25-1133
17	23.13	71.487	1.3186	1.3194	0.0008	AlN	25-1133
18	5.76	72.743	1.2989	1.3007	0.0018	AlN	25-1133
19	2.05	81.031	1.1857	1.1850	0.0007	AlN	25-1133

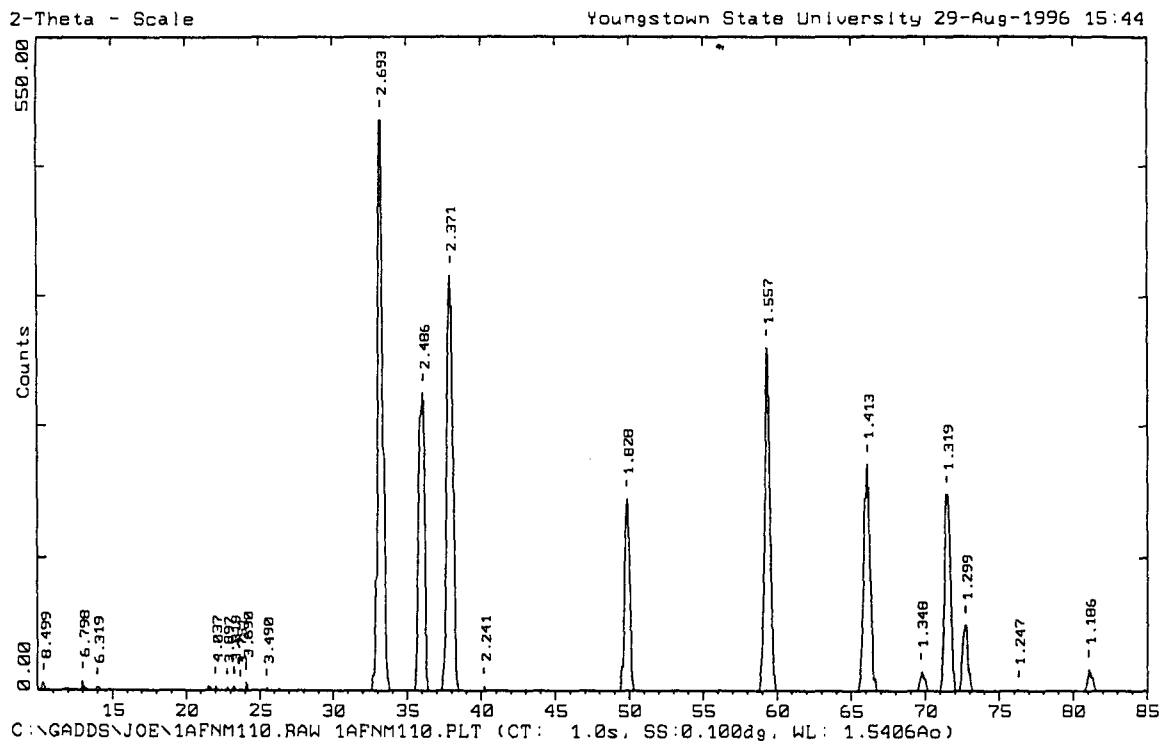

Figure 5.13. X-ray diffraction pattern for $Al_2(FN)_{1.5}$ synthesis trial 1 product 2.

Table 5.14

Statistical Data For Figure 5.13

Peak	Counts (%)	2θ (°)	$d_{Exp.}$ (Å)	$d_{Lit.}$ (Å)	$\lvert d_{Exp.}-d_{Lit.} \rvert$ (Å)	Phase	PDF Card
1	1.21	10.400	8.4992	-	-	-	-
2	1.51	13.014	6.7975	-	-	-	-
3	0.51	14.003	6.3193	-	-	-	-
4	0.67	22.000	4.0370	-	-	-	-
5	0.50	22.800	3.8971	-	-	-	-
6	0.73	23.276	3.8186	-	-	-	-
7	0.19	23.700	3.7512	-	-	-	-
8	1.43	24.100	3.6898	-	-	-	-
9	0.33	25.500	3.4903	-	-	-	-
10	100.00	33.246	2.6927	2.695	0.0023	AlN	25-1133
11	50.64	36.102	2.4859	2.490	0.0041	AlN	25-1133
12	70.92	37.917	2.3710	2.371	0.0000	AlN	25-1133
13	0.81	40.200	2.2415	-	-	-	-
14	32.44	49.851	1.8278	1.829	0.0012	AlN	25-1133
15	58.37	59.325	1.5565	1.5559	0.0006	AlN	25-1133
16	38.49	66.095	1.4125	1.4133	0.0008	AlN	25-1133
17	3.16	69.699	1.3480	1.3475	0.0005	AlN	25-1133
18	33.29	71.472	1.3189	1.3194	0.0005	AlN	25-1133
19	11.07	72.737	1.2990	1.3007	0.0017	AlN	25-1133
20	0.23	76.276	1.2473	1.2450	0.0023	AlN	25-1133
21	3.67	81.044	1.1856	1.1850	0.0006	AlN	25-1133

The data showed that the product was mainly aluminum nitride. This conclusion was based on the fact that the most intense peaks matched the known indexed peaks of AlN.

Product 3. The X-ray diffraction pattern for the bluish powder sampled from the bottom of the reaction vessel is illustrated in Figure 5.14, and the corresponding numerical data is in Table 5.15.

The data showed that this sample also consists mostly of aluminum nitride. Again, the conclusion was based on the fact that the most intense peaks matched the known indexed peaks of AlN. Note that since the sample was scraped from the bottom of the nickel boat, the bluish color observed is quite likely due to the diffusion of nickel into the sample. However, this possibility was not further investigated.

Product 4. The X-ray diffraction pattern for the gray sample of condensed material, which was scraped from the inside of the quartz tube, is shown in Figure 5.15, and the corresponding statistical data is listed in Table 5.16.

The data indicated that this sample consisted of a mixture of the starting materials, aluminum metal and aluminum fluoride along with the reaction product aluminum nitride. Aluminum nitride was experimentally determined to be the main product that was found in the previous three samples that were analyzed, but it was only present in a small amount in this sample. Thus, it can be assumed that

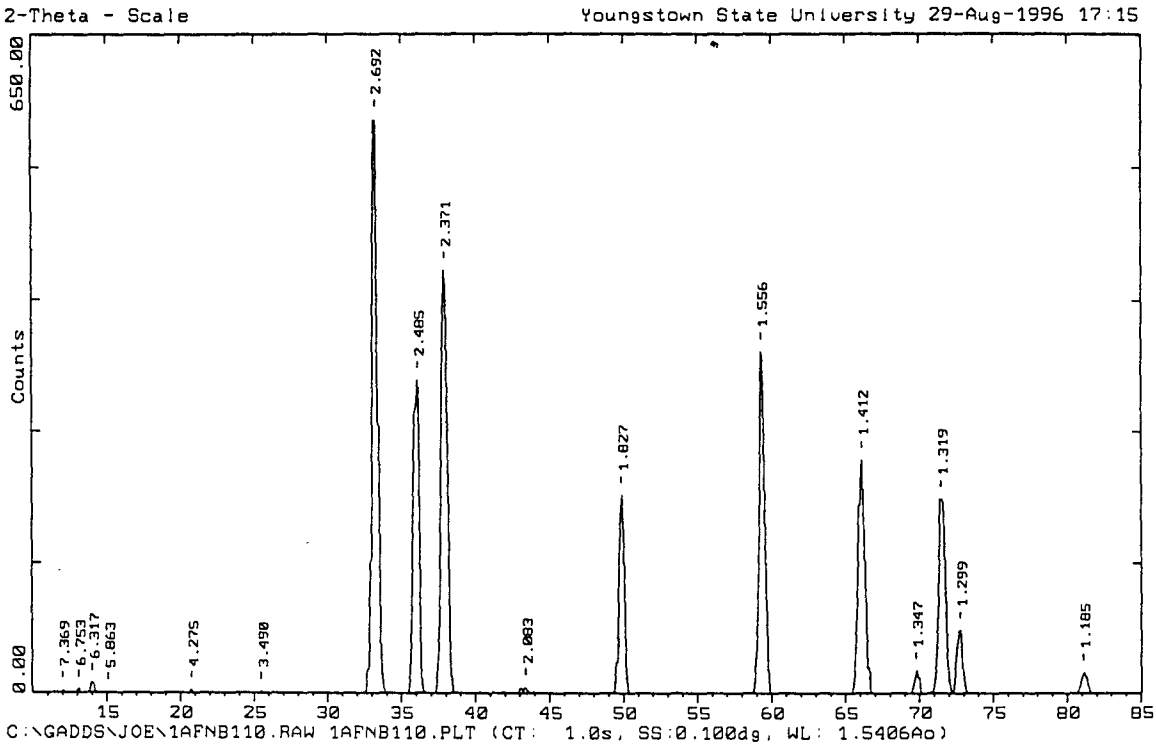

Figure 5.14. X-ray diffraction pattern for $Al_2(FN)_{1.5}$ synthesis trial 1 product 3.

Table 5.15

Statistical Data For Figure 5.14

Peak	Counts (%)	2θ (°)	$d_{Exp.}$ (Å)	$d_{Lit.}$ (Å)	$\lvert d_{Exp.}-d_{Lit.} \rvert$ (Å)	Phase	PDF Card
1	0.34	12.000	7.3693	-	-	-	-
2	0.57	13.100	6.7529	-	-	-	-
3	1.62	14.009	6.3166	-	-	-	-
4	0.16	15.100	5.8626	-	-	-	-
5	0.46	20.763	4.2746	-	-	-	-
6	0.27	25.500	3.4903	3.48	0.0103	Al_2O_3	42-1468
7	100.00	33.249	2.6924	2.695	0.0026	AlN	25-1133
8	51.46	36.117	2.4850	2.490	0.005	AlN	25-1133
9	69.39	37.919	2.3709	2.371	0.0001	AlN	25-1133
10	0.94	43.400	2.0833	2.085	0.0017	Al_2O_3	42-1468
11	32.79	49.878	1.8269	1.829	0.0021	AlN	25-1133
12	56.29	59.332	1.5563	1.5559	0.0004	AlN	25-1133
13	38.52	66.137	1.4117	1.4133	0.0016	AlN	25-1133
14	3.72	69.770	1.3468	1.3475	0.0007	AlN	25-1133
15	32.10	71.483	1.3187	1.3194	0.0007	AlN	25-1133
16	10.39	72.756	1.2988	1.3007	0.0019	AlN	25-1133
17	3.43	81.084	1.1851	1.1850	0.0001	AlN	25-1133

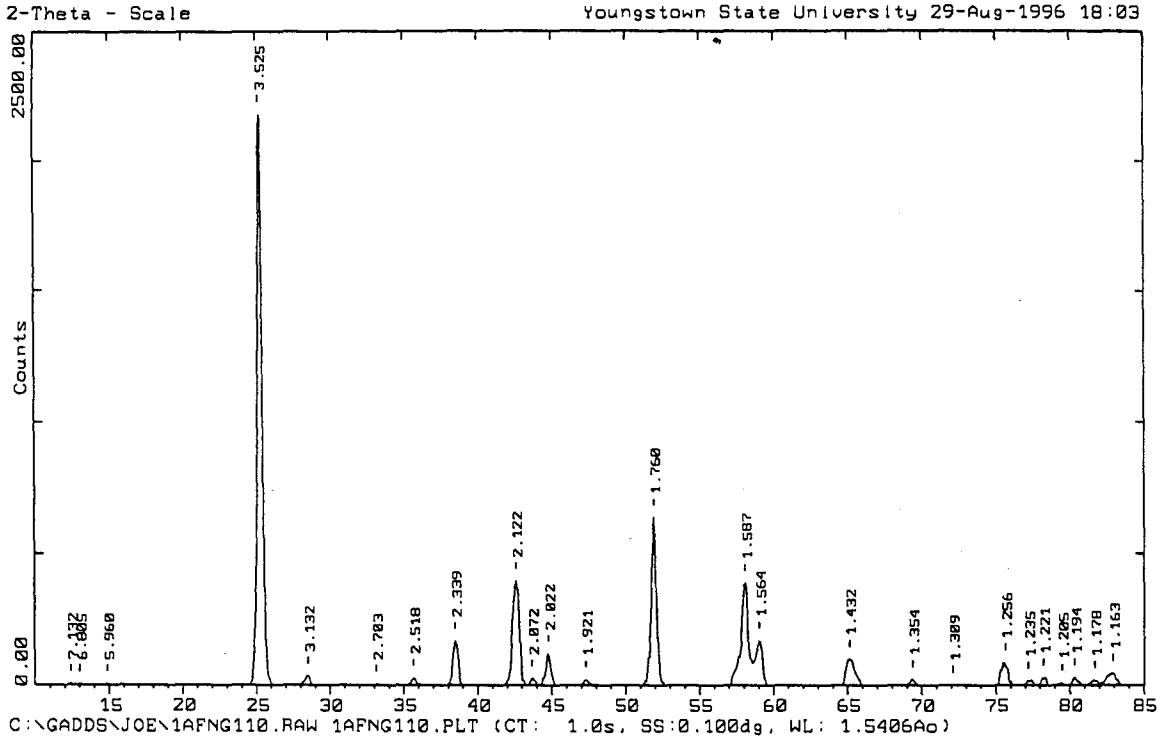

Figure 5.15. X-ray diffraction pattern for $Al_2(FN)_{1.5}$ synthesis trial 1 product 4.

Table 5.16

Statistical Data For Figure 5.15

Peak	Counts (%)	2θ (°)	$d_{Exp.}$ (Å)	$d_{Lit.}$ (Å)	$\lvert d_{Exp.}-d_{Lit.} \rvert$ (Å)	Phase	PDF Card
1	0.18	12.400	7.1325	-	-	-	-
2	0.11	13.000	6.8046	-	-	-	-
3	0.21	14.851	5.9602	6.002	0.0418	β-AlF_3	43-435
4	100.00	25.244	3.5251	3.517	0.0081	AlF_3	44-231
5	1.53	28.476	3.1319	3.1423	-	-	-
6	0.18	33.114	2.7031	2.695	0.0081	AlN	25-1133
7	1.17	35.634	2.5175	2.5137	0.0038	AlF_3	44-231
8	7.32	38.463	2.3386	2.338	0.0006	Al	4-787
9	17.33	42.572	2.1219	2.1187	0.0032	AlF_3	44-231
10	1.03	43.642	2.0723	2.0742	0.0019	AlF_3	44-231
11	5.20	44.780	2.0223	2.024	0.0017	Al	4-787
12	0.91	47.281	1.9210	1.914	0.0070	β-AlF_3	43-435
13	28.10	51.896	1.7605	1.7599	0.0006	AlF_3	44-231
14	17.05	58.065	1.5873	1.5869	0.0004	AlF_3	44-231
15	7.46	59.023	1.5638	1.5614	0.0024	AlF_3	44-231
16	4.30	65.086	1.4320	1.431	0.0010	Al^0	4-787
17	1.01	69.372	1.3536	1.3536	0.0000	AlF_3	44-231
18	0.01	72.100	1.3089	1.310	0.0011	β-AlF_3	43-435
19	3.75	75.630	1.2564	1.2572	0.0008	AlF_3	44-231
20	0.70	77.184	1.2349	1.2319	0.003	AlF_3	44-231
21	1.26	78.209	1.2213	1.2210	0.0003	Al^0	4-787
22	0.36	79.47	1.2051	1.2059	0.0008	AlF_3	44-231
23	1.22	80.32	1.1944	1.1947	0.0003	AlF_3	44-231
24	0.81	81.67	1.1780	1.1783	0.0003	AlF_3	44-231
25	1.96	82.92	1.1635	1.169	0.0055	Al^0	4-787

product four represents aluminum and aluminum fluoride that vaporized from the starting material and condensed on the quartz tube.

Product 5. The X-ray diffraction pattern for the second condensed material, which was scraped from the inside of the quartz tube, is shown in Figure 5.16, and the corresponding numerical data is listed in Table 5.17. The second deposit of condensed material was white in color and was found further from the nickel boat.

The data indicated that product five consisted of a mixture of compounds as observed for product four. An important difference between the compositions of products four and five was that product five consisted of an oxide. The main component of the product mixture was aluminum oxide, corundum. The conclusion was reached because the most intense peaks, in the X-ray diffraction pattern, corresponded to known peaks for the mineral corundum. In addition, several of the less intense peaks corresponded to peaks which have been previously indexed for the aluminum silicate mineral, mullite.

There is a plausible explanation for the failure of the first attempted synthesis for the compound $Al_2(FN)_{1.5}$. It can be stated, with some degree of certainty, that there was little or no fluorine remaining in the bulk of the material since only aluminum nitride was detected in the

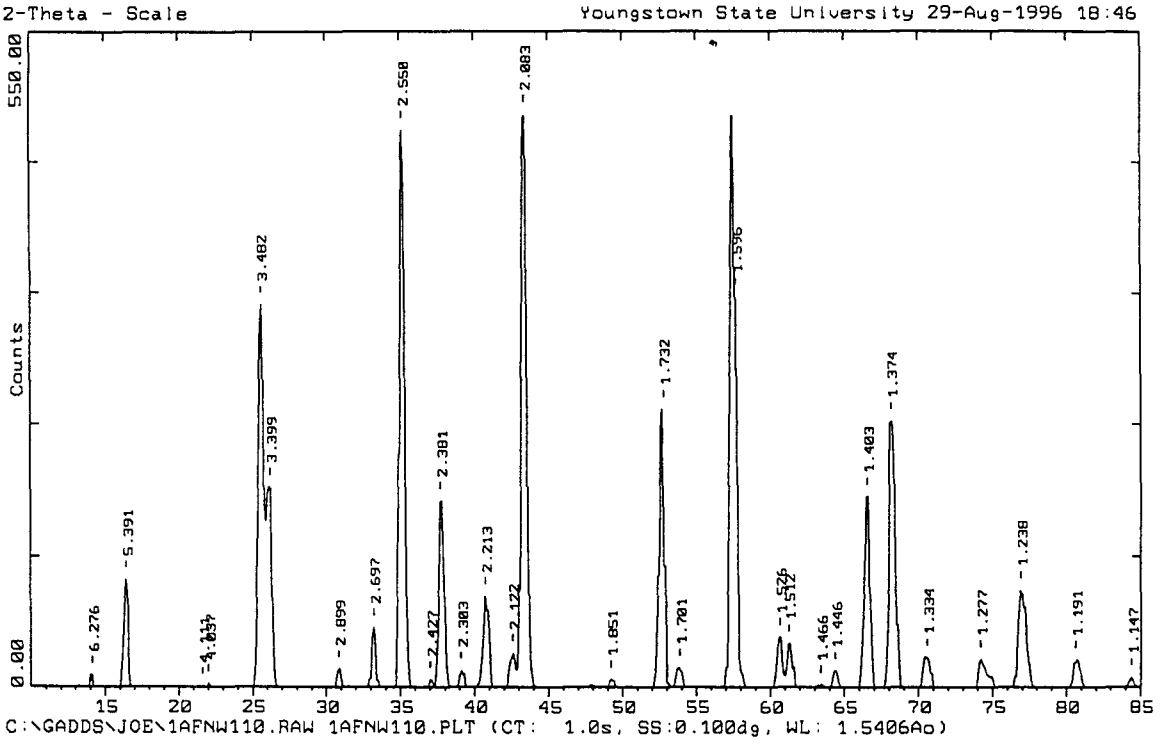

Figure 5.16. X-ray diffraction pattern for $Al_2(FN)_{1.5}$ synthesis trial 1 product 5.

Table 5.17

Statistical Data For Figure 5.16

Peak	Counts (%)	2θ (°)	$d_{Exp.}$ (Å)	$d_{Lit.}$ (Å)	$\lvert d_{Exp.}-d_{Lit.} \rvert$ (Å)	Phase	PDF Card
1	1.94	14.100	6.2761	-	-	-	-
2	18.07	16.431	5.3906	5.39	0.0006	$Al_6Si_2O_{13}$	15-776
3	0.04	21.600	4.1109	-	-	-	-
4	0.53	22.000	4.0370	-	-	-	-
5	64.12	25.563	3.4819	3.48	0.0019	Al_2O_3	42-1468
6	33.66	26.200	3.3986	3.390	0.0086	$Al_6Si_2O_{13}$	15-776
7	3.02	30.820	2.8988	2.8860	0.0128	$Al_6Si_2O_{13}$	15-776
8	10.03	33.193	2.6969	2.694	0.0029	$Al_6Si_2O_{13}$	15-776
9	93.62	35.167	2.5499	2.551	0.0011	Al_2O_3	42-1468
10	1.21	37.015	2.4267	2.428	0.0013	$Al_6Si_2O_{13}$	15-776
11	31.41	37.744	2.3815	2.379	0.0025	Al_2O_3	42-1468
12	2.71	39.086	2.3027	2.308	0.0053	$Al_6Si_2O_{13}$	15-776
13	15.32	40.742	2.2129	2.206	0.0069	$Al_6Si_2O_{13}$	15-776
14	5.69	42.572	2.1219	2.121	0.0009	$Al_6Si_2O_{13}$	15-776
15	100.00	43.408	2.0830	2.085	0.0020	Al_2O_3	42-1468
16	1.25	49.191	1.8508	1.841	0.0098	$Al_6Si_2O_{13}$	15-776
17	46.77	52.800	1.7324	1.7398	0.0074	Al_2O_3	42-1468
18	3.18	53.862	1.7008	1.7001	0.0007	$Al_6Si_2O_{13}$	15-776
19	65.63	57.700	1.5964	1.5999	0.0035	$Al_6Si_2O_{13}$	15-776
20	8.34	60.643	1.5258	1.5242	0.0016	$Al_6Si_2O_{13}$	15-776
21	7.34	61.240	1.5123	1.5109	0.0014	Al_2O_3	42-1468
22	0.39	63.400	1.4659	1.4605	0.0054	$Al_6Si_2O_{13}$	15-776
23	2.70	64.369	1.4462	1.4421	0.0041	$Al_6Si_2O_{13}$	15-776
24	32.08	66.576	1.4035	1.4045	0.001	Al_2O_3	42-1468
25	44.58	68.181	1.3743	1.3738	0.0005	Al_2O_3	42-1468
26	4.97	70.570	1.3335	1.336	0.0025	Al_2O_3	42-1468
27	4.72	74.179	1.2773	1.2755	0.0018	Al_2O_3	42-1468
28	16.34	76.922	1.2385	1.2390	0.0005	Al_2O_3	42-1468
29	4.59	80.609	1.1908	1.1931	0.0023	Al_2O_3	42-1468
30	1.63	84.397	1.1468	1.1471	0.0003	Al_2O_3	42-1468

three sample zones located in the reaction vessel. Furthermore, two compounds, aluminum oxide and aluminum silicate, were identified in the regions of condensed material on the inner surface of the quartz tube suggesting that the quartz tube had reacted with chemical substances within it, and that there was likely an air leak in the system. The results suggest that the aluminum fluoride in the original sample mixture vaporized and condensed on the quartz tube with a reaction occurring at the process interface. Aluminum, which was present in excess, also could have vaporized and traveled to the cooler end of the tube before condensing in the product five region. The fact that oxides were observed only in product five indicates that there was a small air leak near the seal where product five was collected. Since the majority of the aluminum fluoride in the starting materials vaporized and then deposited on the cooler end of the quartz tube where it reacted, there was no zone in which the aluminum, nitrogen, and aluminum fluoride were all able to interact with each other in the bulk material. Since those three ingredients were not able to react together, the compound $Al_2(FN)_{1.5}$ did not have a chance to form.

Based on these results, the following conditions were modified for the second attempt to synthesize $Al_2(FN)_{1.5}$. For trial two, the starting material aluminum fluoride was

used in a large excess in an attempt to combat the loss of it in the dynamic nitrogen atmosphere. Additionally, the reaction temperature was lowered to 700°C to minimize the effects of vaporization of the starting materials.

Trial 2

A sample of 0.293 grams of aluminum metal was mixed with 3.650 grams of AlF_3, which corresponds to a mole ratio of one mole of aluminum metal to four moles of AlF_3. A sample of the starting materials was analyzed on the X-ray diffractometer. The X-ray diffraction pattern for the sample is illustrated in Figure 5.17, and the corresponding numerical data listed in Table 5.18.

The starting materials were placed in a nickel reaction boat, which was placed in a new quartz tube. The tube was placed in the Thermolyne model 21100 tube furnace and subjected to a dynamic nitrogen atmosphere. The sample was fired for one day at 700°C. The X-ray diffraction pattern for that sample is illustrated in Figure 5.18, and the corresponding statistical data is in Table 5.19.

The results illustrated that the experiment was unsuccessful. The data revealed that aluminum nitride was formed and a large amount of aluminum fluoride remained unreacted. The differences between the first and second syntheses were the mole ratio of the starting reactants and

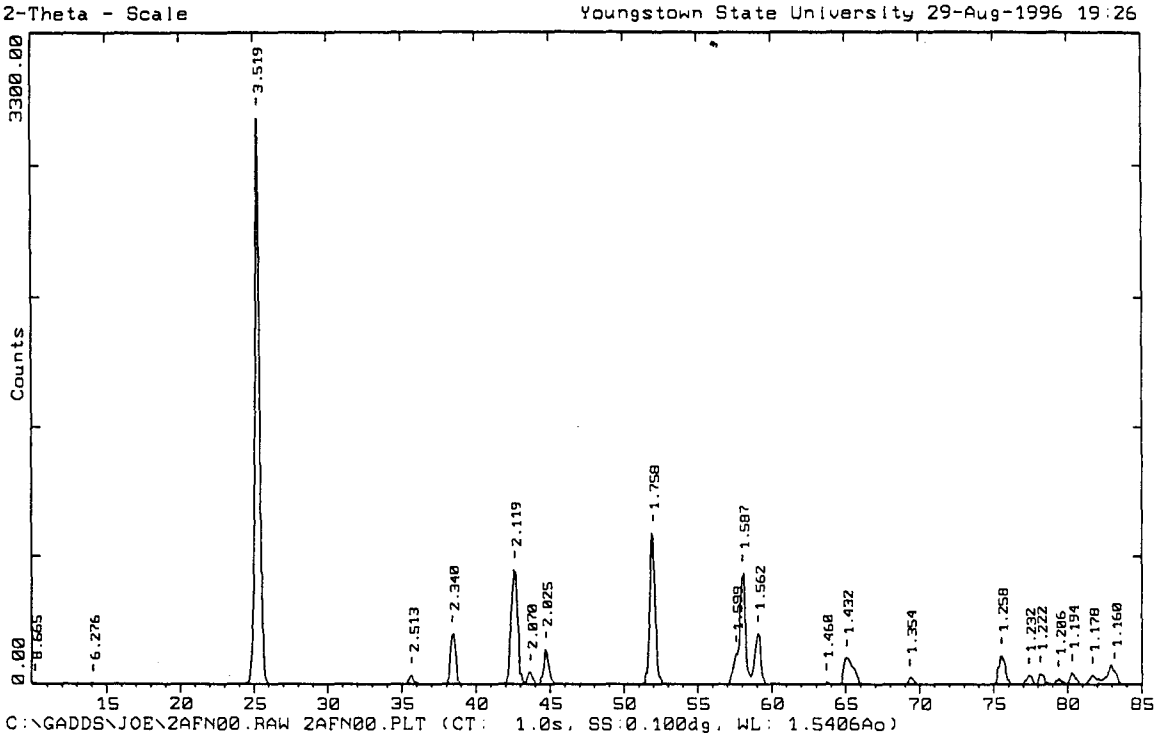

Figure 5.17. X-ray diffraction pattern for $Al_2(FN)_{1.5}$ synthesis trial 2 starting materials.

Table 5.18

Statistical Data For Figure 5.17

Peak	Counts (%)	2θ (°)	$d_{Exp.}$ (Å)	$d_{Lit.}$ (Å)	$\lvert d_{Exp.}-d_{Lit.} \rvert$ (Å)	Phase	PDF Card
1	0.13	10.200	8.6653	-	-	-	-
2	0.15	14.100	6.2761	-	-	-	-
3	100.00	25.290	3.5189	3.517	0.0019	AlF_3	44-231
4	1.46	35.699	2.5131	2.5137	0.0006	AlF_3	44-231
5	8.43	38.441	2.3399	2.338	0.0019	Al^0	4-787
6	19.29	42.638	2.1188	2.1187	0.0001	AlF_3	44-231
7	2.00	43.689	2.0702	2.0742	0.004	AlF_3	44-231
8	5.80	44.714	2.0251	2.0240	0.0011	Al^0	4-787
9	25.53	51.983	1.7577	1.7599	0.0022	AlF_3	44-231
10	5.05	57.600	1.5989	1.5995	0.0006	AlF_3	44-231
11	18.76	58.067	1.5872	1.5869	0.0003	AlF_3	44-231
12	8.57	59.116	1.5615	1.5614	0.0001	AlF_3	44-231
13	0.28	63.702	1.4597	1.4617	0.002	AlF_3	44-231
14	4.38	65.069	1.4323	1.431	0.0013	Al^0	4-787
15	1.07	69.353	1.3539	1.3536	0.0003	AlF_3	44-231
16	4.75	75.529	1.2578	1.2572	0.0006	AlF_3	44-231
17	1.46	77.396	1.2321	1.2319	0.0002	AlF_3	44-231
18	1.72	78.172	1.2218	1.221	0.0008	Al^0	4-787
19	0.85	79.421	1.2056	1.2059	0.0003	AlF_3	44-231
20	1.92	80.321	1.1944	1.1947	0.0003	AlF_3	44-231
21	1.49	81.698	1.1777	1.1783	0.0006	AlF_3	44-231
22	2.23	83.200	1.1602	1.1628	0.0026	AlF_3	44-231

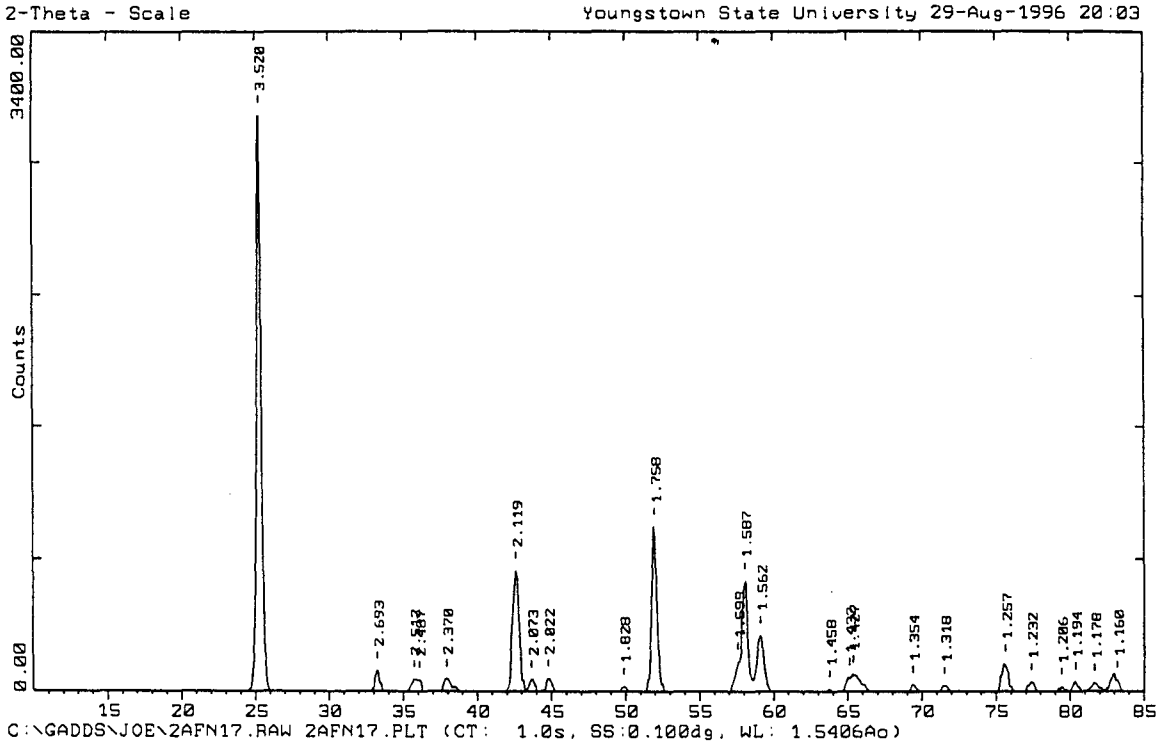

Figure 5.18. X-ray diffraction pattern for $Al_2(FN)_{1.5}$ synthesis trial 2 product.

Table 5.19

Statistical Data For Figure 5.18

Peak	Counts (%)	2θ (°)	$d_{Exp.}$ (Å)	$d_{Lit.}$ (Å)	$\lvert d_{Exp.}-d_{Lit.} \rvert$ (Å)	Phase	PDF Card
1	100.00	25.280	3.5202	3.517	0.0032	AlF_3	44-231
2	3.28	33.238	2.6933	2.695	0.0017	AlN	25-1133
3	1.97	35.722	2.5115	2.5137	0.0022	AlF_3	44-231
4	1.85	36.083	2.4872	2.490	0.0028	AlN	25-1133
5	2.04	37.926	2.3705	2.371	0.0005	AlN	25-1133
6	19.32	42.626	2.1193	2.1187	0.0006	AlF_3	44-231
7	1.86	43.637	2.0726	2.0742	0.0016	AlF_3	44-231
8	2.08	44.779	2.0223	2.0184	0.0039	AlF_3	44-231
9	0.75	49.852	1.8278	1.829	0.0012	AlN	25-1133
10	26.52	51.972	1.7581	1.7599	0.0018	AlF_3	44-231
11	4.82	57.600	1.5989	1.5995	0.0006	AlF_3	44-231
12	17.76	58.072	1.5871	1.5869	0.0002	AlF_3	44-231
13	9.05	59.114	1.5616	1.5614	0.0002	AlF_3	44-231
14	0.32	63.765	1.4584	1.4617	0.0033	AlF_3	44-231
15	2.32	65.100	1.4317	1.4321	0.0004	AlF_3	44-231
16	2.69	65.357	1.4267	1.4226	0.0041	AlF_3	44-231
17	1.08	69.370	1.3536	1.3536	0.0000	AlF_3	44-231
18	0.90	71.509	1.3183	1.3194	0.0011	AlN	25-1133
19	4.46	75.619	1.2565	1.2572	0.0007	AlF_3	44-231
20	1.42	77.370	1.2324	1.2319	0.0005	AlF_3	44-231
21	0.74	79.400	1.2059	1.2059	0.0000	AlF_3	44-231
22	1.65	80.354	1.1940	1.1947	0.0007	AlF_3	44-231
23	1.36	81.657	1.1782	1.1783	0.0001	AlF_3	44-231
24	1.80	83.200	1.1602	1.1628	0.0026	AlF_3	44-231

the reaction temperature. The deficiency of aluminum metal in the second synthesis may account for the failure of the experiment because all of the aluminum metal was consumed to form aluminum nitride. At this point, it was considered that adjusting the mole ratio could alleviate this problem in the next synthesis, although it was beginning to appear as though the formation of aluminum nitride is preferential due to its relative thermodynamic stability.

Trial 3

A third attempt to synthesize the novel nitride-fluoride compound $Al_2(FN)_{1.5}$ was performed. As in the previous two syntheses, aluminum metal and aluminum fluoride were used as the initial starting materials, but with a modified relative starting ratio. Again the presumption was that a dynamic nitrogen atmosphere would provide nitrogen which should react with aluminum and fluorine to produce the proposed nitride-fluoride compound. The starting mixture was made by mixing 0.701 grams of aluminum metal with 2.619 grams of AlF_3. The reactants were ground into a powder with a mortar and pestle. The mole ratio was 1.0 moles of aluminum metal to 1.2 moles of AlF_3. The starting materials were analyzed on the X-ray diffractometer. The X-ray diffraction pattern is illustrated in Figure 5.19, and the corresponding statistical data is listed in Table 5.20.

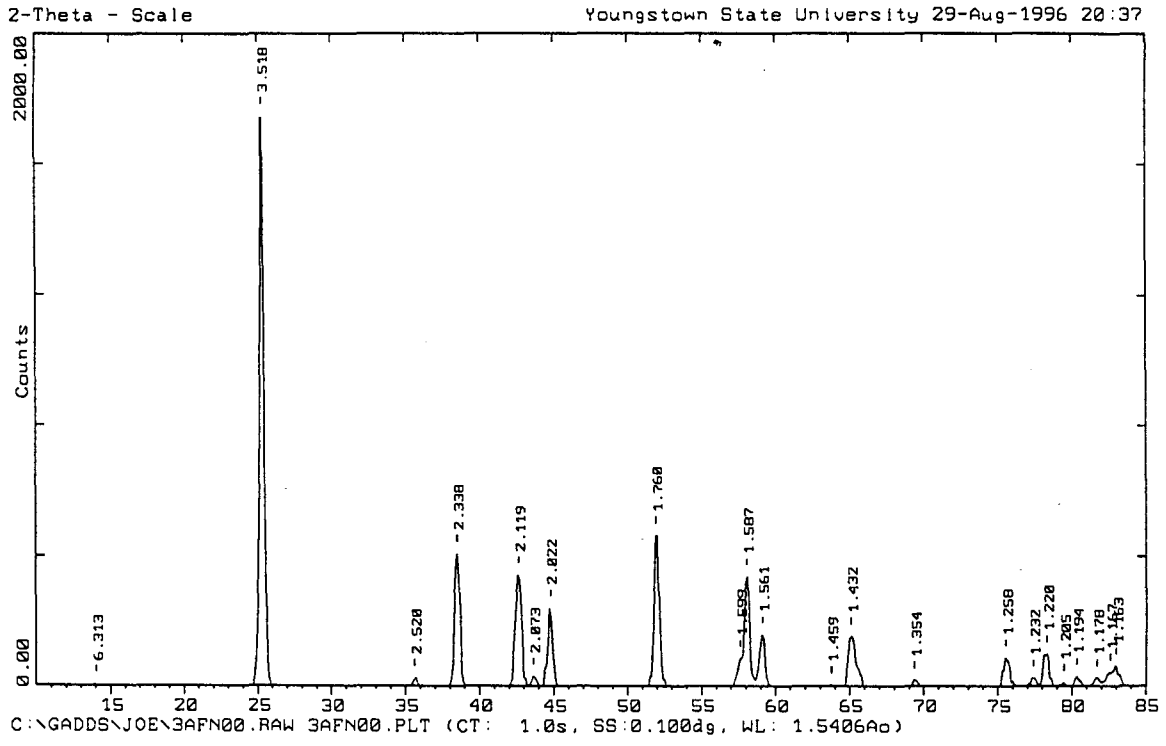

Figure 5.19. X-ray diffraction pattern for $Al_2(FN)_{1.5}$ synthesis trial 3 starting materials.

Table 5.20

Statistical Data For Figure 5.19

Peak	Counts (%)	2θ (°)	$d_{Exp.}$ (Å)	$d_{Lit.}$ (Å)	$\lvert d_{Exp.}-d_{Lit.} \rvert$ (Å)	Phase	PDF Card
1	0.21	14.017	6.3131	-	-	-	-
2	100.00	25.295	3.5181	3.517	0.0011	AlF_3	44-231
3	1.32	35.595	2.5202	2.5137	0.0065	AlF_3	44-231
4	21.78	38.473	2.3380	2.338	0.0000	Al^0	4-787
5	18.20	42.639	2.1187	2.1187	0.0000	AlF_3	44-231
6	1.54	43.621	2.0733	2.0742	0.0009	AlF_3	44-231
7	12.81	44.780	2.0223	2.0240	0.0017	Al^0	4-787
8	24.72	51.913	1.7599	1.7599	0.0000	AlF_3	44-231
9	4.55	57.600	1.5989	1.5995	0.0006	AlF_3	44-231
10	17.94	58.077	1.5870	1.5869	0.0001	AlF_3	44-231
11	8.44	59.117	1.5615	1.5614	0.0001	AlF_3	44-231
12	0.16	63.756	1.4586	1.4617	0.0031	AlF_3	44-231
13	8.28	65.085	1.4320	1.4321	0.0001	AlF_3	44-231
14	0.96	69.357	1.3539	1.3536	0.0003	AlF_3	44-231
15	4.66	75.538	1.2577	1.2572	0.0005	AlF_3	44-231
16	1.30	77.386	1.2322	1.2319	0.0003	AlF_3	44-231
17	5.30	78.307	1.2200	1.2210	0.0010	Al^0	4-787
18	0.51	79.470	1.2050	1.2059	0.0009	AlF_3	44-231
19	1.57	80.333	1.1942	1.1947	0.0005	AlF_3	44-231
20	1.37	81.698	1.1777	1.1783	0.0006	AlF_3	44-231
21	2.33	82.600	1.1671	1.169	0.0019	Al^0	4-787
22	3.30	83.000	1.1625	1.1628	0.0003	AlF_3	44-231

The starting materials were placed in a nickel reaction boat, which was placed in a new quartz tube. The tube was placed inside the Thermolyne model 21100 tube furnace and connected to a dynamic nitrogen atmosphere. The sample was fired for one day at 700°C. The X-ray diffraction pattern for the sample is shown in Figure 5.20, and the corresponding statistical data is in Table 5.21.

The results indicated that the experiment was again unsuccessful. The data showed that AlN formed, and the remaining material was aluminum and AlF_3. The mole ratio was the condition adjusted in the third synthesis. It is unclear why $Al_2(FN)_{1.5}$ did not form. One possible reason may be that the mole ratio was acceptable but the temperature was insufficient to cause the solids to react.

Trial 4

The fourth attempt to synthesize the compound $Al_2(FN)_{1.5}$ was again performed with aluminum metal and AlF_3 in a dynamic nitrogen atmosphere. A mixture of 1.634 grams of aluminum metal and 2.543 grams of AlF_3 were ground into a powder. The mole ratio was 2 moles of aluminum metal to 1 mole of AlF_3. A sample of the starting materials was analyzed on the X-ray diffractometer. The X-ray diffraction pattern for the sample is illustrated in Figure 5.21, and the corresponding statistical data is listed in Table 5.22.

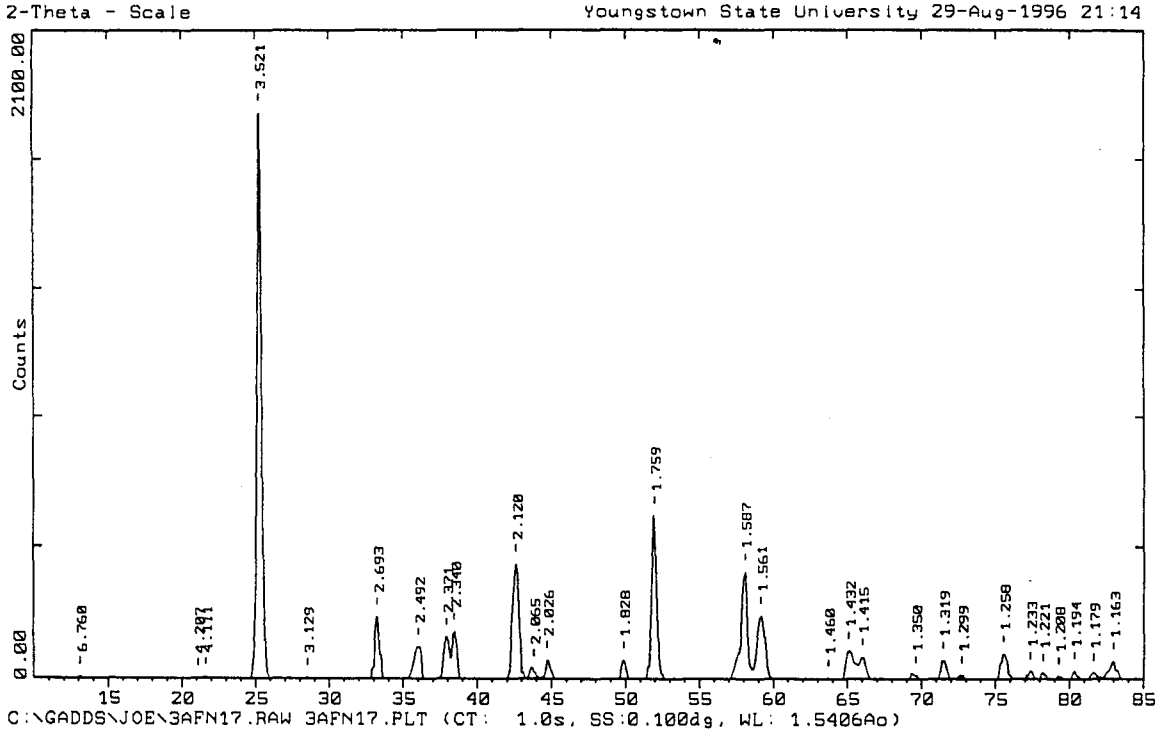

Figure 5.20. X-ray diffraction pattern for $Al_2(FN)_{1.5}$ synthesis trial 3 product.

Table 5.21

Statistical Data For Figure 5.20

Peak	Counts (%)	2θ (°)	$d_{Exp.}$ (Å)	$d_{Lit.}$ (Å)	$\lvert d_{Exp.}-d_{Lit.} \rvert$ (Å)	Phase	PDF Card
1	0.28	13.086	6.7600	-	-	-	-
2	0.00	21.100	4.2071	-	-	-	-
3	0.21	21.600	4.1109	-	-	-	-
4	100.00	25.275	3.5208	3.517	0.0038	AlF_3	44-231
5	0.16	28.500	3.1294	-	-	-	-
6	10.27	33.240	2.6932	2.695	0.0018	AlN	25-1133
7	5.25	36.015	2.4917	2.490	0.0017	AlN	25-1133
8	6.94	37.918	2.3710	2.371	0.0000	AlN	25-1133
9	7.78	38.443	2.3398	2.338	0.0018	Al^0	4-787
10	19.32	42.611	2.1201	2.1187	0.0014	AlF_3	44-231
11	1.65	43.800	2.0652	2.0742	0.0090	AlF_3	44-231
12	3.09	44.700	2.0257	2.024	0.0017	Al^0	4-787
13	3.00	49.858	1.8276	1.829	0.0014	AlN	25-1133
14	27.46	51.957	1.7585	1.7599	0.0014	AlF_3	44-231
15	17.85	58.070	1.5871	1.5869	0.0002	AlF_3	44-231
16	10.59	59.147	1.5608	1.5559	0.0049	AlN	25-1133
17	0.06	63.700	1.4597	1.4617	0.0020	AlF_3	44-231
18	4.62	65.088	1.4319	1.431	0.0009	Al^0	4-787
19	3.55	65.981	1.4147	1.4133	0.0014	AlN	25-1133
20	0.65	69.600	1.3497	1.3475	0.0022	AlN	25-1133
21	3.04	71.454	1.3192	1.3194	0.0002	AlN	25-1133
22	0.56	72.710	1.2995	1.3007	0.0012	AlN	25-1133
23	4.16	75.540	1.2576	1.2572	0.0004	AlF_3	44-231
24	1.28	77.351	1.2327	1.2319	0.0008	AlF_3	44-231
25	0.99	78.215	1.2212	1.221	0.0002	Al^0	4-787
26	0.39	79.261	1.2077	1.2059	0.0018	AlF_3	44-231
27	1.33	80.322	1.1944	1.1947	0.0003	AlF_3	44-231
28	0.96	81.612	1.1787	1.1783	0.0004	AlF_3	44-231
29	2.85	82.976	1.1628	1.1628	0.0000	AlF_3	44-231

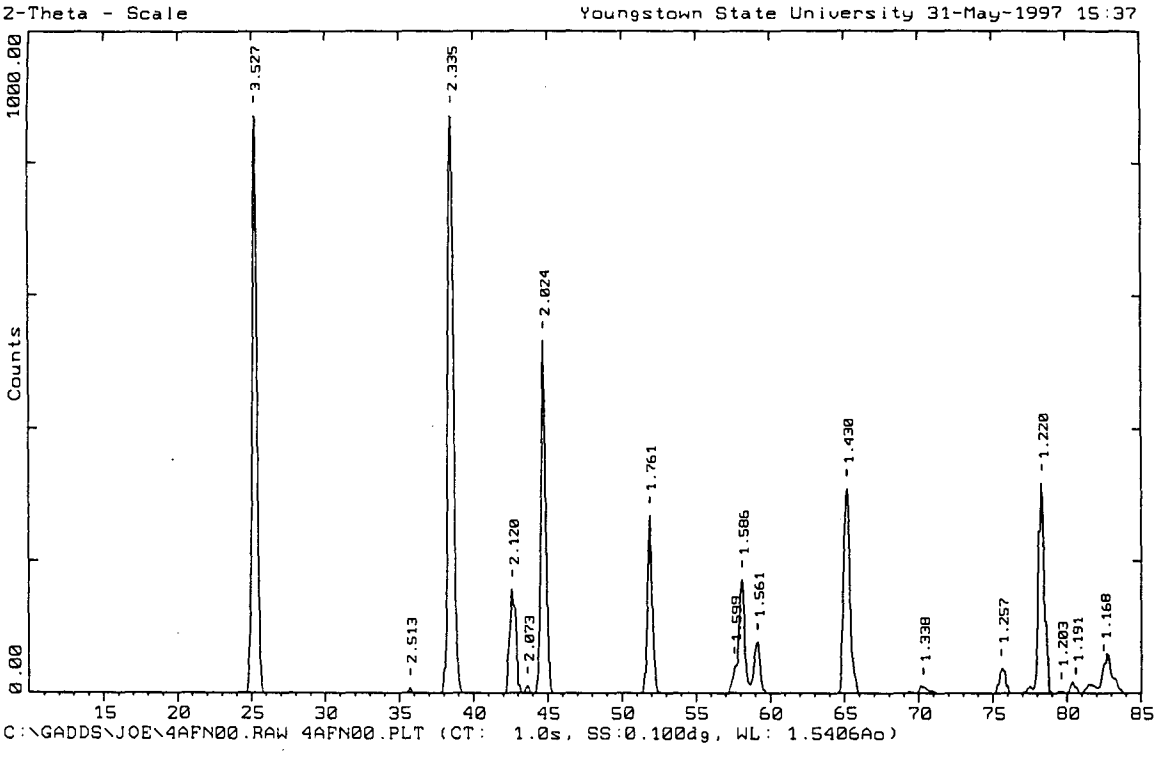

Figure 5.21. X-ray diffraction pattern for $Al_2(FN)_{1.5}$ synthesis trial 4 starting materials.

Table 5.22

Statistical Data For Figure 5.21

Peak	Counts (%)	2θ (°)	$d_{Exp.}$ (Å)	$d_{Lit.}$ (Å)	$\lvert d_{Exp.}-d_{Lit.} \rvert$ (Å)	Phase	PDF Card
1	100.00	25.230	3.5270	3.517	0.0100	AlF_3	44-231
2	0.82	35.705	2.5127	2.5137	0.0010	AlF_3	44-231
3	99.59	38.532	2.3346	2.338	0.0034	Al^0	4-787
4	17.72	42.621	2.1196	2.1187	0.0009	AlF_3	44-231
5	1.24	43.626	2.0731	2.0742	0.0011	AlF_3	44-231
6	60.28	44.746	2.0237	2.024	0.0003	Al^0	4-787
7	30.48	51.874	1.7612	1.7599	0.0013	AlF_3	44-231
8	4.56	57.600	1.5989	1.5995	0.0006	AlF_3	44-231
9	19.39	58.116	1.5860	1.586	0.0000	AlF_3	44-231
10	8.73	59.148	1.5607	1.5614	0.0007	AlF_3	44-231
11	35.06	65.176	1.4302	1.431	0.0008	Al^0	4-787
12	1.09	70.300	1.3380	-	-	-	-
13	4.21	75.593	1.2569	1.2572	0.0003	AlF_3	44-231
14	35.97	78.338	1.2196	1.221	0.0014	Al^0	4-787
15	0.25	79.599	1.2034	1.2059	0.0025	AlF_3	44-231
16	1.10	80.600	1.1910	1.1947	0.0037	AlF_3	44-231
17	5.11	82.500	1.1683	1.169	0.0007	Al^0	4-787

The mixture of aluminum metal and AlF_3 was placed in an unused nickel boat, and a second nickel boat was placed on top to act as a cover. The sample was placed in a new quartz tube, which was placed inside of the Thermolyne model 21100 tube furnace and connected to a dynamic nitrogen atmosphere. The sample was fired for one day at 1000°C. The product was analyzed on the X-ray diffractometer. The X-ray diffraction pattern for the sample is shown in Figure 5.22, and the corresponding data is in Table 5.23.

As noted in the previous three syntheses discussions, the X-ray diffraction analysis of the end product showed that the main species that formed in the solid-state reaction was AlN. Since the temperature was increased from 700°C to 1000°C for the fourth synthesis, it is likely that the solids were molten during the reaction because the product was a harden mass. Unlike the previous three synthesis attempts, a second nickel boat was used to cover the reaction boat in order to keep the reactants from vaporizing. Consequently, there was no deposit discovered on the inner surface of the quartz tube which is evidence that the precursors did not vaporize.

The explanation for the failure of the trial four synthesis of $Al_2(FN)_{1.5}$ is not apparent, but it is quite likely related to the relatively high stability of AlN as compared to the proposed novel nitride-fluoride compound.

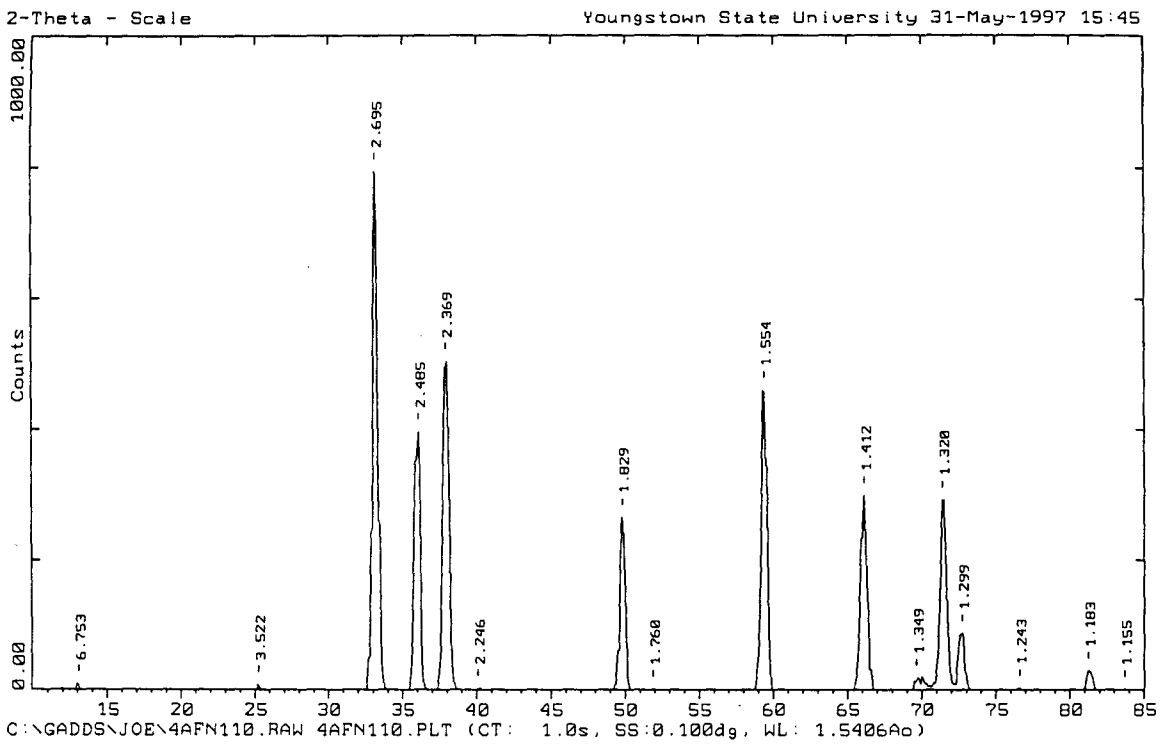

Figure 5.22. X-ray diffraction pattern for $Al_2(FN)_{1.5}$ synthesis trial 4 product.

Table 5.23

Statistical Data For Figure 5.22

Peak	Counts (%)	2θ (°)	$d_{Exp.}$ (Å)	$d_{Lit.}$ (Å)	$\lvert d_{Exp.}-d_{Lit.} \rvert$ (Å)	Phase	PDF Card
1	1.15	13.100	6.7529	-	-	-	-
2	1.01	25.268	3.5218	3.517	0.0048	AlF_3	44-231
3	100.00	33.210	2.6955	2.695	0.0005	AlN	25-1133
4	49.94	36.121	2.4847	2.490	0.0053	AlN	25-1133
5	63.58	37.954	2.3688	2.371	0.0022	AlN	25-1133
6	0.30	40.107	2.2464	-	-	-	-
7	33.56	49.830	1.8285	1.829	0.0005	AlN	25-1133
8	0.15	51.900	1.7603	1.7599	0.0004	AlF_3	44-231
9	57.98	59.418	1.5543	1.5559	0.0016	AlN	25-1133
10	37.76	66.147	1.4115	1.4133	0.0018	AlN	25-1133
11	2.42	69.670	1.3485	1.3475	0.0010	AlN	25-1133
12	36.89	71.427	1.3196	1.3194	0.0002	AlN	25-1133
13	10.85	72.723	1.2993	1.3007	0.0014	AlN	25-1133
14	0.33	76.600	1.2429	1.2450	0.0021	AlN	25-1133
15	3.64	81.263	1.1829	1.1850	0.0021	AlN	25-1133
16	0.06	83.700	1.1546	1.1628	0.0082	AlF_3	44-231

Attempted Synthesis of $NaLi_6Mg_6F_{19}$

An attempt to synthesize the novel mixed metal fluoride compound, $NaLi_6Mg_6F_{19}$, was performed according to the following stoichiometrically balanced equation:

$$NaF + 6LiF + 6MgF_2 \rightarrow NaLi_6Mg_6F_{19}.$$

The details of each trial will be discussed next.

Trial 1

A sample was prepared by mixing 4.916 grams of MgF_2, 2.048 grams of LiF, and 0.552 grams of NaF. The mole ratio was 6 moles MgF_2, to 6 moles LiF, to 1 mole NaF. The mixture was ground into a powder, prepared, and analyzed on the X-ray diffractometer. The X-ray diffraction pattern for the starting materials is illustrated in Figure 5.23, and the corresponding statistical data is listed in Table 5.24.

The starting materials were placed in a new nickel reaction vessel. The nickel boat was loaded into a new quartz tube, which remained open to air. The tube was placed in the Thermolyne model 21100 tube furnace, and the sample was fired for 15 hours at 500°C. The sample product was analyzed on the X-ray diffractometer. The X-ray diffraction pattern for the sample is shown in Figure 5.24, and the corresponding statistical data is in Table 5.25.

The X-ray diffraction pattern indicated that the reaction failed to produce the novel mixed metal fluoride

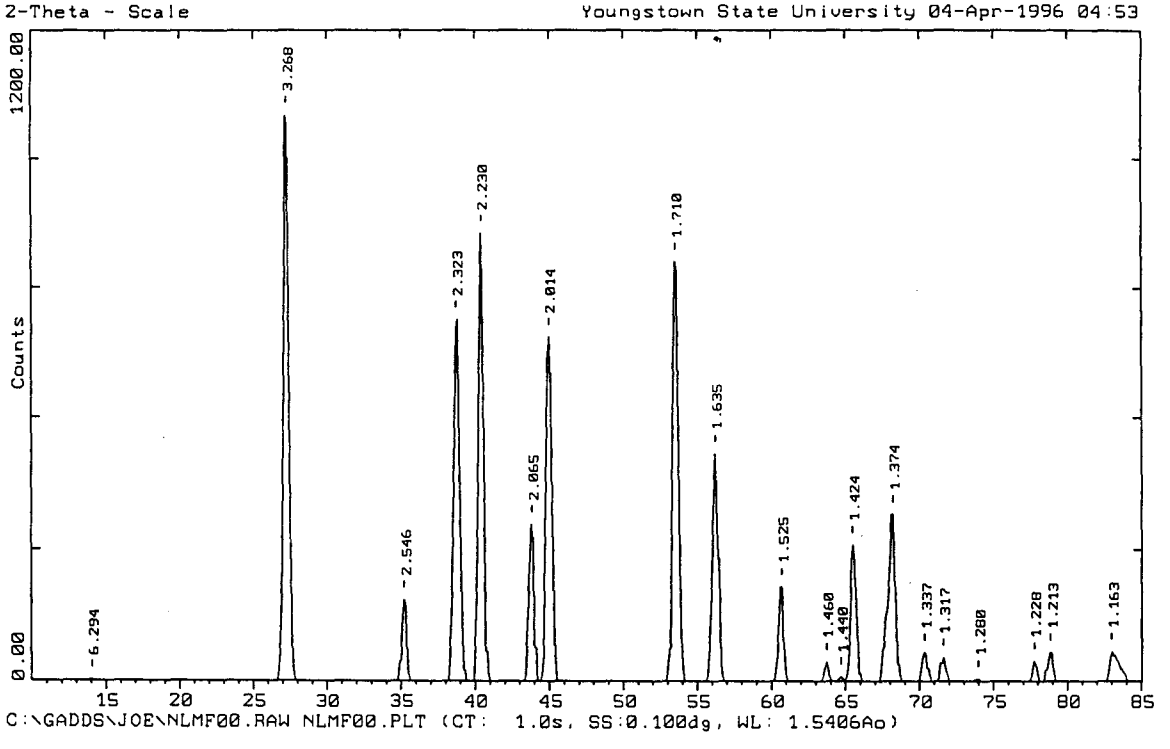

Figure 5.23. X-ray diffraction pattern for $NaLi_6Mg_6F_{19}$ synthesis trial 1 starting materials.

Table 5.24

Statistical Data For Figure 5.23

Peak	Counts (%)	2θ (°)	$d_{Exp.}$ (Å)	$d_{Lit.}$ (Å)	$\lvert d_{Exp.}-d_{Lit.} \rvert$ (Å)	Phase	PDF Card
1	0.18	14.060	6.2937	-	-	-	-
2	100.00	27.264	3.2684	3.267	0.0014	MgF_2	41-1443
3	14.24	35.224	2.5459	2.5474	0.0015	MgF_2	41-1443
4	63.54	38.736	2.3228	2.3166	0.0062	NaF	36-1455
5	79.00	40.409	2.2304	2.2309	0.0005	MgF_2	41-1443
6	27.47	43.812	2.0647	2.0672	0.0025	MgF_2	41-1443
7	60.46	44.974	2.0140	2.013	0.0010	LiF	4-857
8	73.98	53.558	1.7097	1.7112	0.0015	MgF_2	41-1443
9	39.94	56.230	1.6346	1.6381	0.0035	NaF	36-1455
10	16.49	60.700	1.5245	1.5259	0.0014	MgF_2	41-1443
11	3.29	63.692	1.4599	1.4607	0.0008	MgF_2	41-1443
12	0.79	64.667	1.4402	1.4403	0.0001	MgF_2	41-1443
13	23.84	65.489	1.4241	1.424	0.0001	LiF	4-857
14	29.20	68.198	1.3740	1.3821	0.0081	MgF_2	41-1443
15	5.07	70.344	1.3373	1.3375	0.0002	NaF	36-1455
16	4.08	71.589	1.3170	1.3176	0.0006	MgF_2	41-1443
17	0.34	73.975	1.2803	1.2814	0.0011	MgF_2	41-1443
18	3.49	77.727	1.2276	1.2272	0.0004	MgF_2	41-1443
19	4.99	78.865	1.2127	1.214	0.0013	LiF	4-857
20	5.09	82.987	1.1627	1.1625	0.0002	LiF	4-857

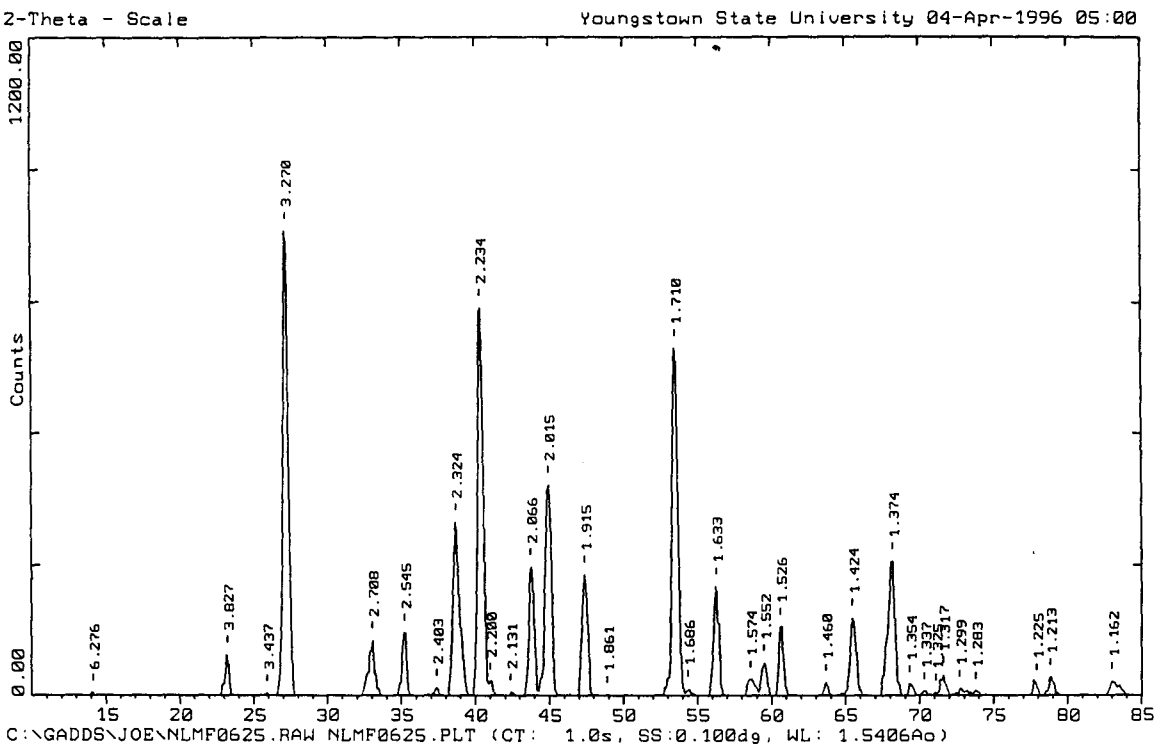

Figure 5.24. X-ray diffraction pattern for $NaLi_6Mg_6F_{19}$ synthesis trial 1 product.

Table 5.25

Statistical Data For Figure 5.24

Peak	Counts (%)	2θ (°)	$d_{Exp.}$ (Å)	$d_{Lit.}$ (Å)	$\lvert d_{Exp.}-d_{Lit.} \rvert$ (Å)	Phase	PDF Card
1	0.54	14.100	6.2761	-	-	-	-
2	8.91	23.227	3.8265	3.83	0.0035	$NaMgF_3$	13-303
3	0.49	25.900	3.4373	3.44	0.0027	$NaMgF_3$	13-303
4	100.00	27.248	3.2703	3.267	0.0033	MgF_2	41-1443
5	11.93	33.053	2.7079	2.71	0.0021	$NaMgF_3$	13-303
6	13.62	35.235	2.5451	2.5474	0.0023	MgF_2	41-1443
7	1.74	37.395	2.4029	2.41	0.0071	$NaMgF_3$	13-303
8	37.51	38.715	2.3240	2.3166	0.0074	NaF	36-1455
9	83.54	40.348	2.2336	2.2309	0.0027	MgF_2	41-1443
10	3.10	40.995	2.1998	2.20	0.0002	$NaMgF_3$	13-303
11	0.74	42.376	2.1313	2.13	0.0013	$NaMgF_3$	13-303
12	27.74	43.776	2.0663	2.0672	0.0009	MgF_2	41-1443
13	45.55	44.955	2.0148	2.013	0.0018	LiF	4-857
14	26.21	47.431	1.9152	1.918	0.0028	$NaMgF_3$	13-303
15	0.21	48.900	1.8611	1.862	0.0009	$NaMgF_3$	13-303
16	74.93	53.539	1.7102	1.7112	0.0010	MgF_2	41-1443
17	1.42	54.368	1.6861	1.689	0.0029	$NaMgF_3$	13-303
18	23.68	56.286	1.6331	1.6335	0.0004	MgF_2	41-1443
19	3.58	58.583	1.5745	1.575	0.0005	$NaMgF_3$	13-303
20	7.04	59.518	1.5519	1.556	0.0041	$NaMgF_3$	13-303
21	14.99	60.615	1.5264	1.5259	0.0005	MgF_2	41-1443
22	2.76	63.666	1.4604	1.4607	0.0003	MgF_2	41-1443
23	16.86	65.476	1.4244	1.424	0.0004	LiF	4-857
24	28.91	68.188	1.3742	1.3745	0.0003	MgF_2	41-1443
25	2.48	69.334	1.3542	2.356	1.0018	$NaMgF_3$	13-303
26	0.87	70.335	1.3374	1.3375	0.0001	NaF	36-1455
27	0.67	71.100	1.3249	1.327	0.0021	$NaMgF_3$	13-303
28	4.44	71.573	1.3173	1.3176	0.0003	MgF_2	41-1443
29	1.42	72.710	1.2995	1.300	0.0005	$NaMgF_3$	13-303
30	0.96	73.797	1.2830	1.2814	0.0016	MgF_2	41-1443
31	2.84	77.90	1.2253	1.2272	0.0019	MgF_2	41-1443
32	3.80	78.82	1.2133	1.214	0.0007	LiF	4-857
33	3.12	83.00	1.1625	1.1625	0.0000	LiF	4-857

compound, $NaLi_6Mg_6F_{19}$. Instead, the compound sodium magnesium fluoride, $NaMgF_3$ was formed. The X-ray diffraction pattern illustrated that all three of the starting materials were present in the reaction product.

Trial 2

The trial 1 product was placed back in the nickel boat, which was loaded back in the quartz tube. The quartz tube was placed back in the tube furnace, and the sample was fired for 20 additional hours at 500°C in air. The sample was removed, prepared, and analyzed on the X-ray diffractometer. The X-ray diffraction pattern for the sample is illustrated in Figure 5.25, and the corresponding statistical data is listed in Table 5.26.

The data indicated that the synthesis attempt of $NaLi_6Mg_6F_{19}$ was again unsuccessful. The data showed that $NaMgF_3$, LiF, MgF_2, and NaF were present in the product. Because the starting materials were in the product, it appears that the reaction was not complete. It is possible that future experiments, attempting to synthesize $NaLi_6Mg_6F_{19}$, may succeed at higher reaction temperatures.

Attempted Synthesis of $CaLi_5Mg_6F_{19}$

All of the attempts to synthesize the novel mixed metal fluoride compound $CaLi_5Mg_6F_{19}$ were performed according to the

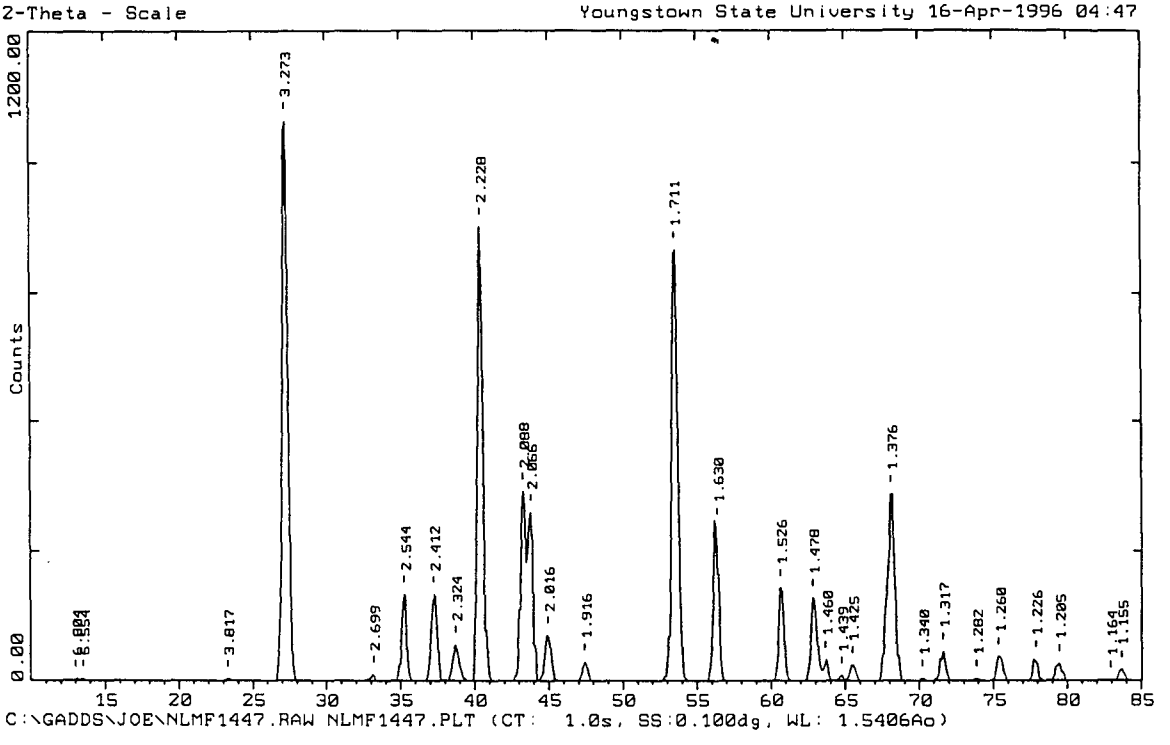

Figure 5.25. X-ray diffraction pattern for $NaLi_6Mg_6F_{19}$ synthesis trial 2 product.

Table 5.26

Statistical Data For Figure 5.25

Peak	Counts (%)	2θ (°)	$d_{Exp.}$ (Å)	$d_{Lit.}$ (Å)	$\lvert d_{Exp.}-d_{Lit.} \rvert$ (Å)	Phase	PDF Card
1	0.26	13.002	6.8038	-	-	-	-
2	0.27	13.500	6.5537	-	-	-	-
3	0.25	23.286	3.8170	3.83	0.0130	$NaMgF_3$	13-303
4	100.00	27.228	3.2726	3.267	0.0056	MgF_2	41-1443
5	1.13	33.162	2.6993	2.68	0.0193	$NaMgF_3$	13-303
6	15.37	35.257	2.5436	2.5474	0.0038	MgF_2	41-1443
7	15.41	37.255	2.4116	2.41	0.0016	$NaMgF_3$	13-303
8	6.39	38.709	2.3243	2.325	0.0007	LiF	4-857
9	81.53	40.448	2.2283	2.23	0.0017	$NaMgF_3$	13-303
10	33.87	43.292	2.0883	-	-	-	-
11	30.03	43.792	2.0656	2.0672	0.0016	MgF_2	41-1443
12	8.12	44.938	2.0155	2.013	0.0025	LiF	4-857
13	3.30	47.422	1.9156	1.918	0.0024	$NaMgF_3$	13-303
14	77.28	53.529	1.7106	1.7112	0.0006	MgF_2	41-1443
15	27.57	56.400	1.6301	1.6335	0.0034	MgF_2	41-1443
16	16.47	60.655	1.5255	1.5259	0.0004	MgF_2	41-1443
17	14.83	62.837	1.4777	1.473	0.0047	$NaMgF_3$	13-303
18	3.77	63.686	1.4600	1.4607	0.0007	MgF_2	41-1443
19	0.87	64.737	1.4388	1.4403	0.0015	MgF_2	41-1443
20	2.75	65.457	1.4247	1.424	0.0007	LiF	4-857
21	33.38	68.108	1.3756	1.3821	0.0065	MgF_2	41-1443
22	0.36	70.196	1.3397	1.3375	0.0022	NaF	36-1455
23	5.12	71.602	1.3168	1.3176	0.0008	MgF_2	41-1443
24	0.37	73.854	1.2821	1.2814	0.0007	MgF_2	41-1443
25	4.28	75.369	1.2601	1.256	0.0041	$NaMgF_3$	13-303
26	3.79	77.844	1.2261	1.2272	0.0011	MgF_2	41-1443
27	3.01	79.443	1.2054	1.213	0.0076	$NaMgF_3$	13-303
28	0.08	82.908	1.1636	1.1625	0.0011	LiF	4-857
29	1.91	83.654	1.1551	1.1549	0.0002	MgF_2	41-1443

following stoichiometrically balanced equation:

$$CaF_2 + 5LiF + 6MgF_2 \rightarrow CaLi_5Mg_6F_{19}.$$

The details of each trial will be discussed next.

Trial 1

A mixture of 0.845 grams of CaF_2, 1.403 grams of LiF, and 4.041 grams of MgF_2 was ground up with a mortar and pestle. The mole ratio was 1 mole CaF_2, to 5 moles of LiF, to 6 moles of MgF_2. A sample was analyzed on the X-ray diffractometer. The X-ray diffraction pattern for the sample is illustrated in Figure 5.26, and the corresponding statistical data is listed in Table 5.27.

The mixture was pressed into a sample pellet, which was placed in a new nickel boat. The nickel boat was placed inside a new quartz tube. The tube was placed inside the Thermolyne model 21100 tube furnace and left open to the room atmosphere to test the relative stability of the proposed novel fluoride relative to oxides. The sample was fired for one day at 650°C. The sample product was analyzed on the X-ray diffractometer. The X-ray diffraction pattern for the sample is illustrated in Figure 5.27, and the corresponding statistical data is listed in Table 5.28.

The X-ray diffraction data showed that no reaction had occurred because only the starting materials were present in the sample product.

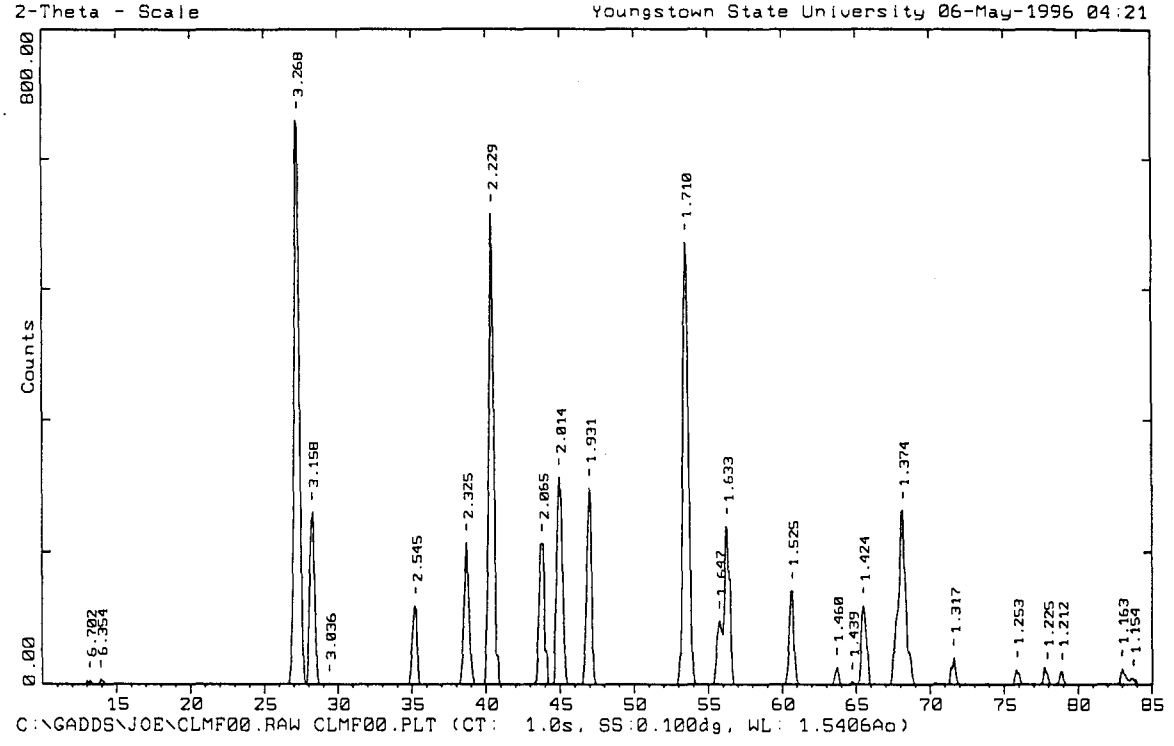

Figure 5.26. X-ray diffraction pattern for $CaLi_5Mg_6F_{19}$ synthesis trial 1 starting materials.

Table 5.27

Statistical Data For Figure 5.26

Peak	Counts (%)	2θ (°)	$d_{Exp.}$ (Å)	$d_{Lit.}$ (Å)	$\lvert d_{Exp.}-d_{Lit.} \rvert$ (Å)	Phase	PDF Card
1	0.70	13.200	6.7019	-	-	-	-
2	0.86	13.926	6.3541	-	-	-	-
3	100.00	27.265	3.2682	3.267	0.0012	MgF_2	41-1443
4	30.36	28.236	3.1580	3.155	0.0030	CaF_2	35-816
5	0.06	29.400	3.0356	-	-	-	-
6	13.80	35.238	2.5449	2.5474	0.0025	MgF_2	41-1443
7	24.78	38.697	2.3250	2.325	0.0000	LiF	4-857
8	83.40	40.426	2.2294	2.2309	0.0015	MgF_2	41-1443
9	24.75	43.809	2.0648	2.0672	0.0024	MgF_2	41-1443
10	36.42	44.985	2.0135	2.013	0.0005	LiF	4-857
11	34.63	47.014	1.9312	1.9316	0.0004	CaF_2	35-816
12	78.28	53.531	1.7105	1.7112	0.0007	MgF_2	41-1443
13	11.18	55.754	1.6474	1.6471	0.0003	CaF_2	35-816
14	27.76	56.280	1.6333	1.6335	0.0002	MgF_2	41-1443
15	16.44	60.686	1.5248	1.5259	0.0011	MgF_2	41-1443
16	3.11	63.681	1.4601	1.4607	0.0006	MgF_2	41-1443
17	0.43	64.726	1.4391	1.4403	0.0012	MgF_2	41-1443
18	13.74	65.493	1.4241	1.424	0.0001	LiF	4-857
19	30.54	68.201	1.3739	1.3745	0.0006	MgF_2	41-1443
20	4.61	71.602	1.3168	1.3176	0.0008	MgF_2	41-1443
21	2.61	75.850	1.2533	1.2533	0.0000	CaF_2	35-816
22	2.29	77.900	1.2253	1.2272	0.0019	MgF_2	41-1443
23	2.22	78.900	1.2123	1.214	0.0017	LiF	4-857
24	2.69	82.952	1.1631	1.1625	0.0006	LiF	4-857
25	1.11	83.749	1.1540	1.1549	0.0009	MgF_2	41-1443

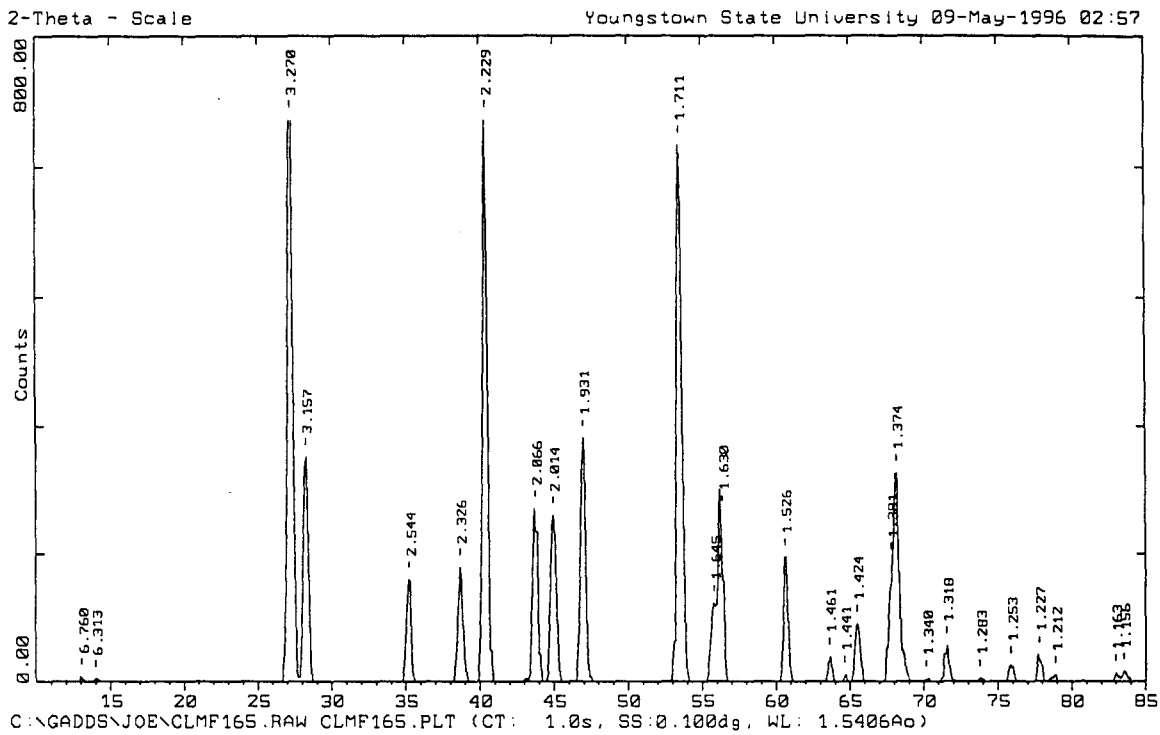

Figure 5.27. X-ray diffraction pattern for $CaLi_5Mg_6F_{19}$ synthesis trial 1 product.

Table 5.28

Statistical Data For Figure 5.27

Peak	Counts (%)	2θ (°)	$d_{Exp.}$ (Å)	$d_{Lit.}$ (Å)	$\lvert d_{Exp.}-d_{Lit.} \rvert$ (Å)	Phase	PDF Card
1	0.81	13.086	6.7600	-	-	-	-
2	0.52	14.017	6.3131	-	-	-	-
3	100.00	27.250	3.2700	3.267	0.0030	MgF_2	41-1443
4	35.51	28.246	3.1569	3.155	0.0019	CaF_2	35-816
5	16.14	35.254	2.5437	2.5474	0.0037	MgF_2	41-1443
6	18.08	38.687	2.3256	2.325	0.0006	LiF	4-857
7	88.78	40.431	2.2292	2.2309	0.0017	MgF_2	41-1443
8	27.34	43.781	2.0661	2.0672	0.0011	MgF_2	41-1443
9	26.39	44.972	2.0141	2.013	0.0011	LiF	4-857
10	38.52	47.018	1.9311	1.9316	0.0005	CaF_2	35-816
11	83.92	53.521	1.7108	1.7112	0.0004	MgF_2	41-1443
12	12.32	55.826	1.6455	1.6471	0.0016	CaF_2	35-816
13	26.58	56.400	1.6301	1.6335	0.0034	MgF_2	41-1443
14	19.64	60.616	1.5264	1.5259	0.0005	MgF_2	41-1443
15	3.98	63.622	1.4613	1.4607	0.0006	MgF_2	41-1443
16	1.18	64.651	1.4406	1.4403	0.0003	MgF_2	41-1443
17	9.07	65.481	1.4243	1.424	0.0003	LiF	4-857
18	18.98	67.800	1.3811	1.3821	0.0010	MgF_2	41-1443
19	32.91	68.178	1.3744	1.3745	0.0001	MgF_2	41-1443
20	0.44	70.184	1.3399	-	-	-	-
21	5.57	71.540	1.3178	1.3176	0.0002	MgF_2	41-1443
22	0.54	73.801	1.2829	1.2814	0.0015	MgF_2	41-1443
23	2.57	75.878	1.2529	1.2533	0.0004	CaF_2	35-816
24	4.17	77.794	1.2267	1.2272	0.0005	MgF_2	41-1443
25	0.99	78.900	1.2123	1.214	0.0017	LiF	4-857
26	1.37	82.984	1.1627	1.1625	0.0002	LiF	4-857
27	1.59	83.556	1.1562	1.1549	0.0013	MgF_2	41-1443

Trial 2

The trial 1 product was repressed into another sample pellet. Unlike trial 1, the sample pellet was placed in a ceramic reaction vessel. The ceramic boat was placed in the quartz tube. As in the first attempted synthesis, the quartz tube was left open to the room atmosphere. The quartz tube was placed inside of the Thermolyne model 21100 tube furnace, and the sample was fired for an additional day at 550°C. The sample was removed and analyzed on the X-ray diffractometer. The X-ray diffraction pattern for the sample is illustrated in Figure 5.28, and the corresponding statistical data is listed in Table 5.29.

The results indicated that the reaction was again unsuccessful. The X-ray diffraction data illustrated that only the starting materials were present in the product. Adjusting the temperature and reaction time may get the reaction to form the desired novel mixed metal fluoride compound in future experiments.

Synthesis of Sr_2NF

The synthesis of Sr_2NF was carried out according to the following stoichiometric equation:

$$3Sr + SrF_2 + N_2 \rightarrow (Sr_2NF)_2.$$

This compound was previously reported in the literature.[9] The purpose for this synthesis was to verify the earlier

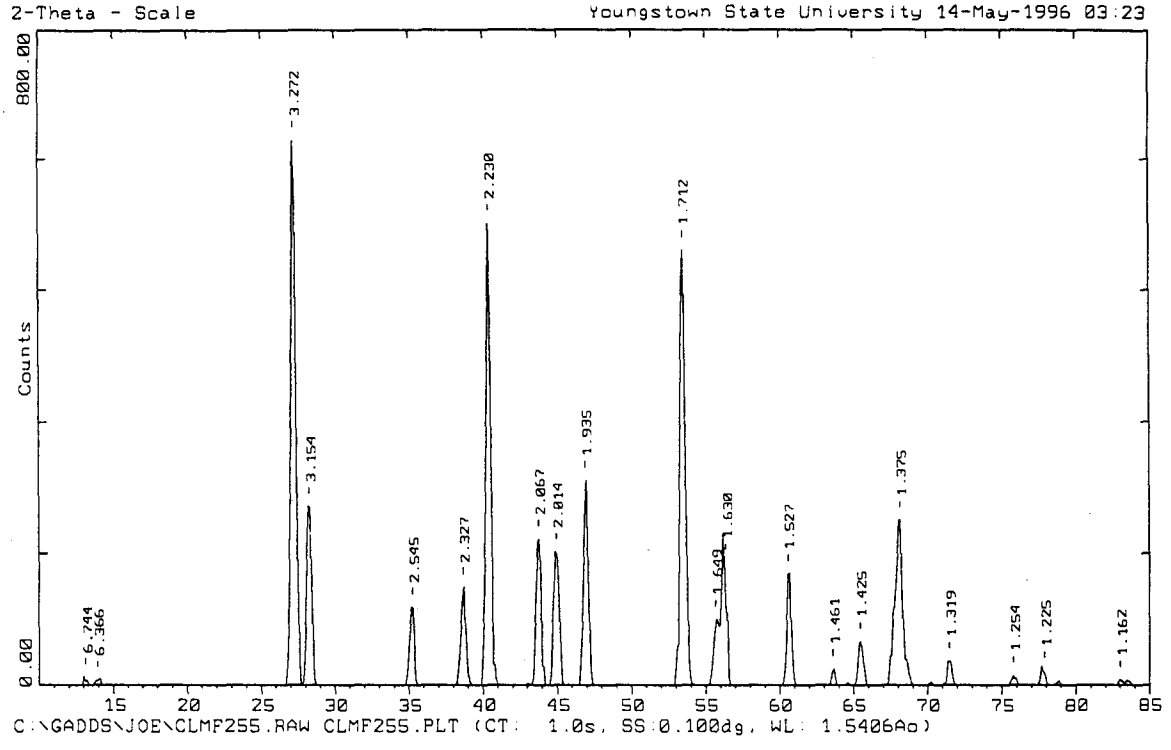

Figure 5.28. X-ray diffraction pattern for $CaLi_5Mg_6F_{19}$ synthesis trial 2 product.

Table 5.29

Statistical Data For Figure 5.28

Peak	Counts (%)	2θ (°)	$d_{Exp.}$ (Å)	$d_{Lit.}$ (Å)	$\lvert d_{Exp.}-d_{Lit.} \rvert$ (Å)	Phase	PDF Card
1	1.60	13.117	6.7442	-	-	-	-
2	1.03	13.900	6.3660	-	-	-	-
3	100.00	27.229	3.2724	3.267	0.0054	MgF_2	41-1443
4	32.87	28.271	3.1542	3.155	0.0008	CaF_2	35-816
5	14.30	35.241	2.5447	2.5474	0.0027	MgF_2	41-1443
6	18.02	38.654	2.3274	2.325	0.0024	LiF	4-857
7	84.53	40.420	2.2298	2.2309	0.0011	MgF_2	41-1443
8	26.85	43.767	2.0667	2.0672	0.0005	MgF_2	41-1443
9	24.35	44.968	2.0142	2.013	0.0012	LiF	4-857
10	37.63	46.921	1.9349	1.9316	0.0033	CaF_2	35-816
11	79.76	53.493	1.7116	1.7112	0.0004	MgF_2	41-1443
12	12.03	55.713	1.6486	1.6471	0.0015	CaF_2	35-816
13	22.51	56.400	1.6301	1.6335	0.0034	MgF_2	41-1443
14	20.43	60.605	1.5267	1.5259	0.0008	MgF_2	41-1443
15	3.04	63.630	1.4612	1.4607	0.0005	MgF_2	41-1443
16	8.02	65.453	1.4248	1.424	0.0008	LiF	4-857
17	30.27	68.168	1.3745	1.3745	0.0000	MgF_2	41-1443
18	4.37	71.482	1.3187	1.3176	0.0011	MgF_2	41-1443
19	1.78	75.802	1.2540	1.2533	0.0007	CaF_2	35-816
20	2.69	77.900	1.2253	1.2272	0.0019	MgF_2	41-1443
21	0.95	83.033	1.1621	1.1625	0.0004	LiF	4-857

results, and further investigate the crystal structure. The reaction conditions will be discussed next.

A sample mixture was prepared by mixing 25.00 grams of strontium metal with 10.00 grams of SrF_2. The mole ratio of the mixture was 1 mole of SrF_2 to 3.6 moles of strontium metal. The starting materials were ground into a powder with a mortar and pestle. The starting materials were placed in a new nickel reaction vessel. The nickel boat was loaded into a new quartz tube, which was connected to a source of dynamic nitrogen. The tube was placed in the Thermolyne model 21100 tube furnace, and the 99.999% pure nitrogen gas was introduced into the system to purge it of air. Initially, the sample was fired for 5.5 hours at 450°C to drive off any oxidation from the strontium metal. Then, the temperature was increased to 950°C, and the sample was heated for an additional 1.5 hours. For safety precautions, the heat on the tube furnace was powered down for the evening, but the nitrogen flow was kept on overnight to continue purging the system. The following day, the temperature was increased back to 950°C, and the sample was heated for an additional 8.0 hours. Again in the evening, the heat was powered down but the nitrogen flow remained on. The next day, the temperature was again increased back to 950°C, and the sample was heated for an additional 8.0 hours. Once more, the heat was powered down in the evening

and the nitrogen flow was left on. The fourth and final day of heating, the temperature was increased back to 950°C as in the previous days, and the sample was heated for an additional 6.5 hours to complete the synthesis. At the conclusion of the synthesis, the sample had been heated 5.5 hours at 450°C and 24 hours total at 950°C. The sample was analyzed on the X-ray diffractometer. The X-ray diffraction pattern for the sample is shown in Figure 5.29, and the corresponding statistical data is listed in Table 5.30.

The structure analysis for this sample indicated that a compound was synthesized that appears to be very similar, but not identical, to the Sr_2NF compound previously reported by Ehrlich[9] et al. This previous Sr_2NF compound was reported as a cubic cell with parameter a = 5.38 Å. Note that the cubic cell with a = 10.714 Å is the one used to calculate the $d_{Lit.}$ values in Table 5.30. The Sr_2NF compound prepared in this work, however, shows a diffraction pattern that can be indexed either as a cubic cell with a = 10.714 Å, or as a tetragonal cell with a = 5.357 Å and c = 10.714 Å. Thus, the compound prepared in this study is based on a slightly smaller cubic cell, which has either doubled in all three dimensions, or has doubled only along the c-axis to give a tetragonal cell. Structural analysis discussed in the section following the next one suggests that the tetragonal structure is the more likely of the two.

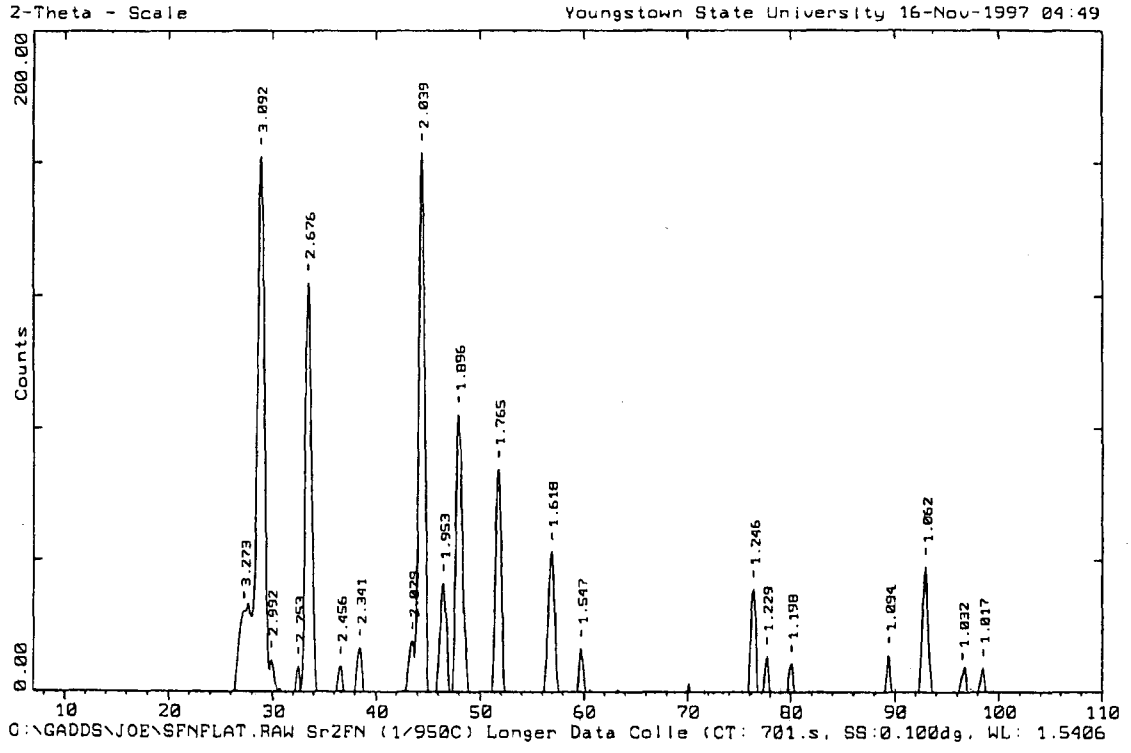

Figure 5.29. X-ray diffraction pattern for Sr_2NF synthesis product.

Table 5.30

Statistical Data For Figure 5.29

Peak	Counts (%)	2θ (°)	$d_{Exp.}$ (Å)	$d_{Lit.}$ (Å)	$\lvert d_{Exp.}-d_{Lit.} \rvert$ (Å)	Phase	PDF Card
1	14.99	27.227	3.2726	3.2305	0.0421	Sr_2NF	*
2	99.21	28.852	3.0919	3.0930	0.0011	Sr_2NF	*
3	5.84	29.840	2.9917	-	-	-	-
4	4.73	32.500	2.7527	-	-	-	-
5	76.02	33.455	2.6762	2.6785	0.0023	Sr_2NF	*
6	4.74	36.563	2.4556	2.4581	0.0025	Sr_2NF	*
7	8.14	38.424	2.3408	2.3381	0.0027	Sr_2NF	*
8	9.40	43.489	2.0792	-	-	-	-
9	100.00	44.394	2.0389	2.034	0.0049	Ni^0	4-850
10	20.16	46.454	1.9532	1.9562	0.0030	Sr_2NF	*
11	51.70	47.937	1.8961	1.896	0.0001	Sr_2NF	24-1228
12	41.46	51.756	1.7648	1.762	0.0028	Ni^0	4-850
13	26.23	56.870	1.6177	1.620	0.0023	Sr_2NF	24-1228
14	8.06	59.738	1.5467	1.547	0.0003	Sr_2NF	24-1228
15	19.04	76.375	1.2459	1.246	0.0001	Ni^0	4-850
16	6.68	77.639	1.2288	1.2290	0.0002	Sr_2NF	*
17	5.26	80.055	1.1977	1.1979	0.0002	Sr_2NF	*
18	6.71	89.462	1.0945	1.0935	0.0010	Sr_2NF	*
19	23.27	92.977	1.0621	1.0624	0.0003	Ni^0	4-850
20	3.79	96.500	1.0325	1.0310	0.0015	Sr_2NF	*
21	4.45	98.477	1.0170	1.0172	0.0002	Ni^0	4-850

*Denotes values calculated using *D-CALC* program.[13]

Examination of Figure 5.29 indicated that another phase was present in the sample product, which was later identified as nickel metal. The nickel metal likely diffused into the sample matrix from the nickel boat that contained the sample mixture.

Attempts to index the X-ray data for this sample as an oxide such as SrO or NiO, or fluorides such as SrF_2 or NiF_2, failed. Also, no absolute match was obtained by comparison of the data with patterns stored in the *JCPDS* database, although the previously reported data for Sr_2NF was given as one possible match, as shown in Figure 5.30. Therefore, it appears that the synthesis succeeded in forming the nitride-fluoride compound Sr_2NF, and the structural analysis of that compound will be discussed in the next section.

Structural Analysis of Sr_2NF

Three possibilities for the structure type of Sr_2NF were considered, based on the X-ray data and previously reported structures for Sr_2NF[9] and related structures[10]: NaCl-type, ZnS (zinc blende)-type, and a structure related to both NaCl and ZnS. The procedure for structure analysis involved calculating the bond lengths for each structure type (with the appropriate cell parameters deduced from the experimental powder pattern), followed by performing an empirical bond-valence sum analysis to test feasibility of

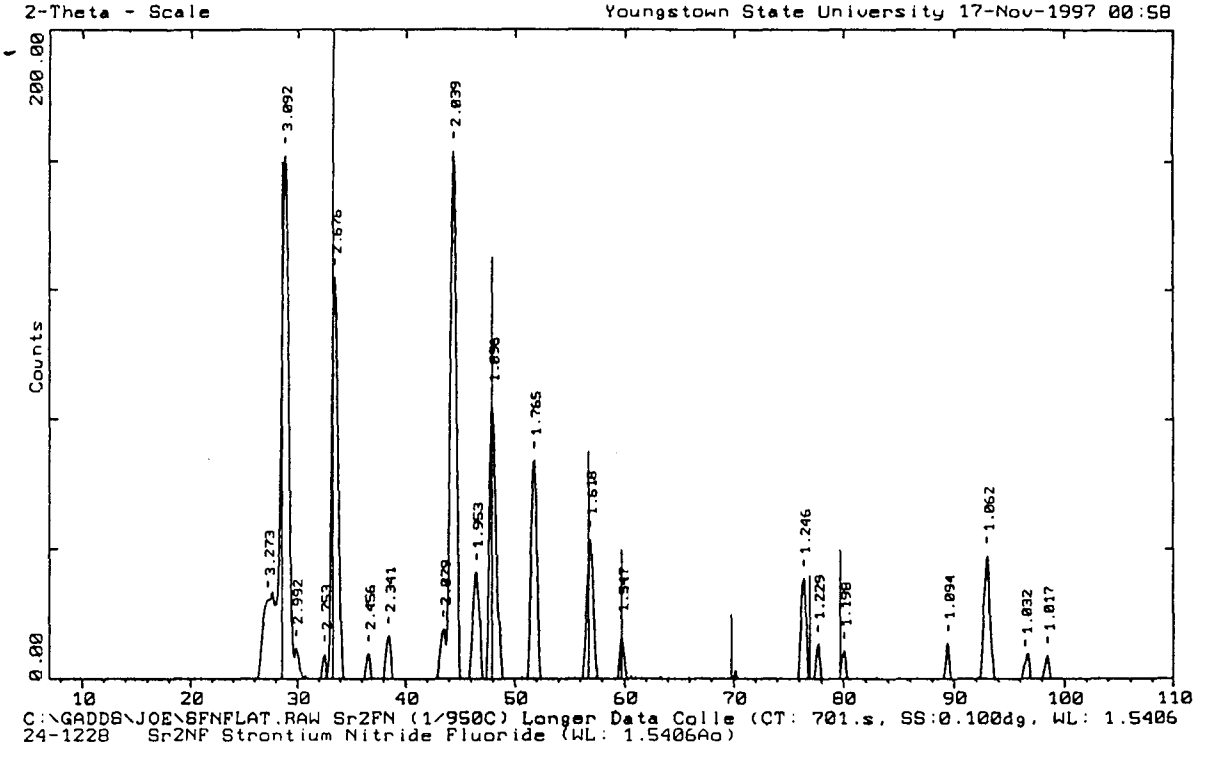

Figure 5.30. X-ray diffraction pattern for Sr_2NF synthesis product indexed to Sr_2NF from *JCPDS* database.

the structure. Since the bond-valence sum method has not been discussed previously in this thesis, it will be summarized next. Results and conclusions of bond-valence sum analysis for each structure type will then be presented.

Empirical Bond-Valence Sum Method

The empirical bond-valence sum method is a powerful diagnostic technique for use in confirming or predicting structural properties of crystalline solids. The method involves calculating valences of individual bonds to an atom of interest, and then summing the bond valences to obtain an experimental value for the valence of that atom. If the bond-valence sum is approximately equal to the oxidation state of the atom of interest, then the local crystal chemistry about the atom of interest is considered feasible. For this study, the bond valences of Sr-N and Sr-F bonds will be calculated using bond lengths for each of the three various structure types considered (see above). A structure-type yielding a bond-valence sum of about 2 (i.e. the ideal oxidation state for Sr) is then considered a feasible structure for Sr_2NF.

Mathematically, the bond valence v_{ij} between two atoms i and j is given by the relation

$$v_{ij} = exp[(R_{ij}-d_{ij})/b_{ij}], \qquad (1)$$

where R_{ij} and b_{ij} are unitless empirical parameters obtained from the literature[16], and d_{ij} is the experimental bond length. For Sr-N and Sr-F bonds, R_{ij} = 2.23 and 2.019 respectively; b_{ij} = 0.37 for both bonds. The valence sum around a central atom is then given by the relation

$$V_i = \Sigma v_{ij}. \qquad (2)$$

Bond-Valence Sum Analysis Results

Table 5.31 shows the results of a bond valence sum analysis around Sr for the three possible structure types considered: NaCl-type, ZnS (zinc blende)-type, and a combined NaCl/ZnS structure. The individual bond valences for each structure were obtained by first calculating ideal bond lengths for each structure, and then substituting these into equation 1 in the previous section. The results for each structure type are discussed next.

NaCl-Type Structure. For the purposes of calculating the bond lengths for Sr_2NF with the NaCl-type structure, the ideal cell with a = 5.357 Å is considered. The fact that the X-ray data actually is better indexed with a doubled parameter (i.e. 10.714 Å) can be explained as due to cation vacancies. This is in fact observed for Mg_3F_3N[10], where one Mg atom is reportedly missing in every other unit cell. The ideal NaCl-type Sr_2NF structure would consist of a unit cell with two formula units, and anions in face-centered cubic

Table 5.31

Bond-Valence Sum Results For Sr_2NF

Bond	Bond Lengths (Å) and Valences (in parentheses) for Structure Types: NaCl	ZnS (zinc blende)	NaCl / zinc blende
Sr-N	3 × 2.678 (3 × 0.30)	2 × 2.320 (2 × 0.78)	2 × 2.704 (2 × 0.28)
Sr-F	3 × 2.678 (3 × 0.17)	2 × 2.320 (2 × 0.44)	2 × 2.704 (2 × 0.16)
Sr-N´	-	-	1 × 2.309 (1 × 0.81)
Sr-F´	-	-	1 × 3.048 (1 × 0.06)
$V_i(Sr)=\Sigma v_{ij}$	1.41	2.44	1.75

packing. Strontium atoms would be coordinated to three nitrogen and three fluorine atoms, and each nitrogen and fluorine atom would be surrounded by six strontium atoms. In order to preserve an ideal NaCl-type structure, the Sr-N and Sr-F bond lengths would necessarily be identical. This bond length is easily obtained as one-half the cell edge length. The resulting bond valence sum for strontium is calculated to be 1.41, which is much less than the expected value of 2.00. Since stable structures have a strong tendency to obey the bond valence sum rule (to at least within 0.20 valence units), the conclusion here is that the NaCl-type structure is not feasible for the compound synthesized in this study.

The fact that Ehrlich[9] et al. reported the structure of their Sr_2NF compound as being of the NaCl-type could be due either to preparation of a different phase (e.g. similar to H-Mg_2NF[10]) than the one presented here, or misassumption of the structure type. The latter explanation is a possibility, because Ehrlich[9] et al. apparently based their conclusion on the fact that their powder pattern could be indexed as a face-centered cubic cell, with a parameter similar to that for SrO. However, no further structural analysis was apparently completed to quantify this result. In any case, the results presented here indicate that the NaCl-type structure is not feasible for Sr_2NF, because the

bond lengths are too large to satisfy local electroneutrality requirements.

ZnS (zinc blende)-Type Structure. One way to reduce the bond lengths is to reduce the coordination number of strontium. If the resulting bond valences are large enough, the bond valence sum for strontium will be favorable despite the decrease in number of bonds. A likely structure with anions packed in a face-centered cubic array which could accomplish this is the zinc blende (ZnS) structure, in which cations are positioned in every other tetrahedral site. There is again only one bond length necessary to describe the structure, which is easily calculated to be 2.320 Å based on the cubic cell parameter a = 5.357 Å. For Sr_2NF with this structure-type, strontium atoms are surrounded by two nitrogen and two fluorine atoms, giving the overall bond valence sum of 2.44. Thus, it appears that strontium is too crowded in this structure, and it is therefore not a feasible choice.

Combined NaCl/ZnS Structure. The fact that strontium is underbonded in the NaCl-type structure and overbonded in the ZnS structure suggests that a structure intermediate between these two is the correct one. Such a structure was reported by Andersson[10] for L-Mg_2FN, which is tetragonal with nitrogen and fluorine atoms in identical positions as anions in MgO (NaCl-type), except that the ordering of nitrogen and

fluorine cause a doubling along one of the axes. The corresponding unit cell parameters for Sr_2NF with this structure would be a = 5.357 Å and c = 10.714 Å, and these can be used to index the experimental diffraction pattern shown previously in Figure 5.29. The cation in this structure is in a square pyramidal site, with two Sr-F and two Sr-N distances of 2.704 Å and one Sr-N distance of 2.309 Å. There is also a relatively weak Sr-F bond with bond distance 3.048 Å. These bond distances were calculated by using the atomic positions given by Andersson[10] for L-Mg_2FN as input in Siemens *SHELXTL* structure plotting program. The relevant crystallographic data used for the calculation are: space group $I4_1/amd$; Z = 4; Sr in 8(e) position with z = 0.1595; N in 4(b) position; and F in 4(a) position. Figure 5.31 then shows a plot of the structure. The bond valence sum for strontium obtained from the calculated distances is 1.75, which is in the vicinity of the ideal valence of 2.00. Note that the strontium position given above has a refinable z parameter, where the value listed above and used in this calculation is the one reported by Andersson[10] for L-Mg_2FN. Quantitative refinement of the structure in future work could yield improved bond valences.

In conclusion, the present study indicates that the most likely structure for the strontium nitride-fluoride compound synthesized here is one that is related to both the

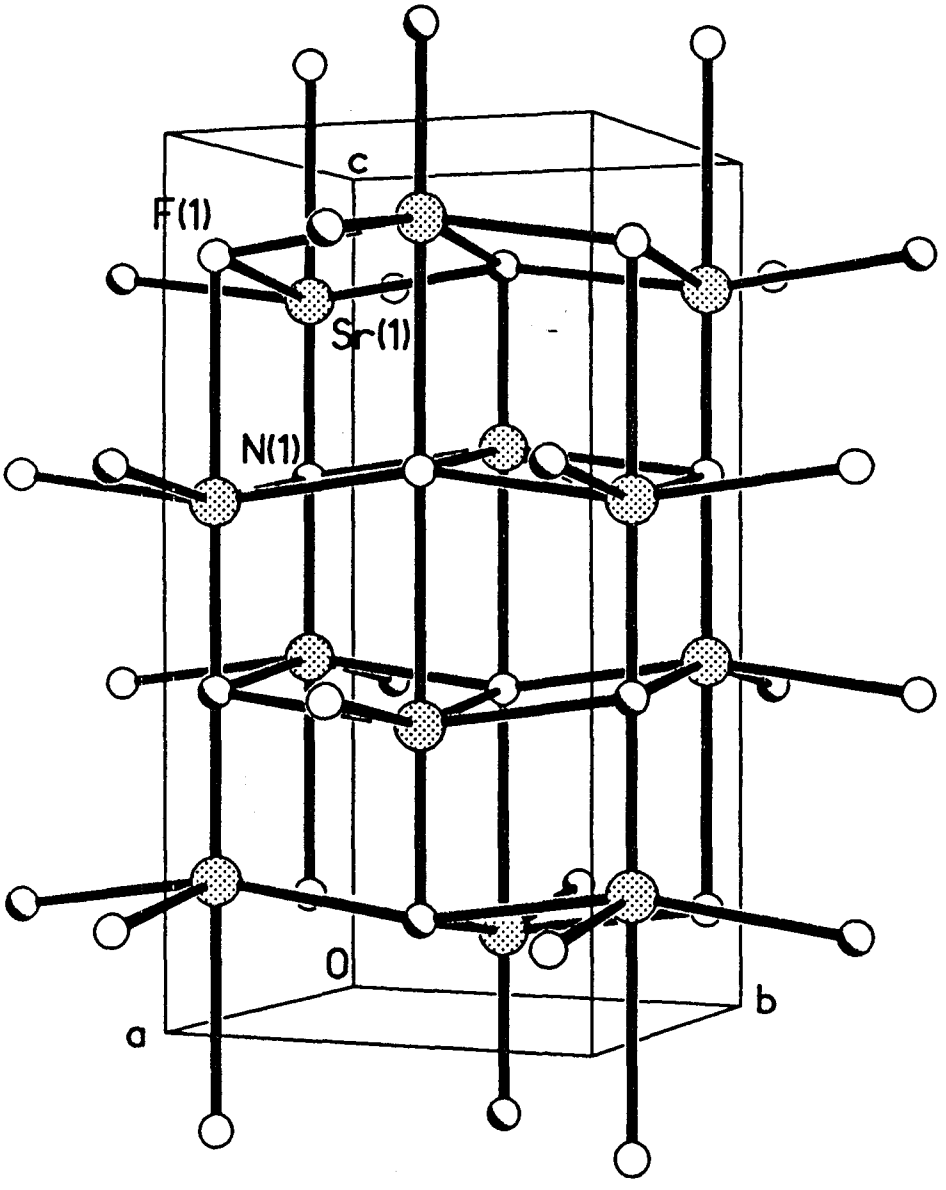

Figure 5.31. Proposed structure plot for Sr_2NF as calculated by Siemens *SHELXTL* structure plotting program.

NaCl and zinc blende structures. This is in agreement with the structure reported for L-Mg_2FN by Andersson[10], but does not agree with the previous structural interpretation for Sr_2NF by Ehrlich[9] et al. It would seem that there is much interesting solid state chemistry to be done on this and related systems.

CHAPTER VI

CONCLUSIONS

An underlying problem in many of the synthesis attempts described in this thesis seems to be related to the stability of aluminum nitride. For those materials where AlN was used as a reactant, $BaMgAl_{11}F_{10}N_9$ and $MgAl_2(FN)_2$, AlN was always prominent in the reaction products. For those reactions in which aluminum metal was reacted with aluminum fluoride in a nitrogen atmosphere, AlN was always observed to form preferentially to the desired product. This suggests that an alternate route must be investigated for the synthesis of aluminum containing nitride-fluoride compounds. One possibility might be carrying out a reaction in a stream of NH_3 instead of N_2. If the preparation of such compounds continues to prove difficult, one can shift focus to the other systems where Al^{+3} is replaced with Fe^{+3}, etcetera.

Another conclusion drawn from some of the results of this thesis is that the number of different reactants needs to be minimized, to simplify the solid-state reaction. For example, the preparation of $BaMgAl_{11}F_{10}N_9$ involved combining 4 different nitride and fluoride reactants. This was a purely exploratory synthesis, and it was realized in

hindsight that the reaction was overly complicated. This minimized the chances for success, because too many reactants must interact simultaneously, which is difficult in the solid state. A better approach would be to synthesize nitride-fluoride precursors and then combine these species to make more complicated nitride-fluoride compounds. Thus, rather than modeling only a specific oxide, the nitride-fluoride synthesis would model the entire reaction. For example, the reaction:

$$\tfrac{1}{2}Ba_2NF + 6Al_2(NF)_{1.5} \rightarrow BaAl_{12}(NF)_{9.5},$$

which models:

$$BaO + 6Al_2O_3 \rightarrow BaAl_{12}O_{19}.$$

Finally, qualitative structural analysis of the Sr_2NF compound synthesized in this project has yielded some new results. Previously, Sr_2NF was reported as having the NaCl-type structure, with cell parameters a=5.38Å. The powder data obtained for the sample prepared in this study can be indexed as a cubic cell, with a=10.714Å. This could be interpreted as a doubling of a cubic cell with dimensions 5.36Å, which is fairly close to the parameters reported by Ehrlich[9] et al. However, a bond-valence sum analysis clearly indicates that the NaCl-type structure is not likely for this material, and that a structure intermediate between NaCl and ZnS (zinc blende) is most likely. However, this result needs to be verified in future work by synthesizing a

pure Sr_2NF sample, and performing a quantitative structure analysis such as Rietveld refinement. It would also be interesting to study Ca_2NF and Ba_2NF, which were also reported by Ehrlich[9] et al, as having the NaCl-type structure.

REFERENCES

1. M. P. Stevens, "Polymer Chemistry an Introduction", 2nd edition, Oxford University Press, Inc., Oxford (1990).

2. F. J. DiSalvo, Science. **247**, 649-655 (1990).

3. I. Amato, Science. **252**, 644-646 (1991).

4. J. P. Bromberg, "Physical Chemistry", 2nd edition, Allyn and Bacon, Inc., Boston (1984).

5. D. Halliday, R. Resnick, "Fundamentals of Physics", 3rd edition, John Wiley & Sons, Inc., New York (1988).

6. B. Douglas, D. McDaniel, and J. Alexander, "Concepts and Models of Inorganic Chemistry", 3rd edition, John Wiley & Sons, Inc., New York (1994).

7. H. H. Willard, L. L. Merritt, J. A. Dean, and F. A. Settle, "Instrumental Methods of Analysis", 7th edition, Wadsworth, Inc., Belmont (1988).

8. F. D. Bloss, "Crystallography and Crystal Chemistry an Introduction", 1st edition, Holt, Rinehart and Winston, Inc., New York (1971).

9. P. Ehrlich, W. Linz, and H. Seifert, Naturwissenschaften. **58**, 219-220 (1971).

10. S. Andersson, Journal of Solid State Chemistry. **1**, 306-309 (1970).

11. R. Marchand, J. Lang, Materials Research Bulletin. **6**, 845-851 (1971).

12. V. W. Jung, R. Juza, Zeitschrift Fur Anorganische Und Allgemeine Chemie. **399**, 129-147 (1973).

13. T. R. Wagner, *D-CALC* (1993).

14. V. Adelsköld, Arkiv. Kemi. Mineral Geol. **12**, 9 (1938).

15. A. R. West, "Solid State Chemistry and Its Applications", John Wiley & Sons Ltd., New York (1992).

16. N. E. Brese, M. O'Keeffe, Acta Cryst. **B47**, 192-197 (1991).